

# Quantitative analysis of tumor heterogeneity based on magnetic resonance images

Student: Elena Trajkovska

Supervisor: Kathrine Røe Redalen

2019, NTNU, Trondheim

# Abstract

**Background:** Solid tumors are commonly heterogeneous because they consist of cancer cells with different aggressiveness. In quantitative cancer imaging, such as magnetic resonance imaging (MRI), the heterogeneity will not be reflected in mean tumor values. The aim of this project was to develop a quantitative image-based tool that reflects tumor heterogeneity by using a machine learning approach with cluster analysis of MR images ( $T_2$ -weighted and diffusion-weighted (DW) images) of 79 rectal cancer patients.

**Materials and methods:** The K-means algorithm is an unsupervised machine learning method that groups the pixel intensities based on similarity. In this project, a K-means clustering algorithm was applied to  $T_2$ -weighted and DW MR images of malignant rectal tumors. The tumors were defined by delineations performed by two radiologists in the  $T_2$ -weighted images. Associations between the resulting clusters and a set of tumor- and patient characteristics were investigated with the Wilcoxon rank-sum test. Progression free survival (PFS) was estimated to identify whether the presence of a certain cluster was linked to patient outcome. Differences in the results between the tumor delineations by the two radiologists were investigated.

**Results:** The results from the clusters defined based on  $T_2$ -weighted images showed statistical significance ( $p < 0.05$ ) for the parameters from the "TNM" staging system. The assessed extent of the primary tumor and the regional lymph nodes after the CRT treatment. ( $p/ypT$ ,  $p/ypN$ ) and the difference in staging before and after CRT ( $\Delta T$ ) were correlated with the presence of some clusters. The DW images with b-values of 50, 100 and 500  $s/mm^2$  demonstrated a significant association between clusters and tumor regression grade (TRG), which is a parameter reflecting the pathologic response to chemoradiotherapy. In the survival analyses, the DW images with b-value = 1000  $s/mm^2$  showed that the most dominant cluster (largest homogenous

region in the tumor) was related to poor survival. The combined data from the T<sub>2</sub>-weighted and DW images also indicated a significant association with PFS.

**Conclusion:** This project showed that K-means clustering of T<sub>2</sub>-weighted and DW MR images is a promising method to extract quantitative properties of tumor heterogeneity in rectal cancer. The results showed correlation to both pathologic treatment response and long-term survival. The combination of data from both T<sub>2</sub>-weighted and DW images improved the predictability of the outcome, so future studies may investigate different combinations of MR sequences for further improvements.

# Preface

This master thesis was written as part of the study program in Biophysics and Medical physics at the Norwegian University of Science and Technology (NTNU). The work was carried out during the autumn and spring semester in the academic year 2018/19. This project is a part of a larger study, where the aim is to examine different MRI techniques for identifying biomarkers of tumor aggressiveness in rectal cancer for improved treatment adaptation.

I would like to thank my supervisor Kathrine Røe Redalen, for giving me the opportunity to work on this project. For all the kindness, understanding, support, availability, consistent guidance and encouragement in the challenging stages of my work. I would also like to thank Franziska Knuth, for the patience to answer all my script questions and for the ease of guiding me while providing meticulous explanations. Thank you to both for showing me how exciting and fulfilling research can be.

Trondheim, August 2019  
Elena Trajkovska



# Table of Contents

List of Abbreviations.....	xiii
<b>1 Introduction.....</b>	<b>15</b>
<b>2 Theory .....</b>	<b>18</b>
<b>2.1 Cancer.....</b>	<b>18</b>
2.1.1 Cancer biology.....	18
2.1.2 Rectal cancer.....	21
<b>2.2 Magnetic Resonance Imaging.....</b>	<b>22</b>
2.2.1 Basic MRI principles.....	22
2.2.2 Image generation.....	26
2.2.3 T <sub>2</sub> -weighted MRI .....	27
2.2.4 Diffusion – weighted MRI .....	29
<b>2.3 Machine Learning .....</b>	<b>32</b>
2.3.1 K-means clustering .....	34
<b>3 Materials and Methods.....</b>	<b>36</b>
<b>3.1 Study population .....</b>	<b>36</b>
3.1.1 Treatment regimens .....	36
3.1.2 Cancer staging.....	37
<b>3.2 Data analysis methods and software.....</b>	<b>40</b>
3.2.1 Acquisition of MR images.....	40
3.2.2 Image Analysis .....	41
3.2.3 Statistical analysis.....	43
3.2.3.1 K-means clustering .....	43
3.2.3.2 Cluster division .....	45
3.2.3.3 Parameter correlation .....	45
3.2.4 Survival analysis .....	47
<b>4 Results.....</b>	<b>52</b>
<b>4.1 Statistical analyses .....</b>	<b>53</b>
4.1.1 T <sub>2</sub> -weighted images .....	53
4.1.1.1 Radiologist -an .....	53
4.1.1.2 Radiologist – shh .....	54
4.1.2 Diffusion-weighted images .....	56
4.1.2.1 b=0 s/mm <sup>2</sup> .....	56
4.1.2.2 b=25 s/mm <sup>2</sup> .....	57
4.1.2.3 b=50 s/mm <sup>2</sup> .....	58

4.1.2.4	b=50 s/mm <sup>2</sup> (shh)	59
4.1.2.5	b= 100 s/mm <sup>2</sup>	60
4.1.2.6	b=500 s/mm <sup>2</sup>	62
4.1.2.7	b=1000 s/mm <sup>2</sup>	63
4.1.2.8	ADC maps	64
4.1.3	T <sub>2</sub> -weighted and diffusion-weighted images	66
<b>4.2</b>	<b>Survival analyses</b>	<b>68</b>
4.2.1	T <sub>2</sub> -weighted images	68
4.2.1.1	Radiologist – “an”	68
4.2.1.2	Radiologist – “shh”	69
4.2.2	Diffusion-weighted images	70
4.2.2.1	b=0 s/mm <sup>2</sup>	70
4.2.2.2	b=25 s/mm <sup>2</sup>	71
4.2.2.3	b=50 s/mm <sup>2</sup>	72
4.2.2.4	b=50 s/mm <sup>2</sup> (shh)	73
4.2.2.5	b=100 s/mm <sup>2</sup>	74
4.2.2.6	b=500 s/mm <sup>2</sup>	75
4.2.2.7	b=1000 s/mm <sup>2</sup>	76
4.2.2.8	ADC maps	77
4.2.3	T <sub>2</sub> -weighted and diffusion-weighted images	78
<b>5</b>	<b>Discussion</b>	<b>80</b>
<b>5.1</b>	<b>Materials and Methods</b>	<b>80</b>
<b>5.2</b>	<b>Results</b>	<b>83</b>
5.2.1	Statistical analyses	83
5.2.1.1	T <sub>2</sub> -weighted images	83
5.2.1.2	Diffusion-weighted images	84
5.2.1.3	T <sub>2</sub> -weighted and diffusion weighted	86
5.2.2	Survival analyses	87
<b>5.3</b>	<b>Clinical implications</b>	<b>88</b>
<b>5.4</b>	<b>Future work</b>	<b>89</b>
<b>6</b>	<b>Conclusion</b>	<b>91</b>
	<b>References</b>	<b>93</b>
	Appendix A Matlab scripts	99
	A1: Image sorting	99
	A2: Grid coordinates	100
	A3: Interpolate DWI to T <sub>2</sub> -weighted image	101
	A4: Extract pixel intensity for ROI	102

A5: Extract voxel coordinates for ROI.....	103
A6: Create matrix for K-means clustering .....	104
A7: K-means clustering .....	105
A8: Calculation of Cluster Volume Fraction (CVF) .....	108
A9: Extract parameter data from Excel for statistical analyses .....	111
A10: Extract parameter data from Excel for survival analyses.....	111
A11: Create datasets for the statistical/survival analyses.....	112
A12: Create delimiter tables in .txt to be used for R-console .....	114
Appendix B R scripts .....	115
B1: Cox proportional-hazards regression.....	115
B2: Wilcoxon rank-sum test .....	115
Appendix C Cluster distribution .....	117
C1: Matlab script for voxel coordinates of tumor median sections.....	117
C2: Matlab script for displaying cluster distribution.....	119
C3: Cluster distribution in median tumor sections .....	120
Appendix D Kaplan-Meier plots.....	121
Appendix E Normality tests .....	122



# List of Abbreviations

ADC	Apparent diffusion coefficient
AJCC	American Joint Committee on Cancer
AI	Artificial intelligence
APR	Abdominal perineal resection
CVF	Cluster volume fraction
CRC	Colorectal cancer
CRT	Chemoradiotherapy
DNA	Deoxyribonucleic acid
DS	Downstaging
DWI	Diffusion weighted imaging
EPI	Echo planar imaging
FID	Free induction decay
FOV	Field of View
GRE	Gradient echo
ICMD	Inter-cluster minimum distance
IORT	Intraoperative radiotherapy
LAR	Low anterior resection
LARC	Locally advanced rectal cancer
MICD	Mean intra-cluster distance
ML	Machine learning
MRI	Magnetic resonance imaging
NCI	National Cancer Institute
NIFTI	Neuroimaging Informatics Technology Initiative
NMR	Nuclear magnetic resonance
PFS	Progression free survival

RF	Radiofrequency
ROC	Receiver operating characteristics
SE	Spin echo
SI	Signal Intensity
SNR	Signal-to-noise ratio
TE	Echo time
TNM	Tumor-Node-Metastasis
TPR	True positive rate
TR	Repetition time
TRG	Tumor regression grade
ROI	Region of interest

# 1 Introduction

Rectal cancer is a form of colorectal cancer, where the primary tumor is confined to the lower 15 centimeters of the rectum [1]. Colorectal cancer is the fourth most common cancer worldwide with an incidence rate of 19.7 per 100 000 population at risk. However, the incidence rate in Norway is two times higher than the median (42.9) which ranks it as the fourth country with highest rate of colorectal cancer. The International Agency for Research on Cancer at the World Health Organization predicts 39.7 percent increase in the number of incidence cases with rectal cancer by 2040 (compared to the baseline of 2018 for both sexes, at all ages) [2].

If the patient is diagnosed with rectal cancer at an early stage, the most common strategy is to surgically remove the cancerous tissue. When the primary tumor has grown through the rectal wall and started to invade the surrounding organs, it is considered locally advanced. The standard treatment procedure for these cases is radiotherapy combined with chemotherapy in order to shrink and downstage the tumor and enable subsequent surgical removal of the remaining tumor components. Although the mortality rate has been reduced by half compared to the 1990s, nowadays the major challenge is that patients develop metastasis and the main cause of death is metastatic disease. Improving the therapeutic strategies could increase the current 68 percent five-year survival for these patients [3].

Rectal cancer is a solid tumor and the solid tumor microenvironment is known to be spatially heterogeneous, which means that it constitutes of different cells with distinct morphologic and phenotypic features. These features are also heterogeneous between tumors of different patients although their diagnosis is the same [4]. The response to treatment varies individually and it is largely contingent on the aggressiveness of the tumor, hence directly dependent on the heterogeneity of the tissue itself. This is a consequence from a multitude

of reasons, among them the different radiosensitivity which cancer cells demonstrate. Locally advanced tumors are generally larger in size, so they can have higher degree of heterogeneity, which gives even more diverse radioresistance in the tumor tissue.

If we can identify, characterize and understand tumor heterogeneity we could contribute to solve one of the key challenges in oncology for designing effective therapeutic and monitoring strategies. Currently, biopsies are used to probe only part of the tumors and they do not necessarily reflect the tumor heterogeneity [5]. Additional techniques using non-invasive quantitative cancer imaging, such as magnetic resonance imaging (MRI), is a potential approach for comprehensively detecting, depicting and quantifying local variations in tumor morphology and function [4]. However, the mean tumor values commonly extracted from the quantitative MRI do not reflect the heterogeneity, so in order to effectively assess it we need to use other statistical measures. This could help us to recognize patterns which can be associated with tumor aggressiveness, radiotherapy response and prognosis.

The potential outcome from such analyses could be used to evaluate heterogeneity as a biomarker for grading the tumor. Regions that are known to show higher treatment resistance can be found and for instance used for escalating the radiotherapy dose so that treatment outcome can be improved in patients having tumors with low radiosensitivity. Also, it can be useful to identify candidates for more intensive treatments, as a high-risk biomarker to recognize patients with high risk for developing metastasis (and death) [6].

This project uses T<sub>2</sub>-weighted and diffusion-weighted MR images of 79 rectal cancer patients at the time of diagnosis. It utilizes image analysis with MATLAB® (MathWorks, Natick, Massachusetts - version R2018a) and K-means clustering which is an unsupervised machine learning method. The obtained results are correlated with data from cancer staging prior and after treatment and survival analyses are conducted based on a five-year follow-up period. The main aims are to:

- Investigate tumor heterogeneity by identifying different regions (clusters) in the tumor with similar properties.

- Investigate if cluster characteristics (for instance size) are related to the treatment outcome.

The thesis begins with a description of the theory used in the project, including MRI, machine-learning and rectal tumor biology, followed by the materials and methods used in Chapter 3. The results are presented in Chapter 4 and discussed followed by the conclusion of the project. In addition, the appendices contain code used for the analyses.

## 2 Theory

This chapter describes cancer biology by focusing on metastatic conditions as one of the most dominant challenges in treatment planning. Subsequently rectal solid tumors are explained, and a short overview of the treatment strategies is provided. A brief theoretical background of magnetic resonance imaging with an emphasis on  $T_2$ -weighting and diffusion-weighting describes the basic physics behind the used images. The section concludes with explanation of machine learning and K-means clustering which are the essential tools for the analyses in the next chapters.

### 2.1 Cancer

Cancer is a term used to describe a heterogeneous group of disorders that are characterized with uncontrolled cell growth and cell spreading that produces abnormal cells [7]. If such excessive cell proliferation of abnormal cells does not invade neighboring tissues, it is called a benign tumor. On the other hand, if these cells can spread to surrounding tissues and/or break away to enter the lymphatic system or bloodstream, they are classified as malignant tumors (usually referred to as 'cancers'). There is a general distinction between tumors depending on whether they are present in body tissues or fluids, as solid or liquid. In the scope of this thesis we look at solid tumors, which are discrete masses made of epithelial or stromal cells that do not contain cysts or liquid areas. [8]

#### 2.1.1 Cancer biology

Solid tumors at the first site of malignancy are considered primary tumors. They tend to grow and become locally advanced as they invade the adjacent organs until a certain time point is reached, when a process known as metastasis occurs. During metastasis secondary tumors start to form at distant sites in the body and gradually invade other organs. This includes several steps

which the metastatic cells undergo with the purpose of reaching successful spreading (Figure 2.1). First, they have to get detached from the primary tumor by reducing the adhesion to neighboring cells and generate a path for migration into local blood or lymph vessels. Then by invading the basal membrane of these vessels (intravasation) they enter and circulate the bloodstream until a secondary site is reached. An inverse process (extravasation) occurs followed by migration in the host's tissue with the purpose of surviving and proliferating to form a secondary tumor. [9]

Metastatic conditions are lethal because of their complexity and the difficulty to identify cancer spreading through magnetic resonance imaging. Also, the treatment strategies become imposed with the additional burden of eliminating secondary sites in addition to the primary tumor [10]. Up to 50% of patients diagnosed with colorectal cancer die from metastatic disease and the overall 5-year survival for patients diagnosed when the primary tumor has already spread is below 10% [11]. The major site of metastasis is in the liver (up to 70% of patients) and the lungs (up to 20%) [10]. This emphasizes the importance of early detection and treatment of the primary tumor, especially in patients that have already developed locally advanced tumor which increases the risk of metastasis occurrence.

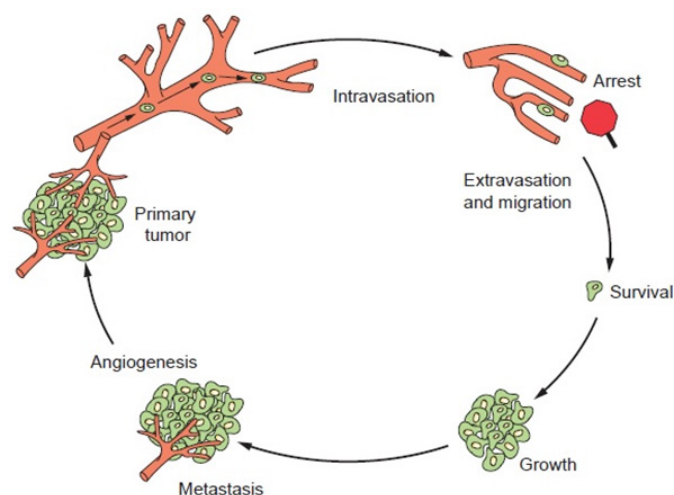


**Figure 2.1** Metastatic process. Metastatic cells detach from the primary tumor and enter the vessels through intravasation. When the secondary site is reached, extravasation and migration help the cells in penetrating the host tissue where they need to survive and proliferate by generating a secondary tumor. [9]

Tumors are considered monoclonal, which means that they are composed of cells that derive from a single starting cell. However, this should not misguide to the conclusion that all tumor cells are the same and it has to be noted that solid tumors are heterogenous (Figure.2.2). [8] There are three levels of heterogeneity depending on the scale of observance: intratumor, intertumor and interpatient. Interpatient refers to differences among tumors within different patients and intertumor differentiates tumors of the same type found in one patient. [11] The most important for this topic is intratumor heterogeneity which describes the morphological differences within a single tumor that can be further divided at two levels. The first level looks at monoclonal tumor cells and various unrelated cells that have infiltrated the tumor from the surrounding environment. They have become part of its microenvironment by being redirected to support tumor activities. The second level defines the phenotypical and molecular distinction between the malignant cells. Various genetic and epigenetic changes can occur and contribute towards cancerous tissues with complicated functional architecture. This gives different asynchronous cell cycles, indicating versatile radioresistance within the solid tumor. [9]

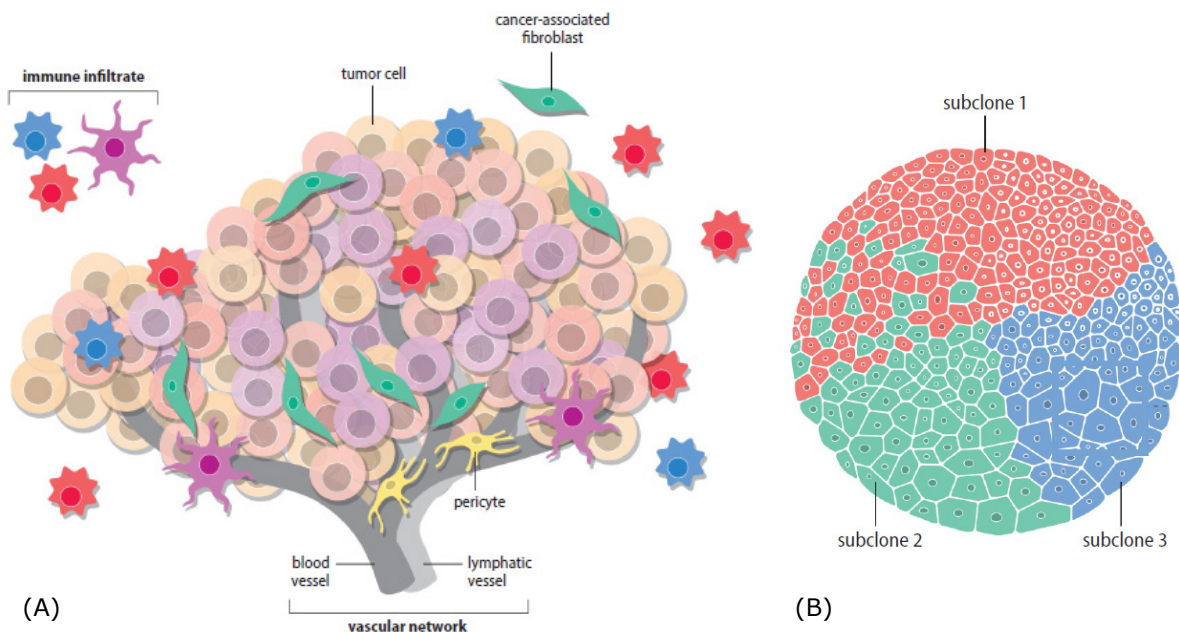


**Figure.2.2** Tumor heterogeneity. (A) Dynamic tumor microenvironment at first level of intratumor heterogeneity with tumor cells and unrelated cells that have been redirected to support tumor activities. (B) Second level of intratumor heterogeneity with distinct tumor subclones. The cells within subclones can intermix (subclones 1 and 2) or be spatially separated (subclone 3) in some cases by physical barriers (ex. blood vessels). [8]



### 2.1.2 Rectal cancer

The rectum is the final straight portion of the large intestine that terminates at the anus, with an average length of 12 centimeters. Rectal cancer is a form of colorectal cancer, where the primary tumor is confined to the lower 15 centimeters of the rectum [1]. Most of the cells in our body do not divide actively, but certain types of cells have high turnover, especially in the gastrointestinal tract. The tissues that have more actively dividing cells tend to have higher risk of developing tumors because of the higher rate of mutations caused by errors in DNA replication and DNA repair. The colon has one of the highest rates with 15-20% of the epithelial cells dying and being replaced every day, which yields larger proneness to tumorigenesis contributing to high colorectal cancer rates. [8]

Rectal cancer can be detected at different stages of growth, which require different treatment strategies. The main treatment options include surgery, radiotherapy and chemotherapy depending on the circumstances and disease development. If the patient is diagnosed with rectal cancer at an early stage, the most common strategy is to surgically remove the cancerous tissue. Additional radiation therapy is used after the surgery to diminish tumor cells that could remain in the area after the operation. On the other hand, in cases where there is locally advanced rectal cancer (LARC), neoadjuvant therapy is prescribed. This approach combines pre-surgery radiation (usually combined with chemotherapy) aimed at shrinking the cancer, so that surgical removal could be performed. However, there are cases where operational interventions are not possible, so chemoradiotherapy (CRT) is the only option, but in such conditions the survival is significantly lower. [13]

Surgery is most commonly used in rectal cancer treatments, but the type of operation depends on the extent and location of the cancer. In cases where the cancer is localized well above the anus, low anterior resection (LAR) is performed. If the tumor is close to the anus, the only option is to undergo abdominoperineal resection (APR). In this procedure the anus is removed, which significantly decreases the patient's quality of life because a replaceable bag that encloses the colostomy must be worn. There are novel interventions,

such as local excision that allows preservation of the anus, but this can only be applied to small cancers that lie close (within 5 centimeters) to it. Otherwise, for smaller incisions further up on the rectum a transcoccygeal excision is applied. [13] This leads to the conclusion that patients can get better life quality, if the tumor is detected earlier or if efficient CRT shrinks the LARC to a size acceptable for the elaborated techniques.

## 2.2 Magnetic Resonance Imaging

One of the most powerful medical imaging techniques today is the Magnetic Resonance Imaging, which provides good contrast resolution and great versatility. A full comprehension of the physical principles in MRI is demanding and would require lengthy elaborations, so this thesis will focus only on aspects relevant to the topic. For details, the reader is referred to *Magnetic Resonance Imaging: Physical Principles and Sequence Design* [16].

### 2.2.1 Basic MRI principles

If not otherwise stated, information in this section is based on [13]. MRI is a non-invasive imaging technique based on an interaction known as nuclear magnetic resonance. The core of this interaction is a linear dependence between the static magnetic flux density (magnetic field –  $B_0$ ) experienced by a nucleus and the resulting angular frequency of rotation  $\omega_0$  of the nuclear spin:

$$\omega_0 = \gamma B_0 \quad (2.1)$$

where  $\gamma$  is the gyromagnetic ratio which is a constant for every nuclear isotope that has a spin. In the current clinical practice MRI is based on proton NMR, for which we have  $\gamma \approx 2.68 \times 10^8 \text{ rads}^{-1}\text{T}^{-1}$  and the angular frequency is referred to as Larmor frequency  $\omega_L$ .

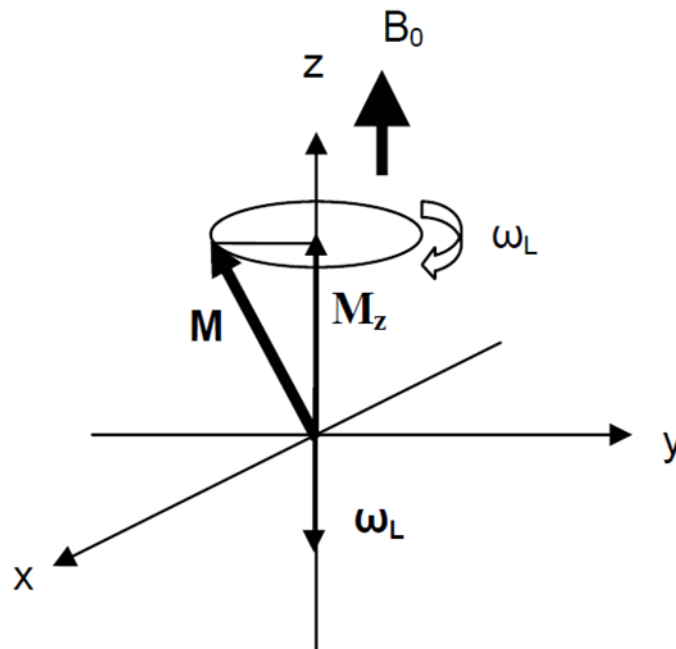


**Figure 2.3:** The magnetic moment  $\vec{M}$  is rotates around  $B_0$  at the Larmor frequency. In equilibrium  $\vec{M}$  coincides with  $\vec{M}_z$ . [14]

The Bloch equation is used to describe the behavior of the macroscopic magnetization vector under the magnetic interactions that were described:

$$\frac{dM}{dt} = \gamma (M \times B) \quad (2.2)$$

where  $B$  is the external magnetic field, and in the presence of two fields  $B = B_0 + B_1$  [15]. In clinical MRI,  $B_1$  has a rotational frequency in the radiofrequency (RF) range, therefore it is called an RF pulse. The angle of rotation induced by this pulse with time of rotation  $t_{rf}$  is given by:

$$\alpha = \gamma B_1 t_{rf} \quad (2.3)$$

The angle can be adjusted to  $90^\circ$  or  $180^\circ$ , for which the RF pulses are named according to the value respectively.

If we observe the induced electrical signal due to the generated  $M_{xy}$  component of the macroscopic magnetization, it will be notable that the signal quickly decays to zero. This is caused by proton relaxation as a repercussion of the proton interactions which lead to exchange and loss of the excitation energy and additionally by the influence of  $B_0$ . The process of relaxation where the protons shift from high-energy states to low-energy states can occur through

spontaneous or stimulated emission. In terms of MRI, we are only interested in stimulated emission and this requires a fluctuating magnetic field with a frequency equal or near to the Larmor frequency. Looking at the magnetization vector it will be possible to detect gradual loss of the  $M_{xy}$  component and increase of the  $M_z$  component until  $M = M_z$  is reached. In reference to the decrease in  $M_{xy}$  and  $M_z$  increase, there are two types of relaxation processes: longitudinal and transverse respectively.

Longitudinal relaxation (also called  $T_1$  or spin-lattice relaxation) (Figure 2.5)

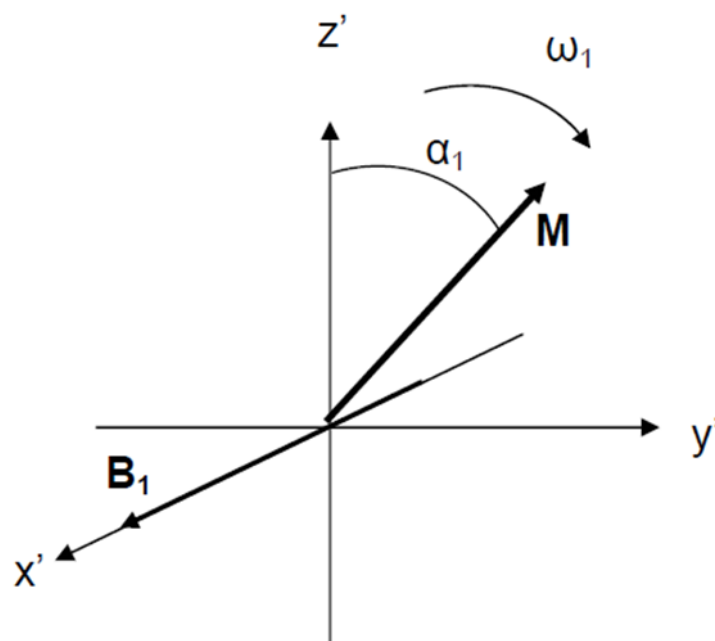


**Figure 2.4:** The RF pulse excites the magnetic moment  $\vec{M}$  at an angle  $\alpha$  which can be adapted to required values [14].

depicts the macroscopic effect of the energy transition that is caused by the stimulated emission from the gradual recovery of the z-component in the magnetization, after the RF pulse. The recovery rate for  $M_z$  is characterized with a time constant  $T_1$  – relaxation time. The relaxation rate  $R_1$  is an inverse of the relaxation time ( $1/T_1$ ). In MRI, pulse sequences that are sensitive to the variations in  $T_1$  are utilized for getting image contrast, as different tissues show variations of several seconds to milliseconds in relaxation times. In the case of longitudinal relaxation these pulse sequences are called  $T_1$ -weighted sequences. Considering  $M_0$  as the initial longitudinal magnetization before the

excitation (at equilibrium), we can quantify this relaxation type with the following:

$$\frac{dM_z}{dt} = \frac{1}{T_1}(M_0 - M_z) \quad [14] \quad (2.4)$$

Transverse relaxation (also called  $T_2$  or spin-spin relaxation) (Figure 2.5) describes the transverse component of the magnetization  $M_{xy}$  after the excitation pulse. Following the same principle explained above,  $T_2$  and  $R_2$  are defined as relaxation time and relaxation rate. Counterintuitively, the transverse component of the magnetization decays at a faster rate compared to the relaxation of the longitudinal component (except in pure water). This is caused by additional relaxation effects which affect the total magnetization in the x-y plane. In vivo,  $T_2$  has higher values for fluids compared to solids, so the changes in  $T_2$  can be valuable when assessing tissue pathology considering that a lot of pathological conditions are related to changes in the tissue water content. This form of relaxation is described with the equation:

$$\frac{dM_{xy}}{dt} = -\frac{1}{T_2}M_{xy} \quad [15] \quad (2.5)$$

Considering (2.4) and (2.5), we can obtain a different form of the Bloch equation (2.2):

$$\frac{dM}{dt} = \gamma M \times B + \frac{1}{T_1}(M_0 - M_z)z - \frac{1}{T_2}M_{xy} \quad (2.6)$$

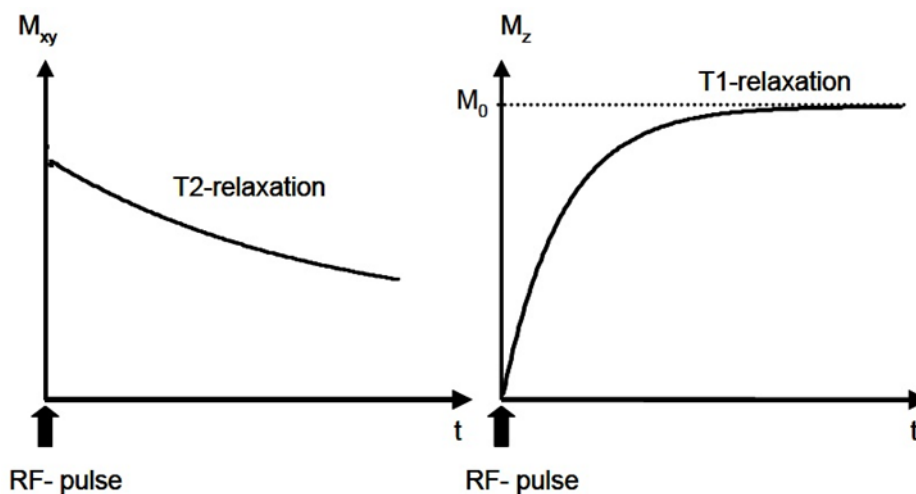


**Figure 2.5:** Transverse and longitudinal relaxation caused by the induced RF pulse

### 2.2.2 Image generation

In clinical MRI there is usually the need to selectively excite a certain part of the body and for such purpose selectivity is achieved with magnetic field gradients. They attain the Larmor frequency as function of the position by producing a spatially varying magnetic field. Figure 2.6 depicts the process of applying a gradient to a slice (5 x 5) in the z- and y-directions and the phase shift that occurs in each of the squares after a certain time [14].

The measured signals are stored as Fourier transform of the object in domain denoted as "k-space". In order to access the stored signals and to obtain an image of the object, the acquired k-space needs to be inverse-Fourier transformed. For the purpose of generating an image with this modality, MRI sequence needs to be performed [16]. It can utilize different gradients and pulses in the process of acquiring the information that are necessary for the user. According to this, there are various combinations that give different sequences depending on the aim of the acquisition. Within the scope of this thesis, we will be looking at acquisition of  $T_2$ -weighted and diffusion-weighted images (DWI).

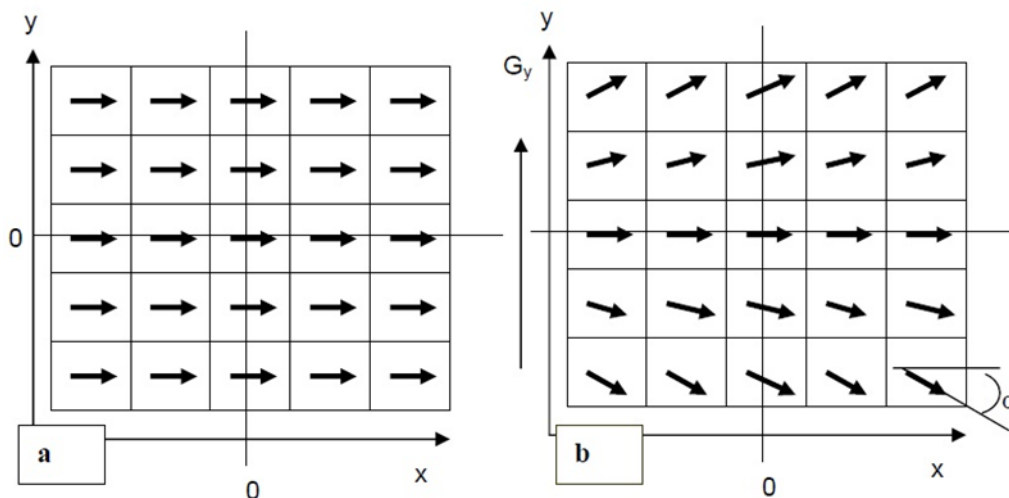


**Figure 2.6:** Transverse magnetization vector phase angles on a slice (5 x 5) a) before applying magnetic field gradient in the y-direction and b) after applying the gradient [14].

### 2.2.3 T<sub>2</sub>-weighted MRI

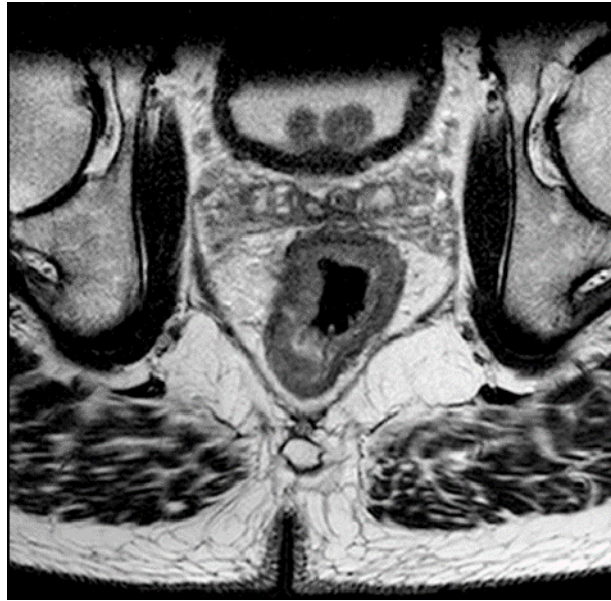


**Figure 2.7:** T<sub>2</sub> – weighted MR image of rectal cancer patient from the OxyTarget study. The fatty tissue has longer relaxation time, so it appears brighter, opposed to the other tissues that contain more water resulting in short T<sub>2</sub> (darker areas).

T<sub>2</sub> – weighted magnetic resonance images are useful for depicting pathological and fluid changes in tissues, which makes them an important asset in visualizing anatomical abnormalities [17]. This type of images is obtained with contrast that depends on the T<sub>2</sub> parameter and the acquisition process usually utilizes a spin echo (SE) sequence (Figure 2.7).

The SE sequence can be explained through the following steps (Figure 2.8-9). First, the longitudinal magnetization is rotated with 90° pulse in the x-y plane, which causes precession under a gradient field where the frequency-encoding (read-out) direction is x and the phase-encoding direction is y. A second pulse of 180° rotates the magnetization around the x- (or y-axis) and the measuring gradient is switched on again. The precession continues in the same direction until the spins meet at the y-axis and form the maximum signal (“echo top”), at  $t = TE$  ( $TE = \text{Echo Time}$ ) [14]. This process samples one line in k-space and in order to acquire more lines, the sequence needs to be repeated with a time interval between the pulses which is called repetition time (TR). The following relation can be used to explain the conditions for obtaining T<sub>2</sub>-weighted image:

$$M_{TE} = M_0 \left( 1 - e^{-\frac{TR}{T_1}} \right) e^{-\frac{TE}{T_2}} \quad [17] \quad (2.7)$$

The different relaxation times among the tissues will generate the contrast in the image, and considering the transverse relaxation rate, we need long TE and long TR in order to obtain images with enough information [16]. This can be explained through the factor  $e^{-\frac{TE}{T_2}}$  that occurs due to  $T_2$  decay during the time delay between the excitation and the echo top. Since the factor is a function of  $T_2$ , it is clear that it causes the weighting of the image.

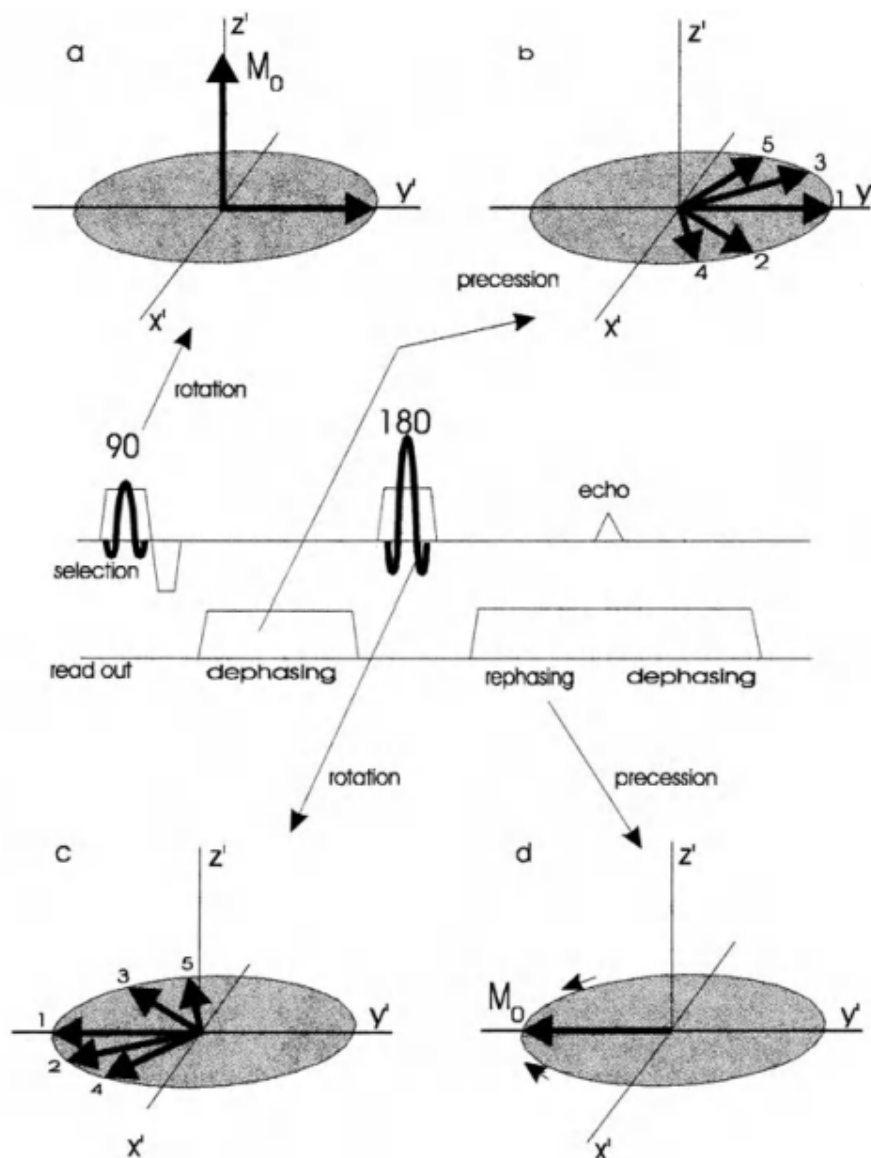


**Figure 2.8:** Steps of the spin-echo sequence a) rotation caused by 90° pulse in x-y plane b) precession, dephasing c) rotation around the x-axis from a 180° pulse d) precession, rephasing [15].



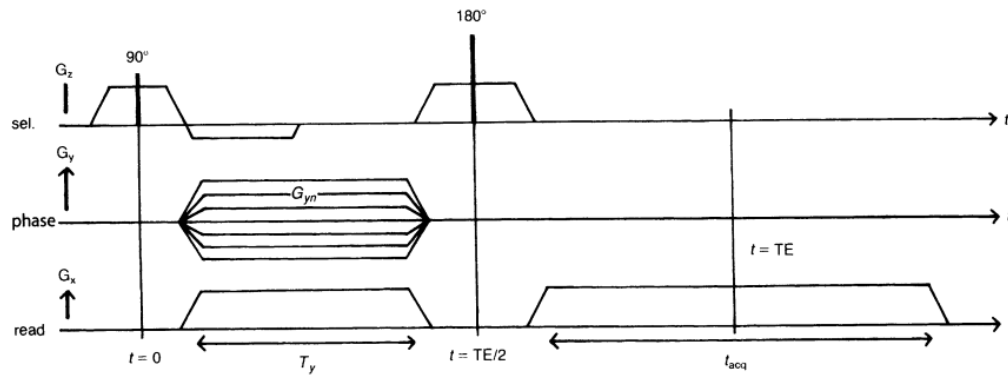


**Figure 2.9:** The spin-echo sequence as function of time following the steps depicted in Figure 2.8 [15].

In cases where  $TE \ll T_2$  the weighting will not be considerable because it will give approximately the same values for all tissues. On the other hand, when we have longer Echo Time (TE) the factor becomes heavily dependent on  $T_2$  and we get more weighting which yields higher contrast.

#### 2.2.4 Diffusion – weighted MRI

Diffusion is a natural process of mass transport that produces molecular and particle mixing without the need of bulk motion. In theory, this phenomenon would result in free molecular motion, but in practice the trajectories of the particles are hindered by restrictions caused from the surrounding particles (Figure 2.10). Diffusion-weighted MRI uses this principle to observe the

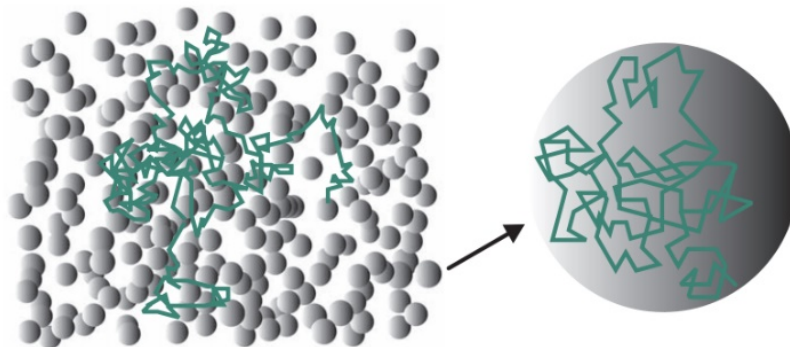


**Figure 2.10:** Trajectory changes in particle movement caused by (a) surrounding cells in the extracellular matrix (b) cell membranes within the cell [19].

movement of water molecules in tissues and their deviations due to influence from cell membranes, cytoskeleton and various other macromolecules [18]. By understanding the different features that contribute to the overall diffusion

process, we can observe complicated tissues by analyzing water molecules and drawing information about biological microstructure from their movement [19].

In order to explain the process of acquiring diffusion-weighted images, we need to briefly look at  $T_2^*$  - weighted MRI. What was previously discussed referred to the  $T_2$  time constant that describes transverse decay of the MR signal within a substance of interest. However, in practice the transverse magnetization decays at a quicker constant compared to the theoretically expected value because of inhomogeneities in the main magnetic field. The “observed” relaxation is represented as  $T_2^*$  and it is always smaller or equal to the “true”



**Figure 2.11:** Diffusion – weighted MR image of rectal cancer patient from the OxyTarget study. The tumor can be detected as a black area resulting from reduced water diffusion, opposed to the surrounding normal tissue which has higher ADC.

$T_2$ . The relation between these two constants is show in:

$$\frac{1}{T_2^*} = \frac{1}{T_2} + \frac{1}{T_2'} \quad (2.8)$$

where  $1/T_2' = \gamma \Delta B_2'$  is relaxation rate from the inhomogeneities ( $\Delta B_2'$ ) in a voxel. Consequently, the process of acquiring  $T_2^*$  - weighted images is slightly different and it usually encompasses the gradient echo sequence, which varies from the spin-echo sequence, because this protocol does not compensate for the field inhomogeneities [17]

DWI uses the principle of attenuating the  $T_2^*$  signal to assess the diffusion of water molecules in a certain region. If a water molecule is able to diffuse (move further around in a sequence), then the initial  $T_2^*$  signal will be more attenuated, and that area will appear dark on the resulting image. Oppositely, when the trajectory of the water molecule is hindered by cell membranes there is less attenuation and these regions appear brighter. (In cases when a region has zero  $T_2^*$  value, it is not possible to observe its diffusion characteristics.) The process of acquiring diffusion information from a ROI starts with obtaining a  $T_2^*$  - weighted image with no attenuation, referred to as the  $b = 0$  image. Then water diffusion is observed in a single direction by applying a strong gradient symmetrically on each side of the  $180^\circ$  pulse used in the gradient sequence. The combination of the area under diffusion gradients, the amplitude and duration of the gradient and the interval between the gradients generates a  $b$ -value, that describes the image. For higher  $b$ -values we have more pronounced diffusion-related signal attenuation. Water molecules which do not diffuse get the phase from the first gradient and after the  $180^\circ$  pulse they flip, but since their location was not changed the effect of the first gradient is reversed. This results in no attenuation of the  $T_2^*$  constant. In contrast, the moving water molecules get the phase from the first gradient and after the pulse, they are exposed to the second gradient since they change their location due to diffusion in the medium. The rephasing results in some loss of the signal depending of the level of movement, which gives higher attenuation of  $T_2^*$ . This process provides a set of images ( $b = 0$  and minimum three diffusion-weighted images for each of the directions) which contain  $T_2^*$  signal attenuation based on water diffusion. The next step utilizes arithmetical combinations of the images for generating  $ADC^1$  maps that do not contain directional information. The  $ADC$  maps are derived from the natural logarithm ( $\ln$ ) of the geometric means of the direction-specific images divided with  $T_2^*$  for  $b = 0$  (Equation 2.10).[20]

---

<sup>1</sup>  $ADC$  – Apparent Diffusion Coefficient

The b-value is mathematically described with the following equation:

$$b = \gamma^2 \delta^2 \left( \Delta - \frac{\delta}{3} \right) \quad (2.9)$$

where  $G$  is the magnitude and  $\delta$  is the width of the two balanced gradients which are symmetrically applied on each side of the  $180^\circ$  pulses.  $\Delta$  is the time between the two gradient pulses. The apparent diffusion coefficient (ADC) is explained through the following formula:

$$\ln \left( \frac{A(b)}{A(b=0)} \right) = -b \text{ADC} \quad [21] \quad (2.10)$$

As it was elaborated previously, ADC is correlated to the measured signal by utilizing  $A(b)$  which is the echo magnitude of the diffusion-weighted signal and  $A(b = 0)$  as the echo magnitude of the non-diffusion-weighted signal [20]. The relation demonstrates that issues which reduce diffusion of water molecules, such as tumors, will produce lower ADC values compared to normal tissues, resulting in clearer image of the region [22, 23].

### 2.3 Machine Learning

The definition of Machine Learning (ML) can be vastly concatenated with different sub-sentences, but the simplest description distinguishes this discipline as a form of Artificial Intelligence (AI) that refers to automated learning from data [24]. It is a complex process of detecting meaningful patterns in various data sets, which has proven to be beneficial when in need of information extraction. Our society uses machine learning in many forms, such as detection of faces with digital cameras, optimization of search results in search engines, voice command recognition etc. Scientific applications are also notable in medicine, astronomy and bioinformatics. The main reason for its applicability, lies in the need for solving tasks which cannot be explicitly programmed in detail because of their complexity. It is based on the principle of learning which we use when acquiring and refining our skills through experience. [25]

A notable difference between AI and ML should be emphasized, because the latter does not attempt to build automated imitation of intelligent behavior and

it only tries to use the strengths and special abilities of machines which are beyond human capabilities in order to complement them. This is the basic reason for developing machine learning programs and using them to detect patterns in enormous databases, which is not possible within the scope of human perception. [26]

The accuracy of the process highly depends on the quality of the data. It is inevitably important that the data should be accurate and meaningful (trusted) so that the produced models are reliable and make sense. If the dataset is not big, the results might be misleading or missing a pattern which would otherwise be detected. Big data is considered a source that has at least one of these four characteristics (Vs):

- Extremely large volume
- Ability to move data at high velocity
- Ever-expanding variety of data sources
- Veracity so that data sources are truthful. [24]

ML differs from traditional statistics for several reasons, but one of the main differences is the "distribution-free" setting, where the computer assumes as little as possible about the nature of the data distribution. A learning algorithm has the task to define the best models which approximate the data-generating process, without any previous information. [27]

Learning is defined as "the acquisition of knowledge or skills through study, experience, or being taught" by the Oxford dictionary [28]. So, in terms of AI we are looking at "teaching" the machine how to solve a task without programming its behavior in every possible variation. This process can occur as supervised or unsupervised according to the nature of interaction between the learner and the environment. We can explain the differences between the two, if we observe a large set of data that needs to be divided in two groups. [24] There are two more types of learning: reinforcement and deep learning, which are out of the scope of this topic, so a detailed explanation will not be provided [26]. We can observe learning as "using experience to gain expertise" where the form of experience creates a distinction between the two methods. For the

supervised learning approach, we would need to “feed” the learner (machine) with training data that helps it create a rule for labeling and dividing the data into two groups. In that case, the experience is provided through the training data. Contrary to this, in unsupervised learning there is no training data and the aim of the learner is to come up with a summary, without being taught through training. A typical example of such approach would be to cluster sets of data into subsets with objects that demonstrate similarity. [24] Essentially, the unsupervised learning attempts to label data, so that it would become supervised. Hence, we can use this approach as a first step, before proceeding with a supervised algorithm [28]. In terms of healthcare, the analysis of big amounts of data for a specific disease can be useful for the purpose of obtaining patterns of symptoms that would be related to outcomes in the patients. This has two main advantages: it takes less time for the machine to observe patterns than in the case of supervised learning and it could avoid guided results without the possibility to oversee certain patterns. [26]

### 2.3.1 K-means clustering

K-means is a type of unsupervised learning algorithm for clustering data. Clustering is a technique which groups objects based on their parameters, without previous labeling (hence the classification is unsupervised) [26]. The data is partitioned into  $k$  clusters, so that each point in a cluster is similar to points from its own cluster rather than with points from other clusters (Figure 2.12). The input for the  $k$ -number that signifies the number of centroids is manual. The algorithm randomly generates the cluster centers and computes all point-to-centroid distances of all observations to each centroid. Every observation is assigned to the cluster with closest centroid. Then, the average of the observations is computed for obtaining  $k$  new centroid locations and the process is repeated until convergence is achieved with the purpose of minimizing total intracluster variance [46].

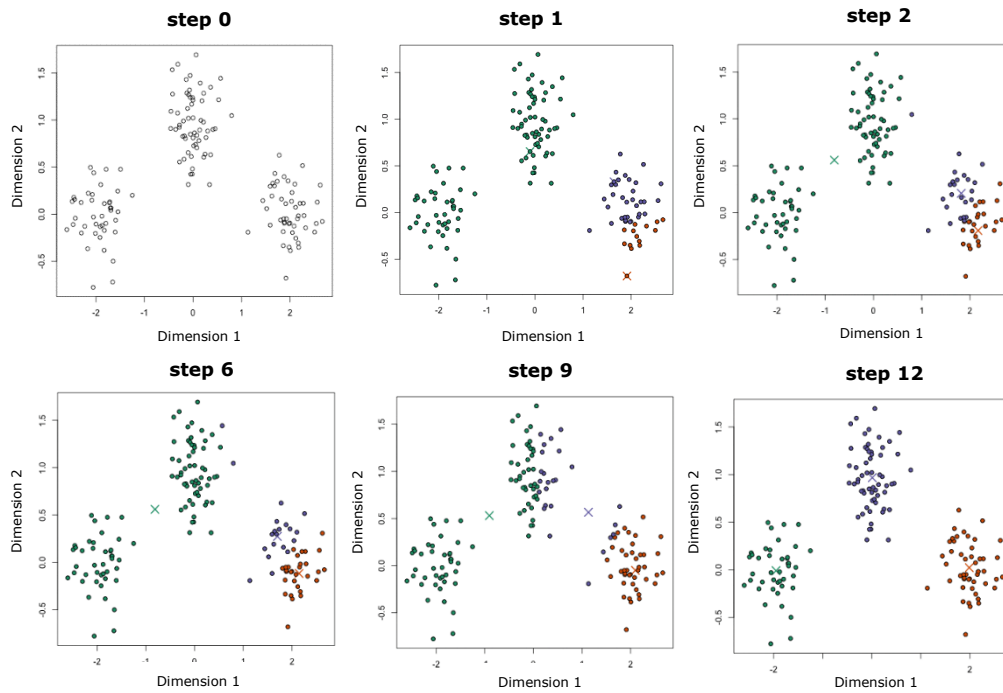


**Figure 2.12** Example steps of the K-means algorithm applied on objects with two parameters (because of space limitation some steps are omitted without compromising clarity): step 0 – the data is unlabeled and no clustering is performed; step 1 – the K value is inputted (in this case  $k=3$ ) and the centroids are randomly dispersed; step 2-12 – every data point is classified by computing the distance between that point and each cluster center. Based on the classified points, the centroids are recomputed from the mean of all vectors in the clusters. The steps are repeated for a set number of iterations until convergence is reached and the group centers do not vary.[51]

The K-means algorithm is easy to understand, fast and relatively efficient for clustering unlabeled data. However, this approach comes with a level of inaccuracy because it requires specification of the  $k$ -number (centroids) and a random selection can produce misleading results (Figure 2.13). Additionally, the Euclidian distance measuring can weigh some underlying factors unequally and it can be problematic with 'noisy' data and in case of outliers<sup>2</sup>. [49] This potentiates the need for optimization in the process of selecting the cluster division which yields best results.

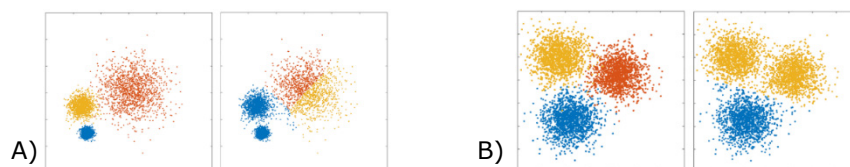


**Figure 2.13** Example situations where the K-means algorithm can underperform: A) expected clustering results (left) and K-means grouping without enough iterations for the system to detect centroids correctly (right). B) expected clustering results (left) and under-partitioning because of inefficient choice of  $k$  value (right). Both can be resolved with enough iterations and optimization of the cluster number, respectively. [48]

<sup>2</sup> An object differing from all other members of a particular group or set [47].

## 3 Materials and Methods

### 3.1 Study population

The patient data used in this thesis comes from the OxyTarget study which is aimed at investigating novel imaging biomarkers for improving CRT response and treatment outcome in rectal cancer [37]. The study included patients that underwent rectal cancer treatment at Akershus University Hospital from 2013 until 2017. The patients agreed to participate in the study by signing a written informed consent according to the protocol approved by the Regional Ethics Committee. All of the 192 enrolled patients were above 18 years old and had not received prior rectal cancer treatment. [38] Seventy-nine patients from this study were chosen because of the adequacy to the scope of the thesis, encompassing various MRI sequences that provide data from a range of intratumoral characteristics important for observing tumor heterogeneity.

#### 3.1.1 Treatment regimens

The patients in the analyzed group (Table 3.1) received surgery only (patients with localized disease) or one of three CRT regimens (patients with LARC). Three patients in the CRT group received radiotherapy without chemotherapy due to health conditions/age:

Xeloda -Fluoropyrimidine carbamate that produces clinically active levels of 5-fluoracil which generate a radiosensitising effect [39].

FLV -5-fluorouracil used to produce a radiosensitising effect [40].



FLOX -Flurouracil-leucovorin-oxaliplatin in combination with folinic acid that generates radiosensitising and neurotoxic effects. It is usually given combined with 5 x 5Gy radiotherapy regimen [45].

The radiotherapy was conducted with one of the two radiation regiments:

5 x 5Gy -5 dose fractions of 5 Gy given in a period of five days, resulting in a total dose of 25 Gy

25 x 2Gy -25 dose fractions of 2 Gy usually given in a period of five weeks, resulting in a total dose of 50 Gy

**Table 3.1:** Information about the study population used in this thesis. The number of patients in each category is calculated in percentage and the age range is given from the youngest to the oldest patient in the group.

Patients	n (%)	Median age (range)
Female	26 (33%)	76 (47-80)
Male	53 (67%)	64 (41-88)
<b>CRT</b>	32 (40%)	60 (41-78)
Female	8 (10%)	61 (49-73)
Male	24 (30%)	60 (41-78)
<b>no CRT</b>	47 (60%)	67 (47-88)
Female	18 (23%)	76 (47-80)
Male	29 (37%)	67 (47-88)
<b>Chemotherapy regime</b>		
FLOX	4 (5 %)	54 (45-64)
Xeloda	22 (28%)	69 (55-83)
FLV	3 (4%)	64 (51-78)
none	3 (4 %)	70 (63-78)
<b>Radiotherapy regime</b>		
2 Gy x 25	26 (33%)	59 (41-78)
5 Gy x 5	6 (7 %)	60 (45-75)

### 3.1.2 Cancer staging

In order to plan an effective treatment, it is vital that the extent of the cancer at the time of diagnosis is precisely defined. It is also important that the evaluation is standardized so that it would allow comparison between patients with the purpose of providing standard care around the world. There are

several staging systems and they are all periodically updated based on the advances in cancer prognosis relevant to the clinical practice. The OxyTarget study uses the TNM" system, which is maintained by the American Joint Committee on Cancer (AJCC) and the International Union for Cancer Control. With this approach, it is possible to stage three parameters: T – the extent of the primary tumor, N – the regional lymph nodes and M – distant metastases. A detailed classification used in TNM is provided in Table 3.3.[41]

After the treatment (in the case of neoadjuvant CRT before surgery) a histopathological investigation on the subsequent resection specimen is performed and the effects of the neoadjuvant therapy are determined. This includes a tumor regression grading (TRG) based on the amount of induced fibrosis related to the residual tumor. There are several most commonly used TRGs and in this study the AJCC system is used. The grading includes four conditions, which are shown in Table 3.2. The TRG system is valuable for rectal cancer treatment because there is evidence that it can be used as an

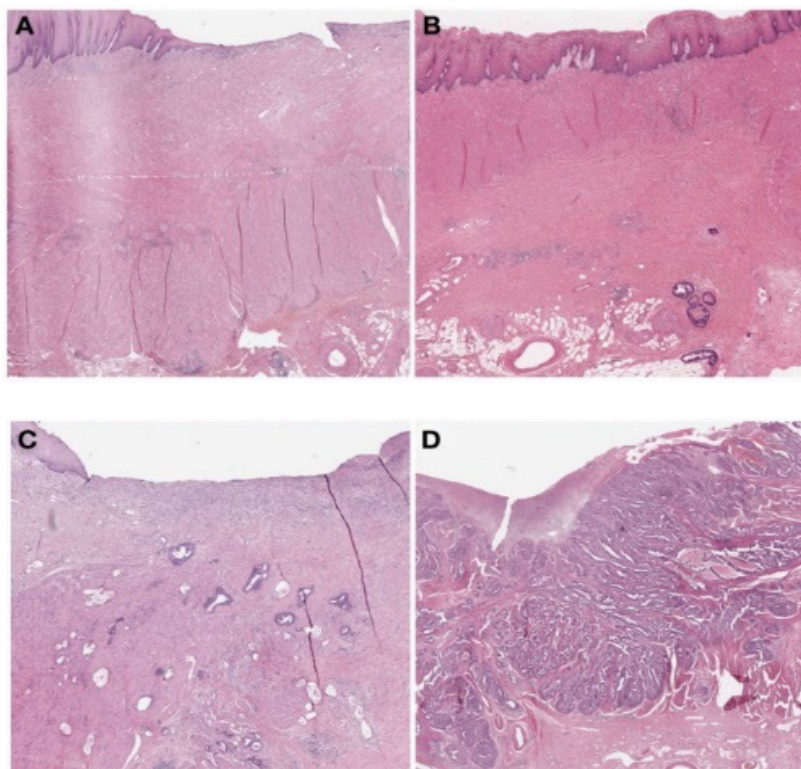


**Figure 3.1:** Examples of tissue with different tumor regression grades according to the TRG staging system: A) Complete regression (TRG0); B) Little residual tumor (TRG1); C) Fibrosis outgrows the residual tumor (TRG2); D) Minimal or no regression (TRG3) [42].

independent predictor for survival. Patients graded as TRG0 have shown improved progression-free survival which generates higher survival rate. [42] The potential for influencing treatment outcome in rectal cancer, makes TRG important for examination in this thesis.

**Table 3.2:** Grading of response to CRT in rectal cancer using the TRG system. The information in the table is extracted from [44].

TRG (Tumor regression grade)	
<b>TRG 0</b>	No viable cancer cells
<b>TRG 1</b>	Single cells or small groups of cancer cells
<b>TRG 2</b>	Residual cancer outgrown by fibrosis
<b>TRG 3</b>	Minimal or no tumor regression. Extensive residual cancer

**Table 3.3:** Different staging in rectal cancer using the TNM system. The information in the table is extracted from [43].

T – Primary tumor		N – Regional lymph nodes		M – Distant metastases	
<b>T0</b>	No evidence of primary tumor	<b>N0</b>	No regional lymph node metastasis	<b>M0</b>	No distant metastasis
<b>T1</b>	Tumor invades submucosa	<b>N1</b>	Metastasis in 1-3 regional lymph nodes	<b>M1</b>	Distant metastasis
<b>T2</b>	Tumor invades muscularis propria	<b>N2</b>	Metastasis in 4 or more regional lymph nodes		
<b>T3</b>	Tumor invades through the muscularis propria into the pericolorectal tissues				
<b>T4</b>	Tumor penetrates to the surface of the visceral peritoneum or directly invades or is adherent to other organs and structures				

Table 3.4 summarizes the general information about the study population included in this thesis. The prefix “mr” indicates that the assessment has been carried out using MRI before the treatment. The prefix “y” indicates that the assessment is completed after the CRT treatment and the prefix “p” refers to the use of pathological examination on a resected specimen.

**Table 3.4:** Tumor characteristics in patients that received neoadjuvant CRT (left) and patients that only underwent surgery (right). The prefixes used in the TNM staging are explained in the text.

CRT	n (%)	no CRT	n (%)
<b>ypTN stage</b>		<b>pTN stage</b>	
ypT0	4 (5%)	pT1	2 (2%)
ypT1	3 (4%)	pT2	15 (19%)
ypT2	3 (4%)	pT3	22 (28%)
ypT3	17 (21%)	pT4	1 (1%)
ypT4	3 (4%)	pN0	24 (30%)
ypN0	18 (23%)	pN1	10 (13%)
ypN1	6 (7%)	pN2	6 (7%)
ypN2	6 (7%)		
<b>mrTNM stage</b>		<b>mrTNM stage</b>	
mrT2	2 (2%)	mrT2	15 (19%)
mrT3	16 (20%)	mrT3	26 (33%)
mrT4	14 (18%)	mrT4	6 (7%)
mrN0	9 (11%)	mrN0	27 (34%)
mrN1	10 (13%)	mrN1	15 (19%)
mrN2	12 (15%)	mrN2	5 (6%)
<b>TRGscore</b>			
TRG0	4 (5%)		
TRG1	7 (9%)		
TRG2	11 (14%)		
TRG3	9 (11%)		

## 3.2 Data analysis methods and software

### 3.2.1 Acquisition of MR images

The MR images of all patients in the study are obtained with Philips Achieva 1.5 Tesla system (Philips Healthcare, Best, The Netherlands) with NOVA Dual HP gradients and a five-channel cardiac coil with parallel imaging capabilities. The T<sub>2</sub>-weighted images of the pelvic cavity and the rectum are obtained in the

sagittal and transversal planes with conventional high-resolution fast spin-echo sequence, where  $TR = 2386-4122$  ms and  $TE = 80$  ms in an acquisition matrix of  $512 \times 512$  (slice thickness 2.5 mm). The DW MR images are acquired with fat-saturated single-shot spin-echo EPI sequence, where  $b = \{0, 25, 50, 100, 500, 1000, 1300\}$  s/mm<sup>2</sup> in a matrix size of  $128 \times 128$  with  $FOV = 160 \times 160$  mm and slice thickness 4 mm. The obtained  $T_2$ -weighted images are used for delineation of the tumors (ROIs) by two radiologists with 7 and 14 years of experience<sup>3</sup>. [45]

### 3.2.2 Image Analysis

The analyses on the images are performed with MATLAB® (MathWorks, Natick, Massachusetts - version R2018a) using the Image Processing Toolbox and the Tools for NIfTI and ANALYZE image toolbox. All the used scripts are included in Appendix A.

The following is in reference to Appendix A.1. The  $T_2$ -weighted images are stored in the DICOM file format (2D), so the first step of the analysis encompasses loading them into the MATLAB workspace, rescaling and sorting into a 3D matrix (x-, y- and z- direction). Sorting is done in the z-direction which is obtained from the DICOM info file. As it was explained in Chapter 3.2.1, ROIs are delineated based on the  $T_2$ -weighted images and stored in a file format called NIfTI (Neuroimaging Informatics Technology Initiative). Therefore, the NIfTI and ANALYZE image toolbox is used to load the ROI which denotes the tumor volume. Further on, after adjusting the ROI (flipping and rotating), it is used to obtain information from the  $T_2$ -weighted images for the tumor region only (via logical indexing). The script in Appendix A.5. extracts the voxel coordinates for the ROI, based on the previous step. A generated table contains the spatial coordinates of the voxels and their corresponding intensity in the pixels from slices. The result is used as a base for all analyses concerning the heterogeneity of the tumor reflected in  $T_2$ -weighted MR images (Appendix A.6).

---

<sup>3</sup> The radiologists are denoted with their initials - "an" and "shh" respectively. In further reading they will be referred to by these abbreviations.

Analogically, a similar procedure is applied on the DW MR images. The initial steps include loading and sorting by the z-direction, which is again obtained

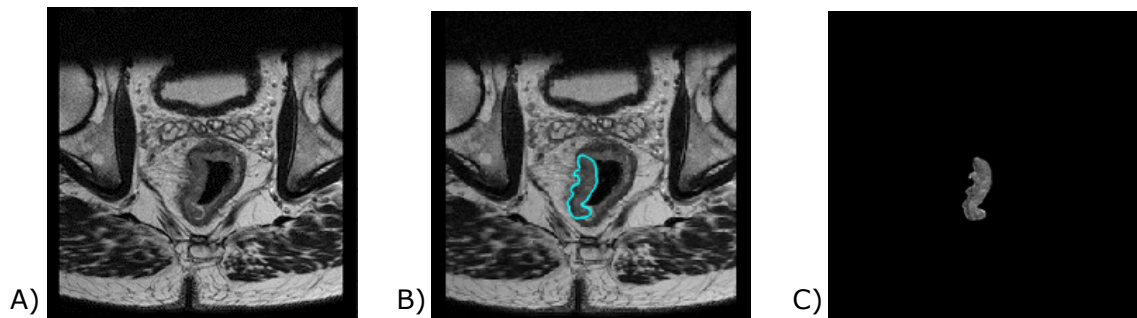


**Figure 3.3:** Quick summary of the image analysis steps (on  $T_2$ -w images): A) load from DICOM files and sort by z-direction. B) Load ROI drawn by a radiologist from a NIfTI file. C) Extract the ROI from the  $T_2$ -w images with logical indexing for further extraction of the voxel coordinates.

Patient_number	X	Y	Z	Intensity
24	96.786	76.351	-17.463	365
24	97.137	76.357	-17.443	365
24	97.488	76.364	-17.423	418
24	97.839	76.37	-17.404	456
24	98.19	76.377	-17.384	433
24	98.541	76.383	-17.364	388
24	98.891	76.39	-17.345	395
24	99.242	76.396	-17.325	448

**Figure 3.2:** Example table with extracted data from the  $T_2$ -w images, depicting the voxel coordinates and the intensity from their corresponding pixels.

from the DICOM info file. However, as it was explained before, the acquisition matrix for the DW images is  $128 \times 128$ , which is different from the acquisition matrix for the  $T_2$ -weighted images  $512 \times 512$ . Therefore, the DWI need to be interpolated to the  $T_2$ -w images in order to be able to apply the ROI from the NIfTI file and extract the tumor information. In continuity, the same steps are applied, until we get another table with voxel coordinates and additional parameters (provided: ADC maps,  $D$ ,  $D^*$  and  $f$ ) which is used for analyzing the tumor heterogeneity on the DW-MR images.

### 3.2.3 Statistical analysis

#### 3.2.3.1 K-means clustering

In continuity of what was discussed previously in Chapter 2.3.1, the K-means unsupervised learning algorithm was used for clustering the data from the obtained tables. In Appendix A.7 the script uses the built-in MATLAB® function 'kmeans' from the Statistics toolbox. The input for the k-number that signifies the number of centroids is manual and values of 2 to 6 are observed. The purpose of this algorithm can be explained mathematically, if we denote the data from the fourth column in Figure 3.3 (Intensity) as  $I = \{125; 456; \dots; I_n\}$ , where each of the  $n$  data points is a dimensional vector defined by the coordinates (columns 1-3). The cluster assignment is associated to each data point and when a data point  $I_i$  belongs to cluster  $k$  it is noted as  $z_i = k$ . The number of observations assigned to a cluster  $k$  is  $N_k$  for  $k \in \{1; \dots; K\}$  and the following objective function is used to find the minimum:

$$E = \frac{1}{2} \sum_{k=1}^K \sum_{i:z_i=k} \|I_i - \mu_k\|_2^2 \quad (3.1)$$

where  $\mu$  are the cluster centroids and  $\frac{1}{2} \|I_i - \mu_k\|_2^2$  is the Euclidian distance measured as the sum of the square of differences of coordinates in each direction. The value of  $E$  cannot increase with each subsequent iteration and eventually it stops changing (therefore a high number of 30 iterations is used in the function) [48].

Appendix A.7 shows the script used to optimize the k-value for each dataset. The mean intra-cluster distance and the minimum inter-cluster distance are used to generate a graph, which indicates the ideal cluster division. This is done by specifying how these two parameters change with  $k$  and by applying functions that generate over-partitioning ( $v_o$ ) and under-partitioning ( $v_u$ ) vectors respectively. Using the notation from before, for the cluster centroids we have a vector containing the centers  $\mu = [\mu_1, \mu_2, \dots, \mu_K]^T$  and an under-partitioning function given by:

$$v_u(K, \mu; I) = \frac{\sum_{k=1}^K MD_k}{K} = \frac{\sum_{k=1}^K \sum_{I_i \in C_k} \frac{\|I_i - \mu_k\|}{N_k}}{K} \quad (3.2)$$

where  $MD_k$  is the mean intra-cluster distance (MICD) for the  $k^{\text{th}}$  cluster. MICD helps define the under-partitioned states because it has high value when at least one of the clusters is under-partitioned, and it shows incident decrease in cases of over-partitioning. The inter-cluster minimum distance (ICMD) can be defined as:

$$d_{min} = \min_{i \neq j} \|\mu_i - \mu_j\| \quad (3.3)$$

When ICMD has a high value, the data can be under-partitioned or optimally partitioned, but in conditions where the inter-cluster minimum distance is very small it indicates that the data is over-partitioned (at least one of the clusters is subdivided). Considering Equation (3.3) we can obtain the over-partitioning function:

$$v_o(K, \mu) = \frac{K}{d_{min}} = \frac{K}{\min_{i \neq j} \|\mu_i - \mu_j\|} \quad (3.4)$$

A parameter called 'validity index' ( $K^*$ ) is used to define the behavior of the two vectors and determine the optimal number of clusters. Equations (3.2) and (3.4) have low values for  $K = K^*$ , so this property is used to obtain  $K^*$ . The script in Appendix A.7 generates matrices containing the values of the two vectors:

$$v_o = [v_o(K_{min}, \mu), \dots, v_o(K_{max}, \mu)] \quad (3.5)$$

$$v_u = [v_u(K_{min}, \mu; I), \dots, v_u(K_{max}, \mu; I)] \quad (3.6)$$

considering that in our case  $K_{min} = 2$  and  $K_{max} = 6$ . These are then normalized to the range [0,1] based on their minimum and maximum values with the following functions:

$$v_u^*(K, \mu; I) = \frac{v_u(K, \mu; I)}{\max_{K=2, \dots, 6} \{v_u(K, \mu; I)\} - \min_{K=2, \dots, 6} \{v_u(K, \mu; I)\}} \quad (3.7)$$

$$v_o^*(K, \mu) = \frac{v_o(K, \mu)}{\max_{K=2, \dots, 6} \{v_o(K, \mu)\} - \min_{K=2, \dots, 6} \{v_o(K, \mu)\}} \quad (3.8)$$



The sum of the Equations (3.7) and (3.8) provides the validity index vector  $v_{sv}$ :

$$v_{sv}(K, \mu; I) = v_o^*(K, \mu) + v_u^*(K, \mu; I) \quad (3.9)$$

where the smallest value is extracted and  $K^*$  is obtained, which gives the optimal number of clusters for the data. [50]

### 3.2.3.2 Cluster division

The next step of the method uses the script from Appendix A.8. The number of voxels assigned to each cluster is counted and the cluster volume fractions (CVF) are calculated for each cluster in every patient:

$$CVF_1 = \frac{\text{Voxels in cluster 1}}{\text{Total number of voxels}} \quad (3.10)$$

Then, the median values of all CVFs are obtained with the purpose of dividing every cluster into high and low values above and below the median, respectively. The division of the clusters from every patient is inputted into a new matrix that contains two groups of voxels above and below median. The two groups are then used in both the statistical and survival analyses for observing if they are associated to the treatment outcomes.

### 3.2.3.3 Parameter correlation

The next step aims to investigate correlation between the parameters from the summarization in Table 3.4 and the two groups from each cluster. The obtained dataset of parameters that define the staging of the tumor is measured on a scale, which indicates that the data is continuous and two types of tests (parametric and non-parametric) can be used to evaluate the correlation. In order to find out which test would be better suited the distribution of the data needs to be probed with the Shapiro-Wilk (1965) normality test.

This test is chosen because of its good power properties [62]. The original test from 1965 for an ordered random sample where we have  $y_1 < y_2 < \dots < y_n$ , is given with:

$$W = \frac{(\sum_{i=1}^n a_i y_i)^2}{\sum_{i=1}^n (y_i - \bar{y}_i)^2} \quad (3.11)$$

where  $y_i$  is the  $i^{\text{th}}$  order statistic,  $\bar{y}$  is the sample mean and  $a$  is defined by  $m$  which are the expected values of the order statistics. This form is limited to a sample size smaller than 50, so it has been continuously improved. The calculations in this thesis are based on the improved algorithm AS R94 which gives calculation power of  $3 \leq n \leq 5000$  [63] The test results are in Appendix E.

In case of normal data distribution, a t-test is utilized. This is a parametric method which can be used when the samples satisfy the conditions of normality, equal variance and independence. There are two types of t-tests: independent (when the compared groups are independent of each other) and paired (when the two groups are dependent on each other). Considering that the parameters and the cluster groups are unpaired, in case of normal distribution, the optimal choice is «two independent samples t-test». This approach is suitable for the purpose of comparing a group treated with A and B components. Independent t test can provide intergroup comparison of postA and postB or preA and postA (Table 3.5).[64]

**Table 3.5:** Example table indicating the potential of “Independent samples t-test” (patient: patient number; preA/B: parameter measured before treatment, postA/B: parameter measured after treatment).

Treatment A			Treatment B		
patient	preA	postA	patient	preB	postB
1	2	1	2	3	0
3	3	0	4	2	3
4	2	0	13	1	2
11	1	3	14	3	2
13	3	2	22	2	1
14	2	2	34	3	0

If the data is not normally distributed a non-parametric test would yield more precise conclusions. In this case the Wilcoxon rank-sum test was chosen as it has some advantages over other methods, because it is more robust and will not detect significance based on outliers. Even if the data is normally distributed the Wilcoxon rank-sum is only 5% less efficient than the unpaired sample t-test (for large samples like our data).[65]

The tests are conducted with two softwares: R console (version 3.5.3) and MedCalc® (version 14.8.1). Appendix A.12 shows the creation of tab delimited

text tables with the divided clusters based on the median, below (value "1") and above (value "2") and the corresponding parameters that grade the tumor. The .txt files are used by the script for the R console calculations (shown in Appendix B). For the control the data is rearranged into two columns containing the parameters corresponding to each group and inputted into the MedCalc® software.

### 3.2.4 Survival analysis

The survival analyses are performed with the software R (version 3.5.3) with the Survival package for computing and the Survminer package for visualizing the results. They are based on the survival data, which is obtained from the observed endpoints in the OxyTarget study. According to the NCI Dictionary of Cancer Terms an endpoint is referring to the outcome which can be measured objectively to determine if an intervention being studied is beneficial [52]. This indicates that the term does not always refer to death or survival, but it can evaluate various parameters according to the objective of the study. The patient data analyzed in this thesis has observed three endpoints for the purpose of determining progression free survival (PFS), which shows that the tumor has no signs of progression. They are: local recurrence (reappearance of the tumor near the place of the primary tumor), metastasis (metastasis to distant sites as described in Chapter 2.1.1) and death. The data from the study contains information about the date of occurrence for the three parameters and in cases where none of the endpoints were reached, the field is left empty (NaN). PFS shows the time interval between the inclusion in the study (at diagnosis) to reaching any of the endpoints. The information contained in the distributed Excel file, is translated into a binary code which registers "an event" if at least one of the endpoints has occurred. Then for all events the PFS is calculated for the outcome which has been reached first (in cases where more than one endpoint is included). Table 3.7 displays a mock-up of PFS calculation for the survival analyses.

Table 3.6 and Table 3.7 show that the analyzed cohort contains patients that have not reached an outcome in the follow-up time, which means that we do not know their true time to event (if it occurred). The lack of event in the

observed time frame, is called 'censoring' and it refers to the incomplete data. After the last time point at which the patient did not experience any of the outcomes, the information becomes censored. [53] Additionally, the PFS data is not normally distributed and it shows skewedness with many early events and relatively few late ones, which emphasizes the need of an adequate method for survival analyses [54].

**Table 3.6:** Example of data preparation for the statistical analyses, showing than an event is registered if a date input exists for any of the three endpoints, and PFS is calculated according to the first occurring event.

Date of inclusion	Date of local recurrence	Date of metastasis	Death		Event		PFS[days]
04-11-14	10-02-16	15-11-16	NaN	→	1	→	455
20-01-15	NaN	02-05-17	NaN	→	1	→	833
27-01-15	NaN	NaN	NaN	→	0		NaN

**Table 3.7:** Number of patients which have reached one of the three endpoints. For 45 patients an event is not registered within the time frame of the study, so they need to be censored.

Patients	n (%)	PFS median (range) [days]
<b>Events</b>	34 (43%)	
Local recurrence	2 (2%)	547 (183-911)
Metastasis	18 (23%)	453 (2-904)
Death	14 (18%)	747 (40-1454)
<b>Non-events (censored)</b>	45 (57%)	

The most commonly used approach for analyzing survival time in medical research is the Cox proportional hazards model [55]. It is a multivariate survival analysis regression model that uses the hazard function and relates it to a set of covariates (risk factors). A hazard is defined as the probability of occurrence of an individual observed event within a time frame centered around that event [56]. In terms of this topic, the hazard is described with value "1" in the "event" tab from Table 3.4. The Cox model can be expressed mathematically with the relation:

$$h(t) = h_0(t) e^{\{b_1x_1 + b_2x_2 + \dots + b_px_p\}} \quad (3.12)$$

where  $(x_1, \dots, x_k)$  are a set of covariates, whose impact is measured by the coefficients  $(b_1, \dots, b_p)$ .  $h_0(t)$  is the baseline hazard at time  $t$ , representing the hazard for a person with the value NaN for all predictor variables [53]. The

baseline hazard function is estimated non-parametrically, which means that the survival times are not assumed to follow a particular statistical distribution. If we divide both sides of Equation (3.11) and take natural logarithm (ln), we obtain the hazard ratio:

$$HR = \ln\left(\frac{h(t)}{h_0(t)}\right) = b_1x_1 + b_2x_2 + \dots + b_px_p \quad (3.13)$$

This shows that the Cox model basically is a multiple linear regression of the logarithm of the hazard on variables  $x_i$ , where  $h_0(t)$  could be referred to as the "intercept" term which varies with time. For two groups of patients  $k$  and  $k'$  that have different covariates, their hazard functions (3.11) would be written as:

$$h_k(t) = h_0(t) e^{\{b_1x_1 + b_2x_2 + \dots + b_px_p\}} \quad (3.14)$$

$$h_{k'}(t) = h_0(t) e^{\{b_1x'_1 + b_2x'_2 + \dots + b_px'_p\}} \quad (3.15)$$

which yields a hazard ratio for the two groups:

$$\frac{h_k(t)}{h_{k'}(t)} = \frac{e^{\{b_1x_1 + b_2x_2 + \dots + b_px_p\}}}{e^{\{b_1x'_1 + b_2x'_2 + \dots + b_px'_p\}}} \quad (3.16)$$

From here, we can define the main assumption of this model, that the hazard of the event in any group is a constant multiple of the hazard in any other group and it does not depend on time. This explains why it is named "proportional hazards" and it shows that the curves of the groups are expected to be proportional and should not cross. [57]

Appendix B.1 contains the script used in R, for computing the Cox regression. Based on Equation (3.11) the computer calculates the regression coefficients ( $b_1, \dots, b_p$ ) and displays the hazard ratio  $\exp(b_i)$  for the second group relative to the first group in column "coef". Therefore, an example coefficient of -0.5129 would indicate that the second group of patients have lower risk of death (lower survival rates) than the first group. In case of a positive sign, the result would direct to higher risk of death which yields worse prognosis for the subjects of the second group. The results include "exp(coef)" which are the exponentiated coefficients that are also called 'hazard ratios' showing the size of effect from the covariate. Hence, in the example this means that the second group reduces

the hazard by a factor of 0.5988. An additional column displays the Wald statistic value calculated as ratio of the coefficient and its standard error:

$$z = \frac{\text{coef}}{\text{se}(\text{coef})} \quad (3.17)$$

This is the base for the Wald statistic test (also known as Wald Chi-squared test) which generates the p-value used as an indicator for assessing whether the difference between the two groups has statistical significance. A p-value defines the probability of finding an observed result when the null hypothesis is true [58]. In the case of comparing two groups of patients, we use this parameter to evaluate if the absolute value of the sample mean difference between the compared groups is greater or equal to the observed results [59].

The survival package in R, uses two alternative tests for calculating the overall significance of the model (p-value) besides the Wald statistical test: Likelihood-ratio test and Log-rank statistics. For the sake of brevity, these tests will not be explained in detail. The three methods are asymptotically equivalent and for large data they give similar results, opposite to cases with smaller datasets where they can show some variation. [60] The likelihood-ratio test has been denoted as behaving better for smaller sample sizes, so it is generally preferred [59]. However, as it was previously stated in the Chapter 2.3, the unsupervised learning technique which we use requires extremely large volumes of data, and in this study the dataset is sufficiently big, so no variations are expected to be observed. The results where  $p < 0.05$  are considered significant, otherwise the conclusion is that there is no important correlation [58].

The results from the model are visualized with Kaplan-Meier plots that show the survivals of the two groups of patients (script for R console in AppendixB.1). The Kaplan-Meier plot is plotted between the estimated survival probability (on the y-axis) and the time past after the inclusion into the study (on x-axis). The result is horizontal and vertical lines that generate a stepping function for each group (Figure 3.4) [61]. Note that it is incorrect to join the calculated points by sloping lines [57]. As the Cox proportional hazard model maintains the proportionality between the groups, we can observe three possible relations between the plotted functions. If there is a vertical gap between the lines, this

means that at a specific time point one of the groups had a smaller fraction of surviving patients. Analogously, a horizontal gap would indicate that one group

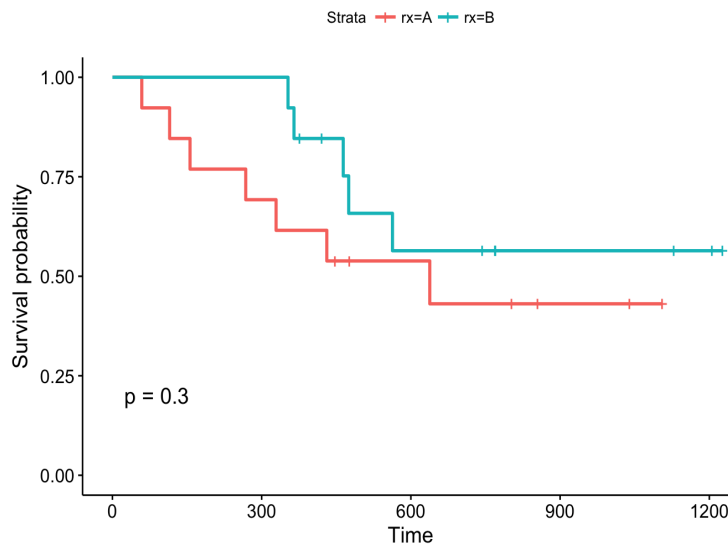


**Figure 3.4:** Example of a Kaplan-Meier plot from the results of the Cox proportional hazards model comparing two patient groups. The stepping functions are plotted against the survival probability (y-axis) and the time after inclusion in the study (x-axis) (censored patients are denoted with '|'). The plot is taken from [61].

took longer time to experience a fraction of deaths. If there is no difference in the outcome between the two groups, then the lines would overlap. [61] Moreover, the censored patients are marked with '|'-sign on the graph.

## 4 Results

This chapter presents the results from the statistical and survival analyses. Figure 4.1 displays sorted T<sub>2</sub>-weighted images for one of the patients, with delineations of the tumor by the two radiologists («an» and «shh»). In this example the ROI is selected on a total of 24 slices, with varying difference in the detection. In some of the slides only one of the radiologists delineated presence of a tumor.

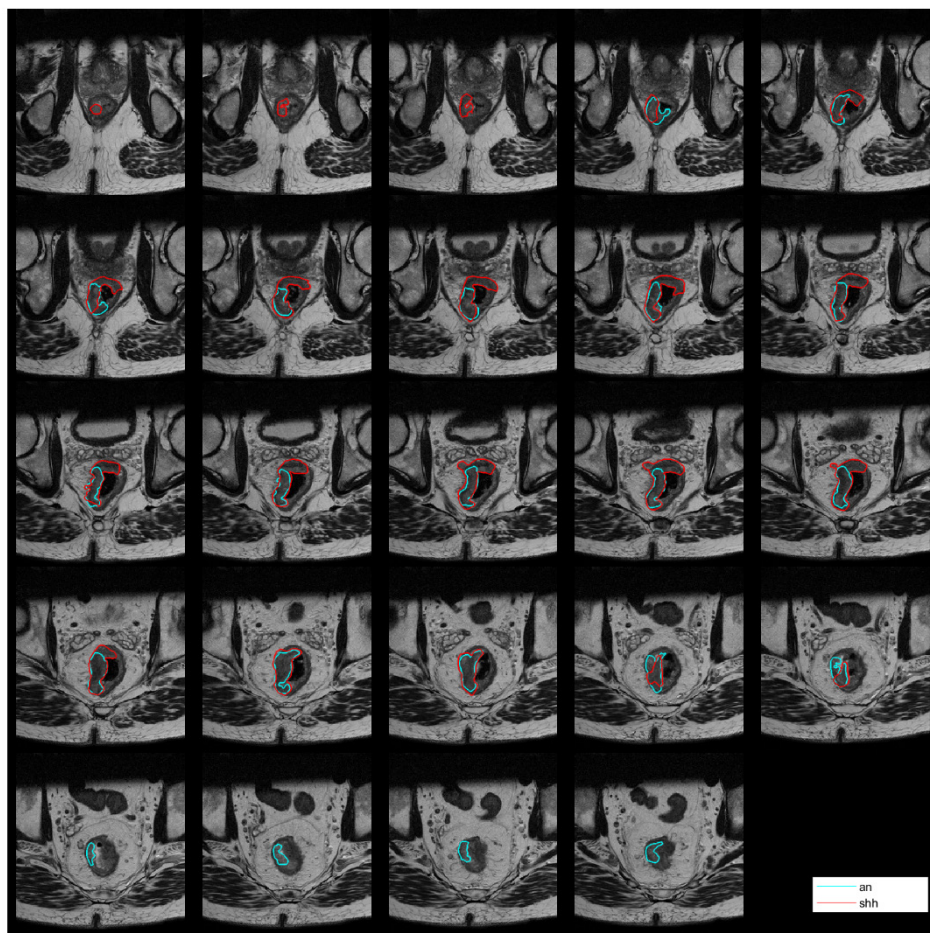


**Figure 4.1:** Sorted T<sub>2</sub>-weighted images with superimposed delineations of the ROI by the two radiologists (“an” and “shh”), presented as two contours in cyan and red color respectively.



The visual inspection of the slices from the other patients showed that there is a noticeable difference in the delineations among all cases. The difference in the selected pixels, corresponds to different voxel coordinates in the tables, which ultimately leads to different clustering results. The analyses were performed on the ROIs from the radiologist «an», but for some cases which showed statistical significance, the delineations from the radiologist «shh» were probed too.

## 4.1 Statistical analyses

### 4.1.1 T2-weighted images

#### 4.1.1.1 Radiologist -an

The obtained patient data with the voxel coordinates and the intensities of the corresponding pixels in the T<sub>2</sub>-weighted images were used to perform the k-means clustering with the script from Appendix A.7. For the ROI from the radiologist “an” the optimal cluster number has been attained at k=4 ( $v_{sv} = 0.63$ ) and the analyses have been conducted according to this grouping factor (Figure 4.3). The resulting clustered data with the corresponding cluster centers is shown in Table 4.1 and Figure 4.2. The results indicate statistical significance ( $p < 0.05$ ) for Cluster 2 in relation to the parameters “p/ypT” and “ΔT” and Cluster 3 related to “p/ypT”.

**Table 4.1:** Table displaying the values of the cluster centers and the median volume fractions for each cluster in data from T<sub>2</sub>-weighted images (radiologist – an).

Cluster number	Intensity (cluster center)	Median volume fraction (CVF)
1	448	29.9%
2	640	44.4%
3	849	19.5%
4	1344	6.2%

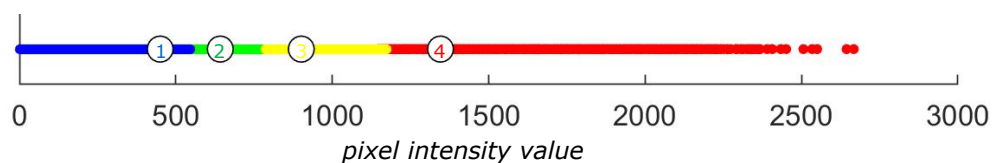


**Figure 4.2:** Tumor cluster affiliation based on K-means clustering of the intensity parameter for k=4 from the T<sub>2</sub>-weighted images (radiologist – an). Clustering is based on all patient’s voxels. The cluster centers are marked by the corresponding cluster number.

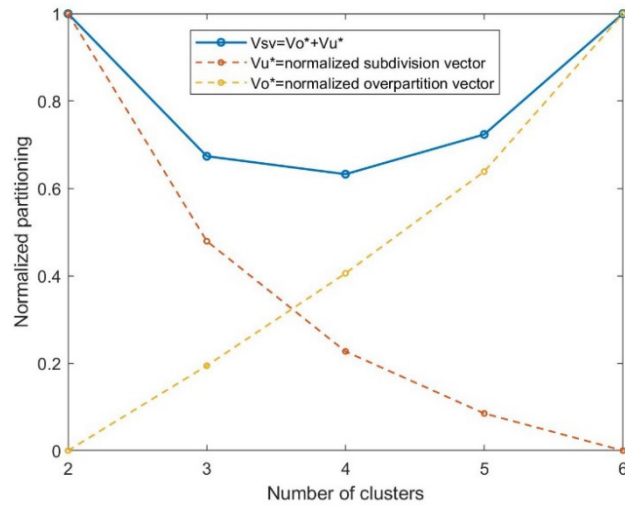


**Figure 4.3:** Plot of the normalized values of the over-partitioned and under-partitioned vectors with the validity index vector ( $v_{sv}$ ). The minimal value of  $v_{sv}$  defines the optimal number of clusters.  $v_u(K_{max}, \mu; I) = 0$  (normalized), because the clustering is done for  $K_{max} = 6$  clusters. ( $T_2$ -weighted images (radiologist – an))

**Table 4.2:** P-values from the Wilcoxon rank-sum test on the two groups (above and below median) for each of the specified parameters that investigate statistical significance in the difference between the two groups. ( $T_2$ -weighted images (radiologist – an))

$T_2$ (an)	mrT	p/ypT	$\Delta T$	mrN	p/ypN	$\Delta N$	TRG
Cluster 1	0.8678	0.1460	0.1805	0.4947	0.6035	0.9842	0.1902
Cluster 2	0.1804	<b>0.0235</b>	<b>0.0429</b>	0.7821	0.2576	0.6168	0.8906
Cluster 3	0.7429	<b>0.0475</b>	0.2000	1.0000	0.1653	0.8897	0.9190
Cluster 4	0.3237	0.7932	0.1639	0.4148	0.8767	0.3662	0.3226

4.1.1.2 Radiologist – shh

**Table 4.3:** Table displaying the values of the cluster centers and the median volume fractions for each cluster in data from  $T_2$ -weighted images (radiologist – shh).

Cluster number	Intensity (cluster center)	Median volume fraction (CVF)
1	446	24.0%
2	624	50.0%
3	837	17.8%
4	1212	3.1%

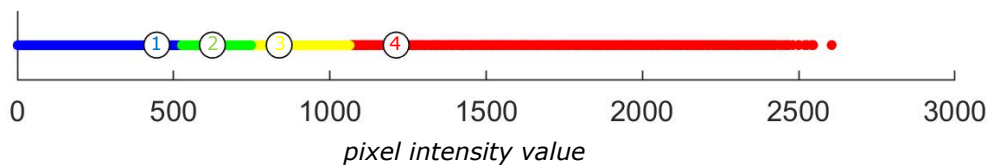


**Figure 4.4:** Tumor cluster affiliation based on K-means clustering of the intensity parameter for  $k=4$  from the  $T_2$ -weighted images (radiologist – shh). Clustering is based on all patient’s voxels. The cluster centers are marked by the corresponding cluster number.

For the ROI from the radiologist “shh” the optimal cluster number has been attained at  $k=4$  ( $v_{sv} = 0.67$ )(Figure 4.5). The resulting clustered data with the corresponding cluster centers are shown in Table 4.3 and Figure 4.4. The results indicate statistical significance ( $p<0.05$ ) for Cluster 1 and Cluster 2 in relation to the parameters “p/ypT” and “TRG” and Cluster 1 for “ $\Delta T$ ” and “p/ypN”.

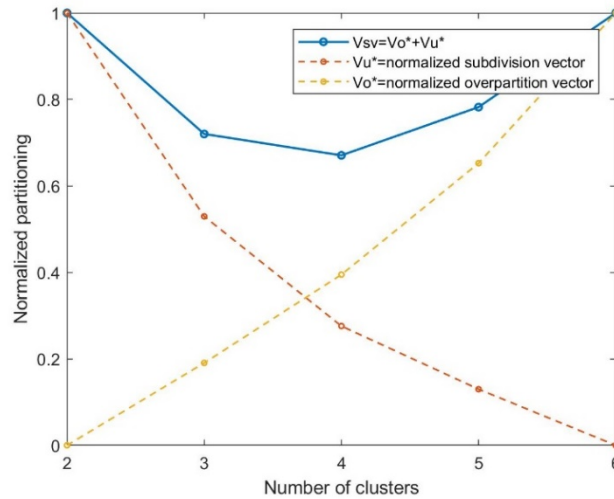


**Figure 4.5:** Plot of the normalized values of the over-partitioned and under-partitioned vectors with the validity index vector ( $v_{sv}$ ). The minimal value of  $v_{sv}$  defines the optimal number of clusters for the  $T_2$ -weighted images (radiologist – shh)

**Table 4.4:** P-values from the Wilcoxon rank-sum test on the two groups (above and below median) for each of the specified parameters that investigate statistical significance in the difference between the two groups. ( $T_2$ -weighted images (radiologist – shh))

$T_2$ (shh)	mrT	p/ypT	$\Delta T$	mrN	p/ypN	$\Delta N$	TRG
Cluster 1	0.7259	<b>0.0220</b>	<b>0.0387</b>	0.6372	<b>0.0301</b>	0.9690	<b>0.0027</b>
Cluster 2	0.8646	<b>0.0492</b>	0.2895	0.8646	0.0685	0.5000	<b>0.0553</b>
Cluster 3	0.4197	0.3334	0.4214	0.7937	0.0614	0.7311	0.7311
Cluster 4	0.6494	0.7026	0.3198	0.6283	0.1105	0.8054	0.8054

### 4.1.2 Diffusion-weighted images

#### 4.1.2.1 $b=0$ s/mm<sup>2</sup>

The same script as in Chapter 4.1.1 is applied to the diffusion-weighted images and the procedure is repeated. For the images with  $b=0$  s/mm<sup>2</sup> the optimal cluster number is defined at  $k=4$  ( $v_{sv} = 0.58$ ) (Figure 4.6), with the cluster centers and median volume fractions displayed in Table 4.5 and Figure 4.7.

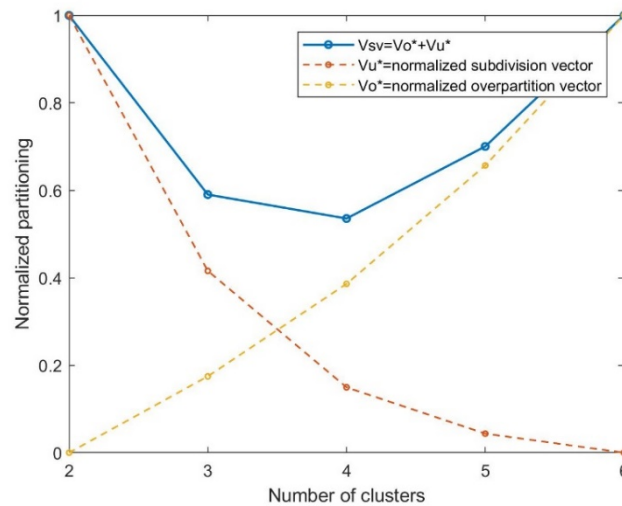


**Figure 4.6:** Plot of the normalized values of the over-partitioned and under-partitioned vectors with the validity index vector ( $v_{sv}$ ). The minimal value of  $v_{sv}$  defines the optimal number of clusters for the diffusion-weighted images with  $b=0$  s/mm<sup>2</sup>.

**Table 4.5:** Table displaying the values of the cluster centers and the median volume fractions for each cluster in data from diffusion-weighted images with  $b$ -value of 0 s/mm<sup>2</sup>.

Cluster number	Intensity (cluster center)	Median volume fraction (CVF)
1	401	16.8%
2	687	36.1%
3	989	24.9%
4	1453	4.1%

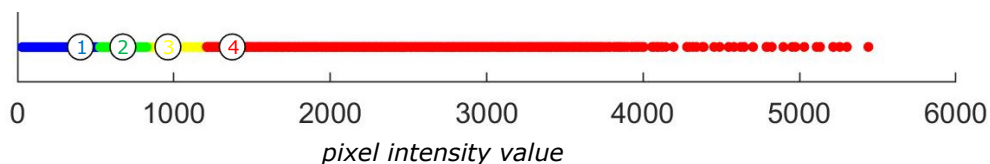


**Figure 4.7:** Tumor cluster affiliation based on K-means clustering of the intensity parameter for  $k=4$  from the diffusion-weighted images. Clustering is based on all patient's voxels. The cluster centers are marked by the corresponding cluster number.

There is no significant difference between the two groups in the clustered data for the DW images with  $b=0$  s/mm<sup>2</sup> (Table 4.6).

**Table 4.6:** P-values from the Wilcoxon rank-sum test on the two groups (above and below median) for each of the specified parameters that investigate statistical significance in the difference between the two groups (DWI;  $b=0$  s/mm<sup>2</sup>).

$b=0$ [s/mm <sup>2</sup> ]	mrT	p/ypT	$\Delta T$	mrN	p/ypN	$\Delta N$	TRG
Cluster 1	0,0972	0,6569	0,6555	0,2116	0,2336	0,9338	0,4804
Cluster 2	0,1298	0,3211	0,1981	0,3490	0,1362	0,9313	0,5866
Cluster 3	0,5104	0,0992	0,5235	0,8902	0,2360	0,3281	0,4078
Cluster 4	0,3237	0,3383	0,2448	0,4894	0,8517	0,5631	0,8252

#### 4.1.2.2 $b=25$ s/mm<sup>2</sup>

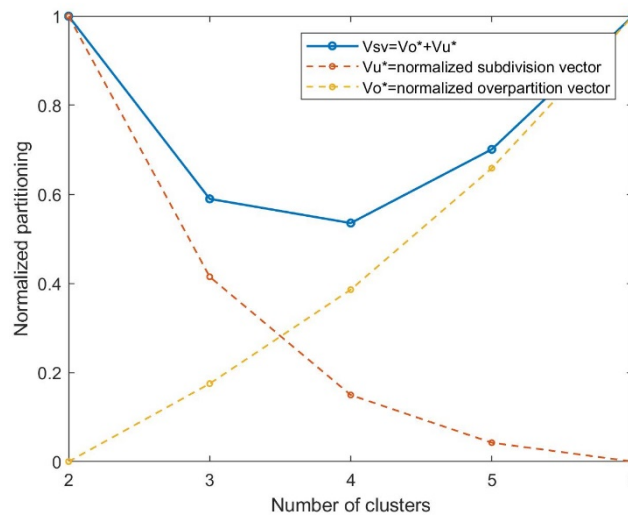


**Figure 4.8:** Plot of the normalized values of the over-partitioned and under-partitioned vectors with the validity index vector ( $v_{sv}$ ). The minimal value of  $v_{sv}$  defines the optimal number of clusters for the diffusion-weighted images with  $b=25$  s/mm<sup>2</sup>.

**Table 4.7:** Table displaying the values of the cluster centers and the median volume fractions for each cluster in data from diffusion-weighted images with  $b$ -value of 25 s/mm<sup>2</sup>.

Cluster number	Intensity (cluster center)	Median volume fraction (CVF)
1	421	16.7%
2	684	35.9%
3	970	24.9%
4	1381	4.2%

There is no significant difference between the two groups in the clustered data for the DW images with  $b=25$  s/mm<sup>2</sup> (Table 4.8).

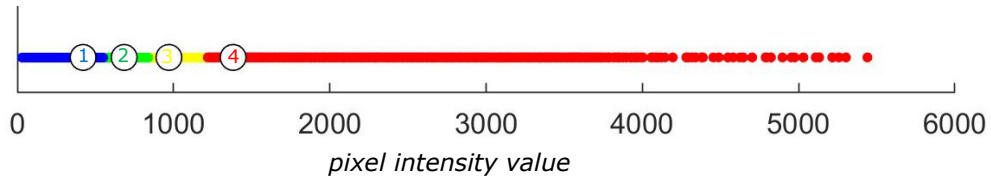


**Figure 4.10:** Tumor cluster affiliation based on K-means clustering of the intensity parameter for  $k=4$  from the diffusion-weighted images. Clustering is based on all patient’s voxels. The cluster centers are marked by the corresponding cluster number.

**Table 4.8:** P-values from the Wilcoxon rank-sum test on the two groups (above and below median) for each of the specified parameters that investigate statistical significance in the difference between the two groups (DWI;  $b=25$  s/mm<sup>2</sup>).

<b>b=25</b> [s/mm <sup>2</sup> ]	mrT	p/ypT	$\Delta T$	mrN	p/ypN	$\Delta N$	TRG
Cluster 1	0.1013	0.2507	0.6001	0.1650	0.2019	0.5599	0.1335
Cluster 2	0.4963	0.0988	0.5993	0.8941	0.3732	0.1682	0.1473
Cluster 3	0.3292	0.6944	0.7046	0.3607	0.7778	0.9055	0.1116
Cluster 4	0.1780	0.6761	0.5299	0.4530	0.1414	0.5032	0.0852

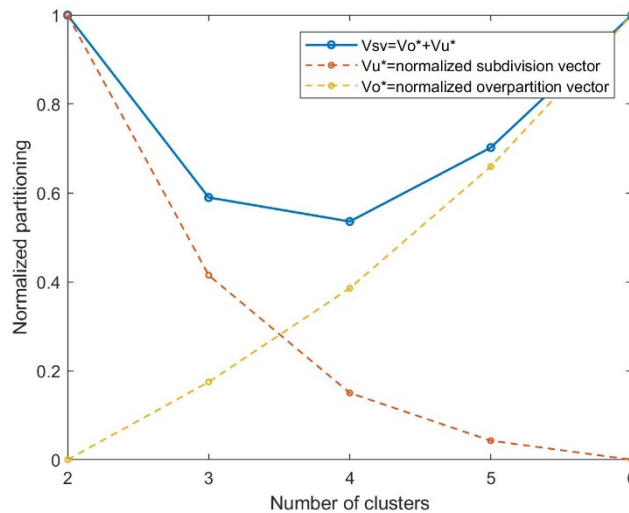


**Figure 4.9:** Plot of the normalized values of the over-partitioned and under-partitioned vectors with the validity index vector ( $v_{sv}$ ). The minimal value of  $v_{sv}$  defines the optimal number of clusters for the diffusion-weighted images with  $b=50$  s/mm<sup>2</sup>.

4.1.2.3  $b=50$  s/mm<sup>2</sup>

**Table 4.9:** Table displaying the values of the cluster centers and the median volume fractions for each cluster in data from diffusion-weighted images with b-value of 50 s/mm<sup>2</sup>.

Cluster number	Intensity (cluster center)	Median volume fraction (CVF)
1	420	22.4%
2	683	38.2%
3	969	22.6%
4	1380	3.9%

There is a significant difference between the two groups in the clustered data for the DW images with  $b=50 \text{ s/mm}^2$  ("an") for the 'p/ypN' parameter in Cluster 3 and the 'TRG' parameter in Cluster 1 and Cluster 2. (Table 4.12).

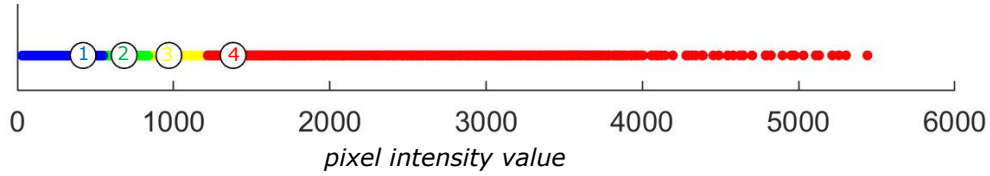


**Figure 4.11:** Tumor cluster affiliation based on K-means clustering of the intensity parameter for  $k=4$  from the diffusion-weighted images. Clustering is based on all patient's voxels. The cluster centers are marked by the corresponding cluster number.

**Table 4.10:** P-values from the Wilcoxon rank-sum test on the two groups (above and below median) for each of the specified parameters that investigate statistical significance in the difference between the two groups (DWI;  $b=50 \text{ s/mm}^2$ ).

$b=50$ [s/mm <sup>2</sup> ]	mrT	p/ypT	$\Delta T$	mrN	p/ypN	$\Delta N$	TRG
Cluster 1	0.4200	0.1135	0.2647	0.8209	0.8885	0.6961	<b>0.0393</b>
Cluster 2	0.1443	0.8085	0.09304	0.1572	0.1592	0.0739	<b>0.0406</b>
Cluster 3	0.0966	0.4455	0.6987	0.7451	<b>0.0493</b>	0.6164	1.0000
Cluster 4	0.4763	0.3216	0.7360	0.9214	0.9258	0.3990	0.4454

#### 4.1.2.4 $b=50 \text{ s/mm}^2$ (shh)

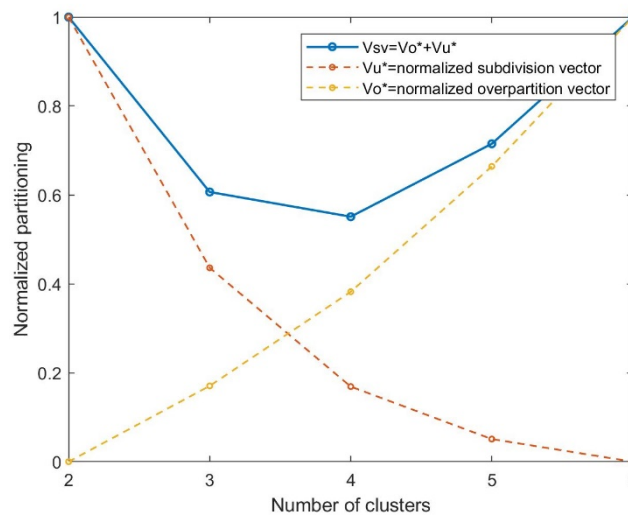


**Figure 4.12:** Plot of the normalized values of the over-partitioned and under-partitioned vectors with the validity index vector ( $v_{sv}$ ). The minimal value of  $v_{sv}$  defines the optimal number of clusters for the diffusion-weighted images with  $b=50 \text{ s/mm}^2$  (shh).

**Table 4.11:** Table displaying the values of the cluster centers and the median volume fractions for each cluster in data from diffusion-weighted images with b-value of 50 s/mm<sup>2</sup> for ROI delineated by radiologist “shh”.

Cluster number	Intensity (cluster center)	Median volume fraction (CVF)
1	356	20.2%
2	593	37.0%
3	846	22.9%
4	1227	3.7%

There is significant difference between the two groups in the clustered data for the DW images with b=50 s/mm<sup>2</sup> (“shh”) for the “p/ypT” parameter in Cluster 2 and Cluster 4 and the  $\Delta T$  parameter for Cluster 4. (Table 4.12).

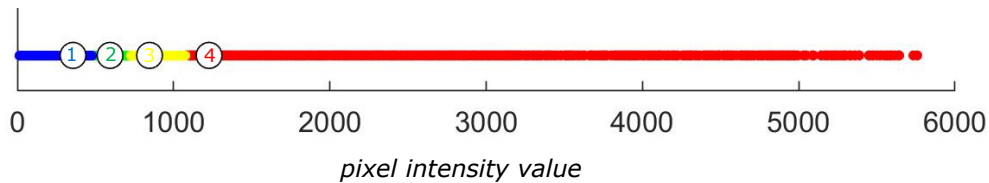


**Figure 4.13:** Tumor cluster affiliation based on K-means clustering of the intensity parameter for k=4 from the diffusion-weighted images. Clustering is based on all patient’s voxels. The cluster centers are marked by the corresponding cluster number.

**Table 4.12:** P-values from the Wilcoxon rank-sum test on the two groups (above and below median) for each of the specified parameters that investigate statistical significance in the difference between the two groups (DWI; b=50 s/mm<sup>2</sup> (shh)).

b=50 (shh) [s/mm <sup>2</sup> ]	mrT	p/ypT	$\Delta T$	mrN	p/ypN	$\Delta N$	TRG
Cluster 1	0.0691	0.9392	0.2539	0.5542	0.7671	0.8935	0.9500
Cluster 2	0.1297	<b>0.0394</b>	0.5501	0.5774	0.9874	0.1924	0.4723
Cluster 3	0.1895	0.6770	0.2539	0.3590	0.6290	0.4980	0.8801
Cluster 4	0.4790	<b>0.0451</b>	<b>0.0413</b>	0.9806	0.3776	0.8000	0.6968

#### 4.1.2.5 b= 100 s/mm<sup>2</sup>

**Table 4.13:** Table displaying the values of the cluster centers and the median volume fractions for each cluster in data from diffusion-weighted images with b-value of 100 s/mm<sup>2</sup>.

Cluster number	Intensity (cluster center)	Median volume fraction (CVF)
1	420	22.2%
2	682	38.2%
3	968	22.6%
4	1378	3.9%



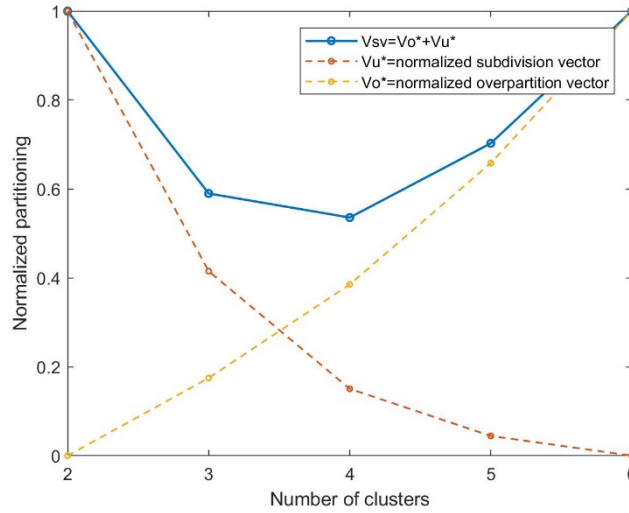


**Figure 4.15:** Plot of the normalized values of the over-partitioned and under-partitioned vectors with the validity index vector ( $v_{sv}$ ). The minimal value of  $v_{sv}$  defines the optimal number of clusters for the diffusion-weighted images with  $b=100$  s/mm<sup>2</sup>.

There is a significant difference between the two groups in the clustered data for the DW images with  $b=100$  s/mm<sup>2</sup> (Table 4.14) for the 'TRG' parameter in Cluster 1 and Cluster 2.

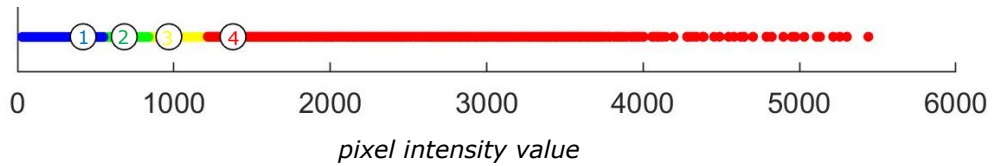


**Figure 4.14:** Tumor cluster affiliation based on K-means clustering of the intensity parameter for  $k=4$  from the diffusion-weighted images. Clustering is based on all patient's voxels. The cluster centers are marked by the corresponding cluster number.

**Table 4.14:** P-values from the Wilcoxon rank-sum test on the two groups (above and below median) for each of the specified parameters that investigate statistical significance in the difference between the two groups (DWI;  $b=100$  s/mm<sup>2</sup>).

<b>b=100</b> [s/mm <sup>2</sup> ]	mrT	p/ypT	$\Delta T$	mrN	p/ypN	$\Delta N$	TRG
Cluster 1	0.4200	0.1135	0.2647	0.8209	0.8499	0.9000	<b>0.0393</b>
Cluster 2	0.1443	0.8085	0.0930	0.1572	0.2413	0.2001	<b>0.0406</b>
Cluster 3	0.0966	0.4455	0.7634	0.7451	0.0734	0.2284	0.9827
Cluster 4	0.4763	0.3216	0.7360	0.9214	0.8488	0.6765	0.4454

4.1.2.6  $b=500 \text{ s/mm}^2$

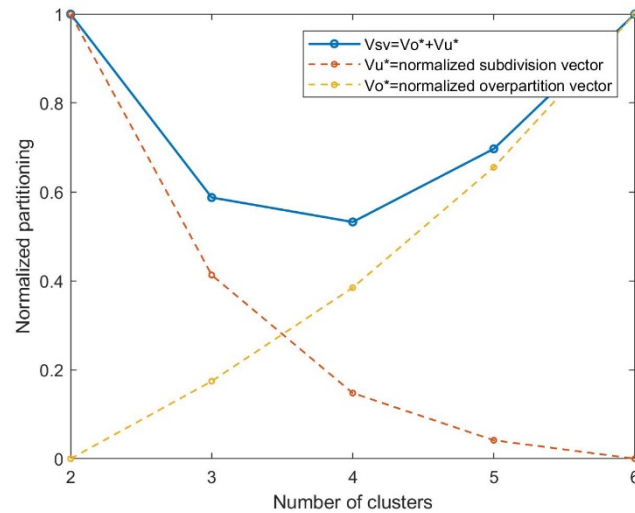


**Figure 4.16:** Plot of the normalized values of the over-partitioned and under-partitioned vectors with the validity index vector ( $v_{sv}$ ). The minimal value of  $v_{sv}$  defines the optimal number of clusters for the diffusion-weighted images with  $b=500 \text{ s/mm}^2$ .

**Table 4.15:** Table displaying the values of the cluster centers and the median volume fractions for each cluster in data from diffusion-weighted images with b-value of  $500 \text{ s/mm}^2$ .

Cluster number	Intensity (cluster center)	Median volume fraction (CVF)
1	410	22.8%
2	676	38.9%
3	963	22.9%
4	1374	3.7%

There is significant difference between the two groups in the clustered data for the DW images with  $b=500 \text{ s/mm}^2$  (Table 4.16) for the parameter 'TRG' in Cluster 1 and Cluster 2.

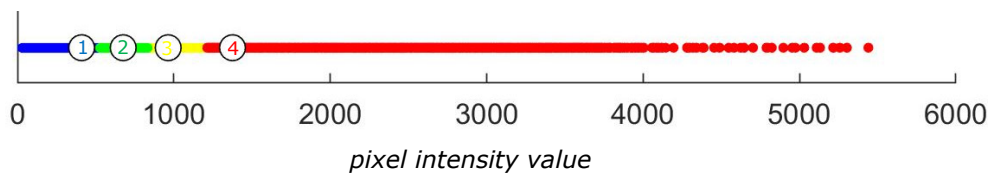


**Figure 4.17:** Tumor cluster affiliation based on K-means clustering of the intensity parameter for  $k=4$  from the diffusion-weighted images. Clustering is based on all patient's voxels. The cluster centers are marked by the corresponding cluster number.

**Table 4.16:** P-values from the Wilcoxon rank-sum test on the two groups (above and below median) for each of the specified parameters that investigate statistical significance in the difference between the two groups (DWI;  $b=500$  s/mm<sup>2</sup>).

$b=500$ [s/mm <sup>2</sup> ]	mrT	p/ypT	$\Delta T$	mrN	p/ypN	$\Delta N$	TRG
Cluster 1	0.5154	0.1657	0.2997	0.6026	0.6243	0.6089	<b>0.0252</b>
Cluster 2	0.0990	0.7436	0.2267	0.0819	0.2777	0.0912	<b>0.0422</b>
Cluster 3	0.0964	0.3755	0.7634	0.9631	0.1398	0.2284	0.9015
Cluster 4	0.4667	0.2530	0.5851	0.8469	0.7209	0.7219	0.5623

#### 4.1.2.7 $b=1000$ s/mm<sup>2</sup>

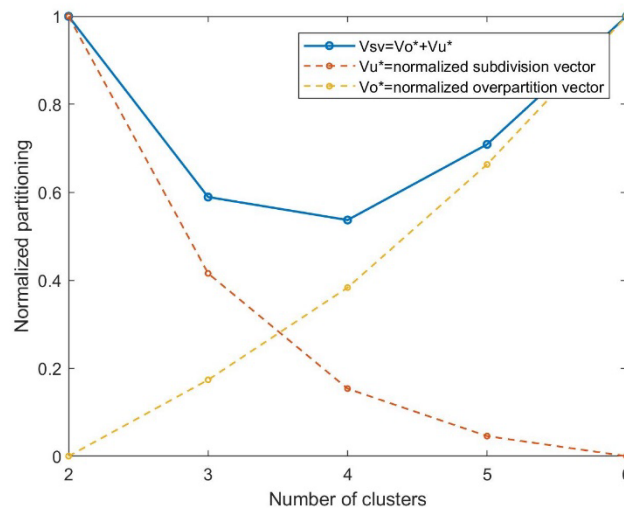


**Figure 4.18:** Plot of the normalized values of the over-partitioned and under-partitioned vectors with the validity index vector ( $v_{sv}$ ). The minimal value of  $v_{sv}$  defines the optimal number of clusters for the diffusion-weighted images with  $b=1000$  s/mm<sup>2</sup>.

**Table 4.17:** Table displaying the values of the cluster centers and the median volume fractions for each cluster in data from diffusion-weighted images with  $b$ -value of 1000 s/mm<sup>2</sup>.

Cluster number	Intensity (cluster center)	Median volume fraction (CVF)
1	402	17.2%
2	674	35.2%
3	962	24.6%
4	1373	4.3%

For the images with  $b=1000$  s/mm<sup>2</sup> the optimal cluster number is defined at  $k=4$  ( $v_{sv} = 0.57$ ) (Figure 4.18), with the cluster centers and median volume fractions displayed in Table 4.17 and Figure 4.19. There is no significant

difference between the groups in the data for the DW images with  $b=1000$   $s/mm^2$  (Table 4.18).

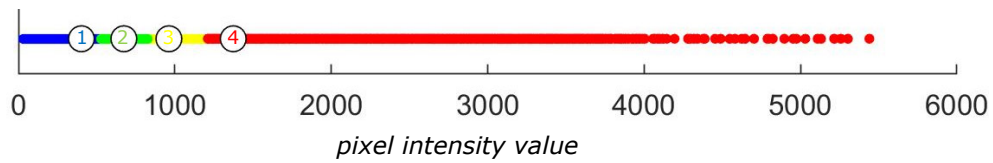


**Figure 4.19:** Tumor cluster affiliation based on K-means clustering of the intensity parameter for  $k=4$  from the diffusion-weighted images ( $b=1000$   $s/mm^2$ ). Clustering is based on all patient's voxels. The cluster centers are marked by the corresponding cluster number.

**Table 4.18:** P-values from the Wilcoxon rank-sum test on the two groups (above and below median) for each of the specified parameters that investigate statistical significance in the difference between the two groups (DWI;  $b=1000$   $s/mm^2$ ).

$b=1000$ [ $s/mm^2$ ]	mrT	p/ypT	$\Delta T$	mrN	p/ypN	$\Delta N$	TRG
Cluster 1	0,0979	0.8494	0,5239	0,2116	0,2342	0,9335	0,7531
Cluster 2	0,8714	0,1357	0,4010	0,8902	0,2360	0,3272	0,3816
Cluster 3	0,3939	0.2848	0,2217	0,3480	0,9919	0,5120	0,5645
Cluster 4	0,2351	0,3469	0,2815	0,7126	0,3092	0,8552	0,4735

#### 4.1.2.8 ADC maps

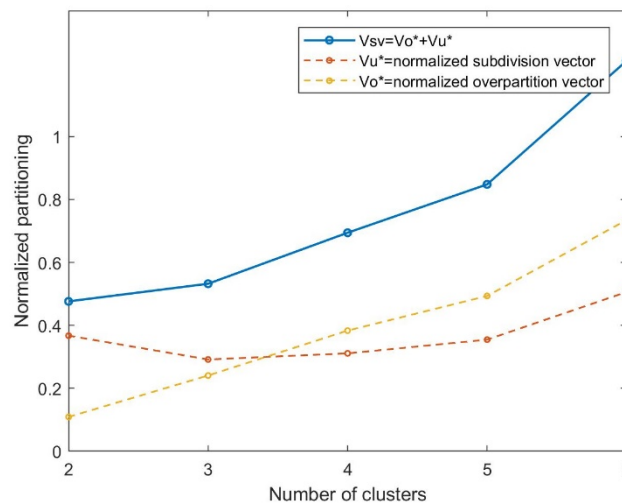


**Figure 4.20:** Plot of the normalized values of the over-partitioned and under-partitioned vectors with the validity index vector ( $v_{sv}$ ). The minimal value of  $v_{sv} = 0.476$  defines the optimal number of clusters for the ADC maps from the diffusion-weighted images.

For the ADC maps the optimal cluster number is defined at  $k=2$  ( $v_{sv} = 0.4112$ ) (Figure 4.20), with the cluster centers and median volume fractions displayed

in Table 4.19 and Figure 4.21. There is no significant difference between the groups in the data for the ADC maps. (Table 4.20)

**Table 4.19:** Table displaying the values of the cluster centers and the median volume fractions for each cluster in data from the ADC maps of the diffusion-weighted images.

Cluster number	Intensity (cluster center)	Median volume fraction (CVF)
1	1093	69.6%
2	1746	30.4%

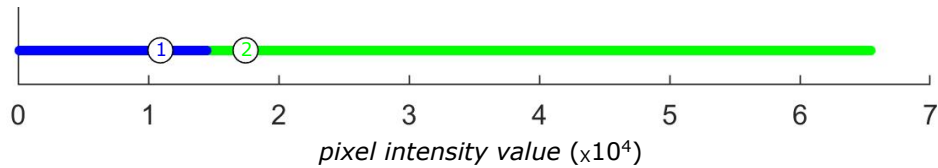


**Figure 4.21:** Tumor cluster affiliation based on K-means clustering of the intensity parameter for  $k=4$  from the ADC maps from the diffusion-weighted images. Clustering is based on all patient's voxels. The cluster centers are marked by the corresponding cluster number.

**Table 4.20:** P-values from the Wilcoxon rank-sum test on the two groups (above and below median) for each of the specified parameters that investigate statistical significance in the difference between the two groups (ADC maps).

ADC	mrT	p/ypT	$\Delta T$	mrN	p/ypN	$\Delta N$	TRG
Cluster 1	0.5756	0.6744	0.3191	0.7118	0.1372	0.2468	0.3060
Cluster 2	0.3841	0.4456	0.2900	0.7981	0.5334	0.8392	0.2341

### 4.1.3 T<sub>2</sub>-weighted and diffusion-weighted images

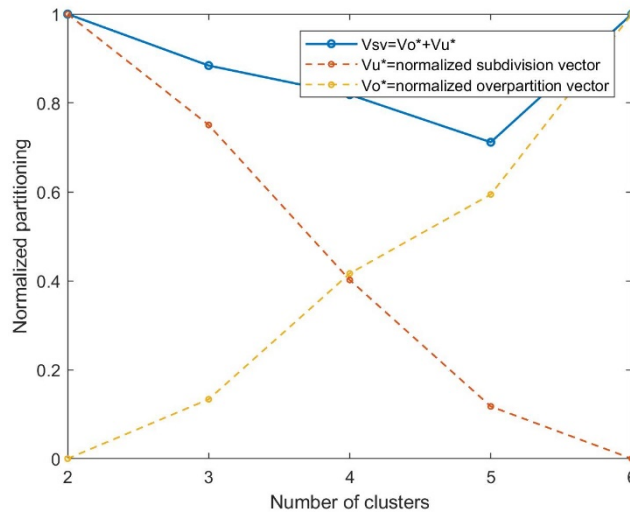


**Figure 4.23:** Plot of the normalized values of the over-partitioned and under-partitioned vectors with the validity index vector ( $v_{sv}$ ). The minimal value of  $v_{sv} = 0.7118$  defines the optimal number of clusters of  $k=5$  for the combined data of diffusion-weighted images with  $b=50 \text{ s/mm}^2$  and T<sub>2</sub>-weighted images where the ROI has been delineated by radiologist “shh”.

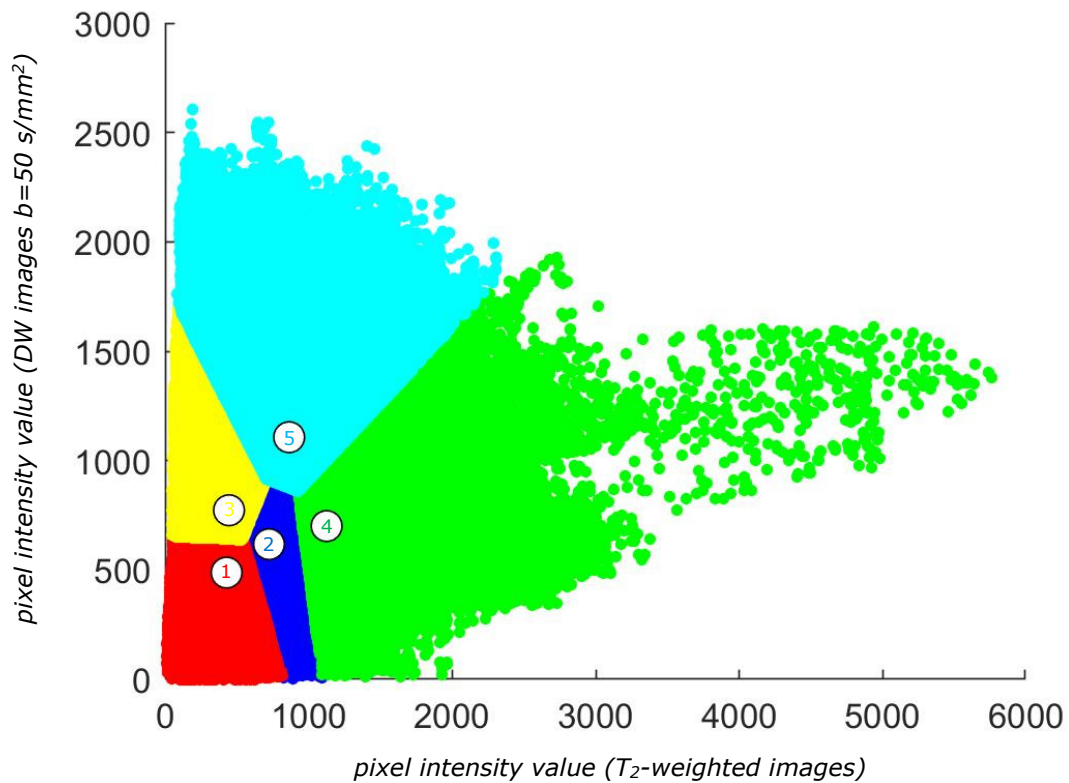


**Figure 4.22:** Tumor cluster affiliation based on K-means clustering of the intensity parameter for  $k=5$  from the combined data of DWI ( $b=50 \text{ s/mm}^2$ ) and T<sub>2</sub>-weighted images from radiologist “shh”. Clustering is based on all patient’s voxels and plotted against the two parameters. The cluster centers are marked by the corresponding cluster numbers.

For the combined data from the  $T_2$ -weighted images and the diffusion-weighted images with  $b=50 \text{ s/mm}^2$  the optimal cluster number is defined at  $k=5$  ( $v_{sv} = 0.7118$ ) (Figure 4.23). The cluster centers with the median volume fractions are plotted against the two parameters ( $T_2$  on the x-axis and DWI on the y-axis) displayed in Figure 4.22.

**Table 4.21:** Table displaying the values of the cluster centers and the median volume fractions for each cluster in data from combined diffusion-weighted images with b-value of  $50 \text{ s/mm}^2$  and  $T_2$ -weighted images for ROI delineated by radiologist "shh".

Cluster number	Intensity (cluster center)	Median volume fraction (CVF)
1	{428; 487}	27.6%
2	{724; 617}	39.6%
3	{445; 772}	12.4%
4	{1125;700}	5.9%
5	{864;1106}	3.6%

There is no significant difference between the two groups in the clustered data from the combined DW images with  $b=50 \text{ s/mm}^2$  and the  $T_2$ -weighted images with the ROI delineated by radiologist "shh". (Table 4.22)

**Table 4.22:** P-values from the Wilcoxon rank-sum test on the two groups (above and below median) for each of the specified parameters that investigate statistical significance in the difference between the two groups (combined DWI ( $b=50 \text{ s/mm}^2$ (shh)) and  $T_2$  (shh)).

$T_2$ +DWI ( $b=50 \text{ s/mm}^2$ ) (shh)	mrT	p/ypT	$\Delta T$	mrN	p/ypN	$\Delta N$	TRG
Cluster 1	0.4231	0.3215	0.6796	0.7218	0.9317	0.8491	0.3856
Cluster 2	0.5237	0.1863	0.1315	0.2491	0.0893	0.3784	1.0000
Cluster 3	0.5001	0.2931	0.1425	0.7767	0.3707	0.8329	0.5173
Cluster 4	0.4162	0.2788	0.2768	0.6582	0.3698	0.8102	0.4647
Cluster 5	0.4958	0.4122	0.8066	0.6905	0.6128	0.5688	0.7728

## 4.2 Survival analyses

### 4.2.1 T<sub>2</sub>-weighted images

#### 4.2.1.1 Radiologist – “an”

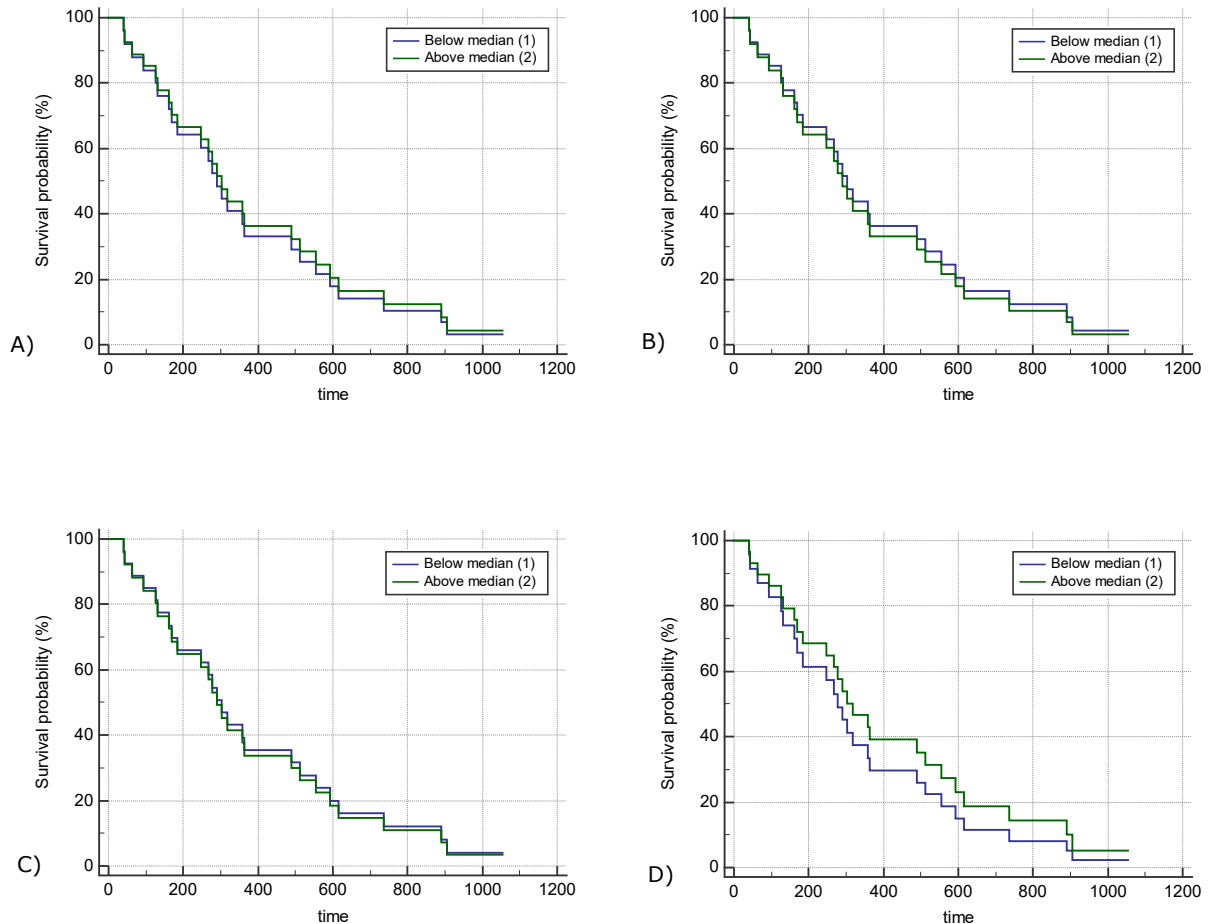


**Figure 4.24:** Kaplan-Meier plots for the survival difference between the two patient groups in cluster 1 (A), cluster 2 (B), cluster 3 (C) and cluster 4 (D) from the T<sub>2</sub>-weighted images (radiologist -an), divided by the median volume with Cox regression analysis (Plotted with MedCalc®). The investigated endpoints are local recurrence, metastasis or death. Survival is indicated in the portion of patients with progression-free survival (PFS). The estimated difference in the two groups results in p-values shown in Table 4.23 (For all clusters there is no significant difference at the selected significance level  $p=0.05$ )

**Table 4.23:** P-values for the comparison of the two patient groups from the Cox-regression analysis (based on Wald test with MedCalc®) and the three tests of the Cox regression with R console for the T<sub>2</sub>-weighted images (radiologist-“an”).

T <sub>2</sub> (an)	Cox regression	Likelihood ratio test	Wald test	Log-rank test
Cluster 1	0.844	0.832	0.822	0.812
Cluster 2	0.834	0.821	0.811	0.823
Cluster 3	0.909	0.900	0.912	0.901
Cluster 4	0.530	0.522	0.532	0.500



## 4.2.1.2 Radiologist – “shh”

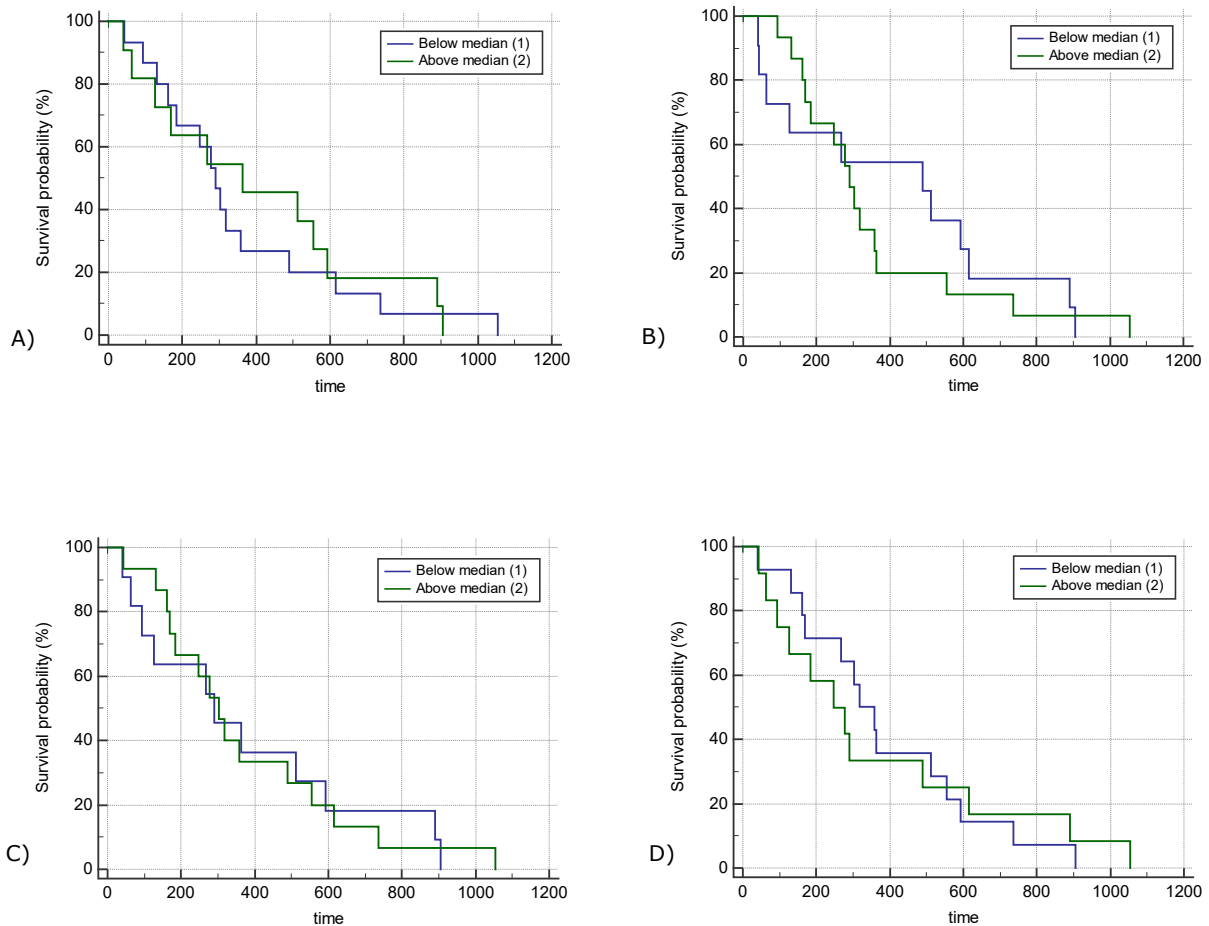


**Figure 4.25:** Kaplan-Meier plots for the survival difference between the two patient groups in cluster 1 (A), cluster 2 (B), cluster 3 (C) and cluster 4 (D) from the T<sub>2</sub>-weighted images (radiologist – “shh”), divided by the median volume with Cox regression analysis (Plotted with MedCalc®). The investigated endpoints are local recurrence, metastasis or death. Survival is indicated in the portion of patients with progression-free survival (PFS). The estimated difference in the two groups results in p-values shown in Table 4.24 (For all clusters there is no significant difference at the selected significance level p=0.05)

**Table 4.24:** P-values for the comparison of the two patient groups from the Cox-regression analysis (based on Wald test with MedCalc®) and the three tests of the Cox regression with R console for the T<sub>2</sub>-weighted images (radiologist – “shh”).

T <sub>2</sub> (shh)	Cox regression	Likelihood ratio test	Wald test	Log-rank test
Cluster 1	0,765	0.799	0.802	0.786
Cluster 2	0,702	0.733	0.720	0.705
Cluster 3	0,937	0.947	0.935	0.923
Cluster 4	0,952	0.969	0.989	0.956

### 4.2.2 Diffusion-weighted images

#### 4.2.2.1 $b=0$ s/mm<sup>2</sup>

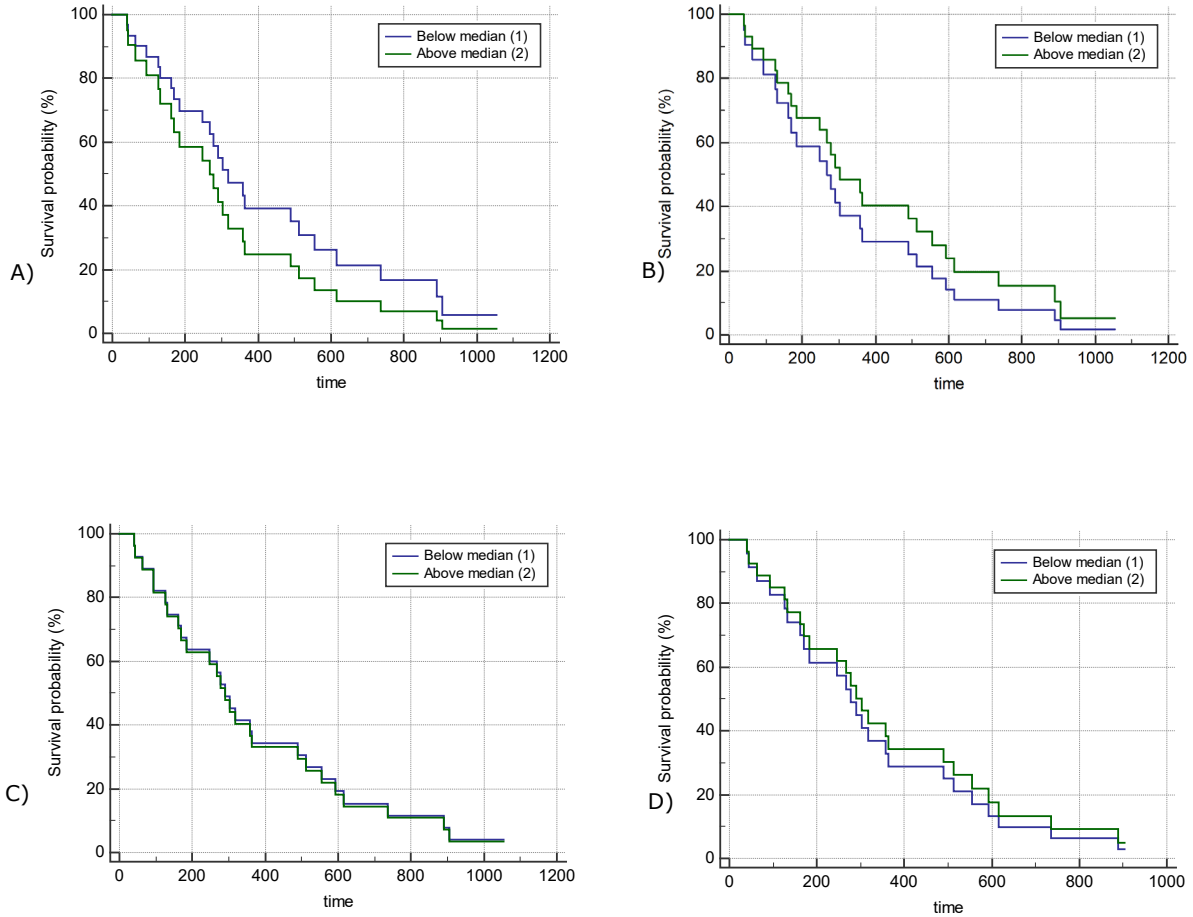
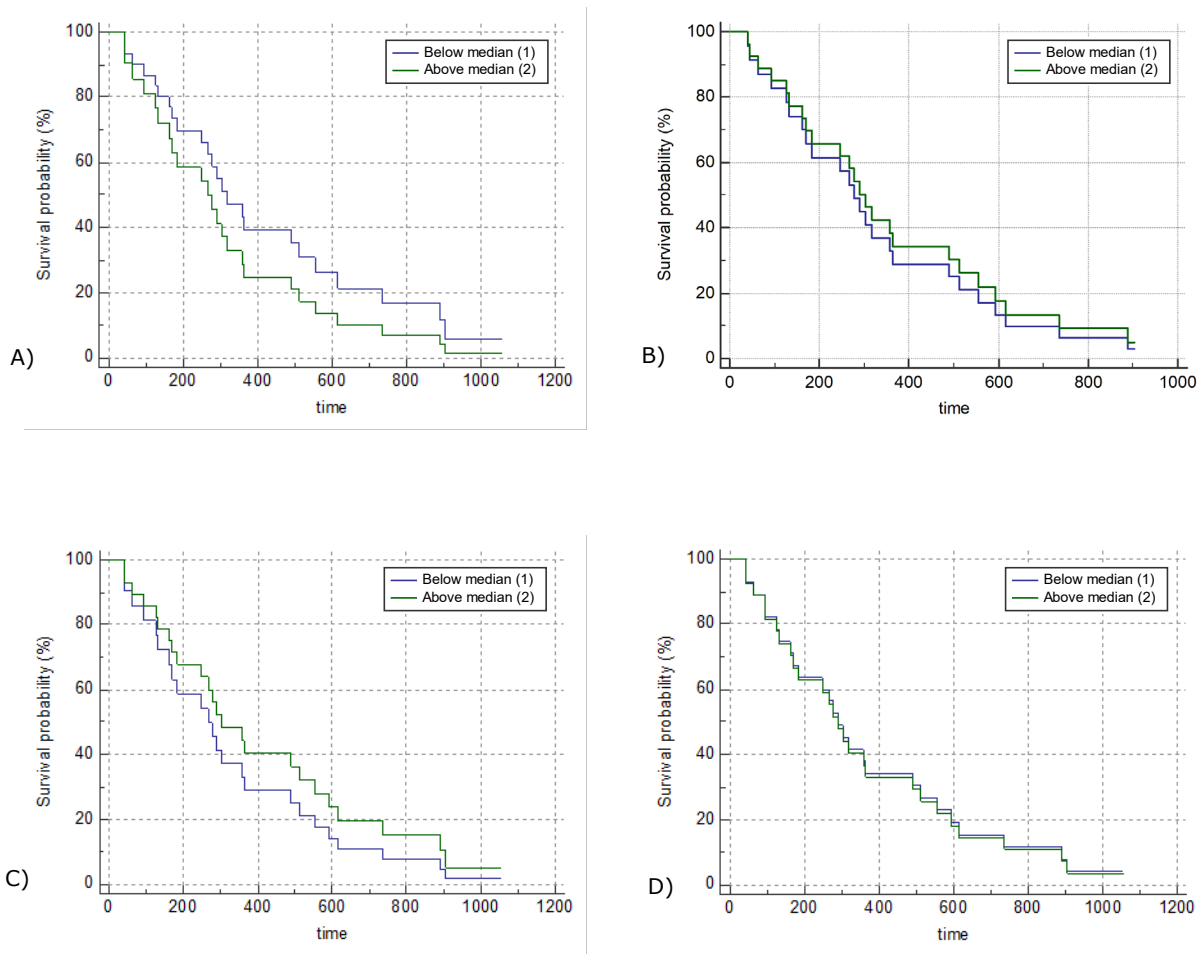


**Figure 4.26:** Kaplan-Meier plots for the survival difference between the two patient groups in cluster 1 (A), cluster 2 (B), cluster 3 (C) and cluster 4 (D) from the diffusion-weighted images ( $b=0$  s/mm<sup>2</sup>), divided by the median volume with Cox regression analysis (Plotted with MedCalc®). The investigated endpoints are local recurrence, metastasis or death. Survival is indicated in the portion of patients with progression-free survival (PFS). The estimated difference in the two groups results in p-values shown in Table 4.25 (For all clusters there is no significant difference at the selected significance level  $p=0.05$ )

**Table 4.25:** P-values for the comparison of the two patient groups from the Cox-regression analysis (based on Wald test with MedCalc®) and the three tests of the Cox regression with R console for the diffusion-weighted images ( $b=0$  s/mm<sup>2</sup>).

<b><math>b=0</math></b> [s/mm <sup>2</sup> ]	Cox regression	Likelihood ratio test	Wald test	Log-rank test
Cluster 1	0.350	0.367	0.354	0.378
Cluster 2	0.469	0.476	0.477	0.452
Cluster 3	0.937	0.934	0.922	0.944
Cluster 4	0.720	0.724	0.735	0.722

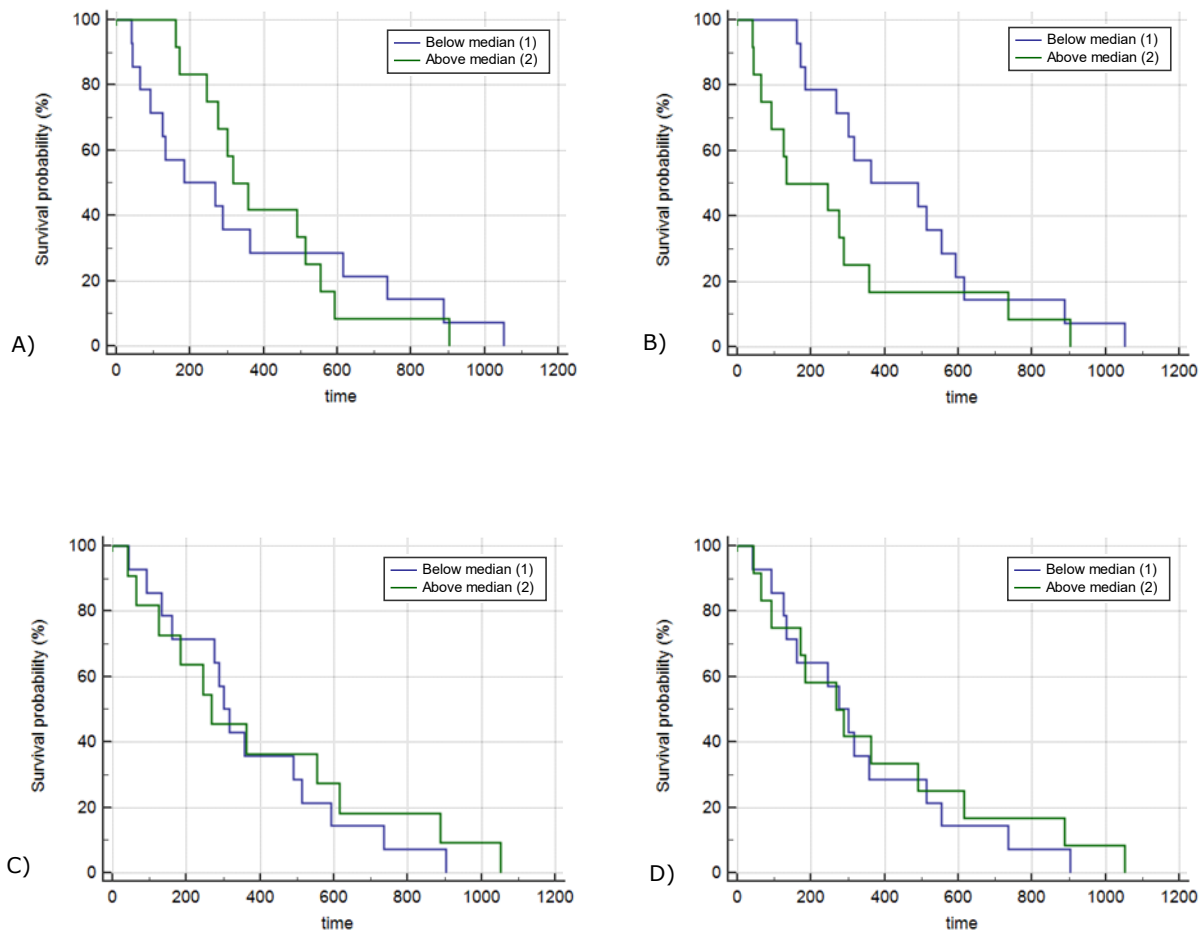
4.2.2.2  $b=25 \text{ s/mm}^2$



**Figure 4.27:** Kaplan-Meier plots for the survival difference between the two patient groups in cluster 1 (A), cluster 2 (B), cluster 3 (C) and cluster 4 (D) from the diffusion-weighted images ( $b=25 \text{ s/mm}^2$ ), divided by the median volume with Cox regression analysis (Plotted with MedCalc®). The investigated endpoints are local recurrence, metastasis or death. Survival is indicated in the portion of patients with progression-free survival (PFS). The estimated difference in the two groups results in p-values shown in Table 4.26 (For all clusters there is no significant difference at the selected significance level  $p=0.05$ )

**Table 4.26:** P-values for the comparison of the two patient groups from the Cox-regression analysis (based on Wald test with MedCalc®) and the three tests of the Cox regression with R console for the diffusion-weighted images ( $b=25 \text{ s/mm}^2$ ).

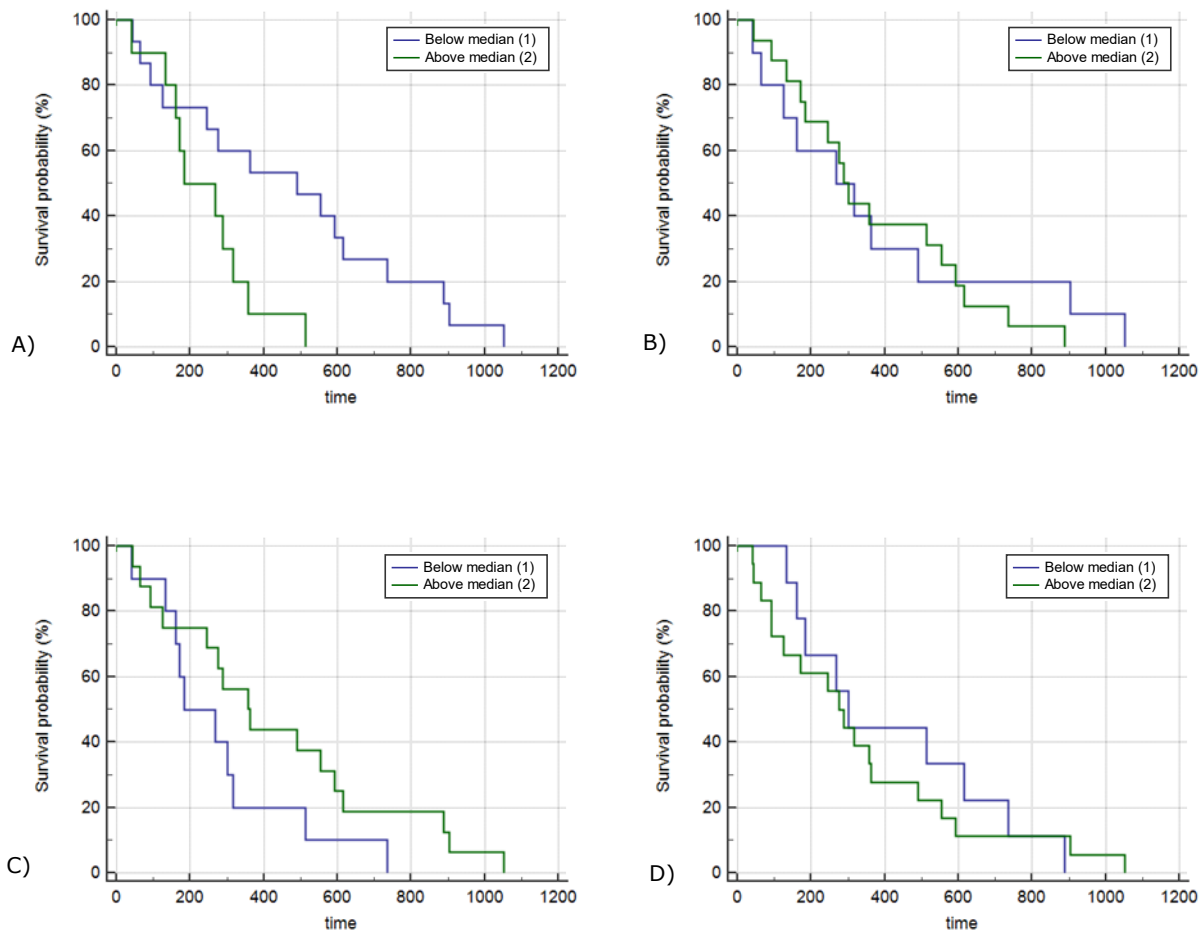
$b=25$ [ $\text{s/mm}^2$ ]	Cox regression	Likelihood ratio test	Wald test	Log-rank test
Cluster 1	0.350	0.364	0.352	0.363
Cluster 2	0.720	0.733	0.725	0.729
Cluster 3	0.469	0.478	0.470	0.466
Cluster 4	0.937	0.942	0.939	0.940

4.2.2.3  $b=50 \text{ s/mm}^2$ 

**Figure 4.28:** Kaplan-Meier plots for the survival difference between the two patient groups in cluster 1 (A), cluster 2 (B), cluster 3 (C) and cluster 4 (D) from the diffusion-weighted images ( $b=50 \text{ s/mm}^2$ ), divided by the median volume with Cox regression analysis (Plotted with MedCalc®). The investigated endpoints are local recurrence, metastasis or death. Survival is indicated in the portion of patients with progression-free survival (PFS). The estimated difference in the two groups results in p-values shown in **Table 4.27** (For all clusters there is no significant difference at the selected significance level  $p=0.05$ )

**Table 4.27:** P-values for the comparison of the two patient groups from the Cox-regression analysis (based on Wald test with MedCalc®) and the three tests of the Cox regression with R console for the diffusion-weighted images ( $b=50 \text{ s/mm}^2$ ).

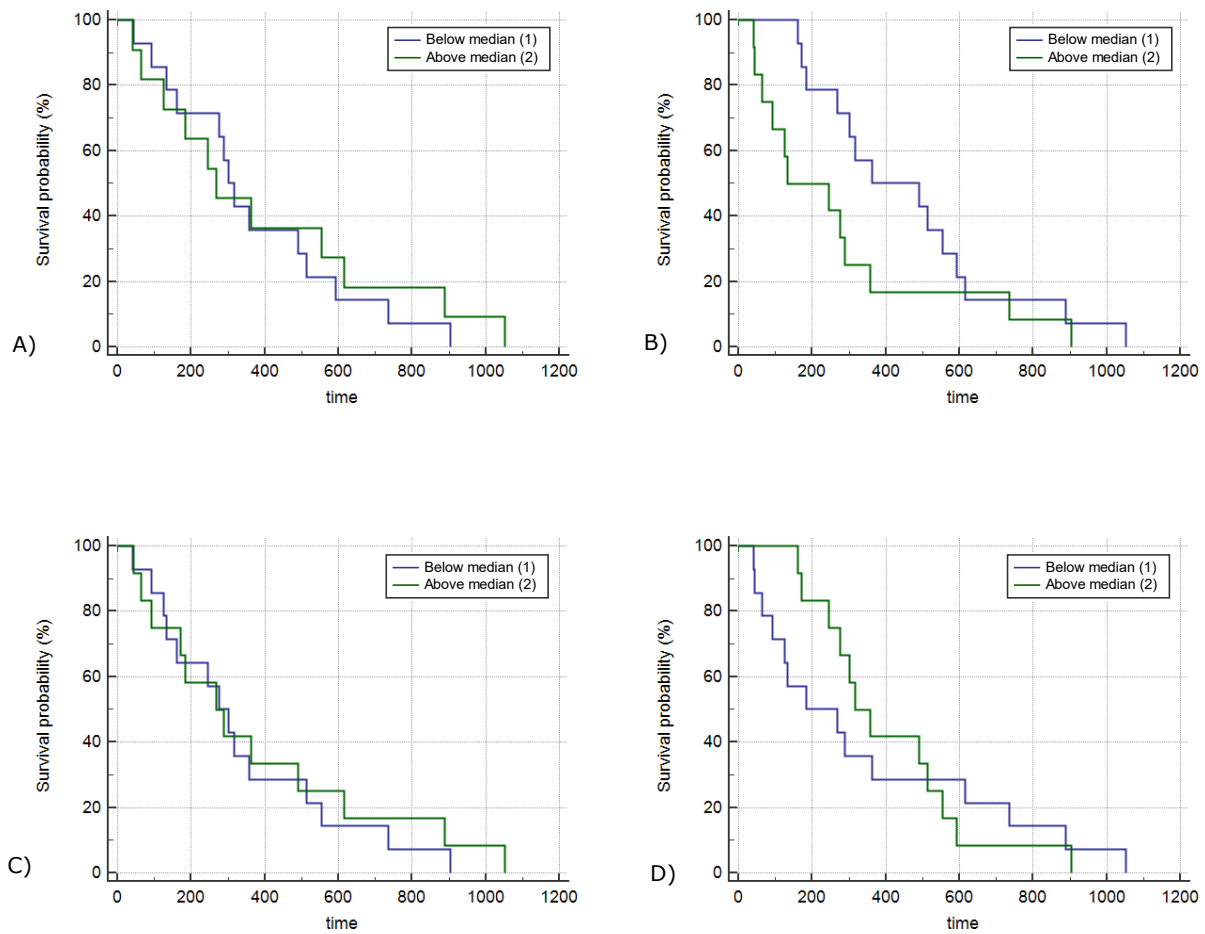
$b=50$ [ $\text{s/mm}^2$ ]	Cox regression	Likelihood ratio test	Wald test	Log-rank test
Cluster 1	0,843	0.847	0.838	0.854
Cluster 2	0,123	0.122	0.131	0.128
Cluster 3	0,705	0.711	0.708	0.700
Cluster 4	0,684	0.690	0.688	0.680

4.2.2.4  $b=50 \text{ s/mm}^2$  (shh)

**Figure 4.29:** Kaplan-Meier plots for the survival difference between the two patient groups in cluster 1 (A), cluster 2 (B), cluster 3 (C) and cluster 4 (D) from the diffusion-weighted images ( $b=50 \text{ s/mm}^2$  – radiologist “shh”), divided by the median volume with Cox regression analysis (Plotted with MedCalc®). The investigated endpoints are local recurrence, metastasis or death. Survival is indicated in the portion of patients with progression-free survival (PFS). The estimated difference in the two groups results in p-values shown in **Table 4.28** (For Cluster 1 there is significant difference at the selected significance level  $p=0.05$ )

**Table 4.28:** P-values for the comparison of the two patient groups from the Cox-regression analysis (based on Wald test with MedCalc®) and the three tests of the Cox regression with R console for the diffusion-weighted images ( $b=50 \text{ s/mm}^2$  – radiologist “shh”).

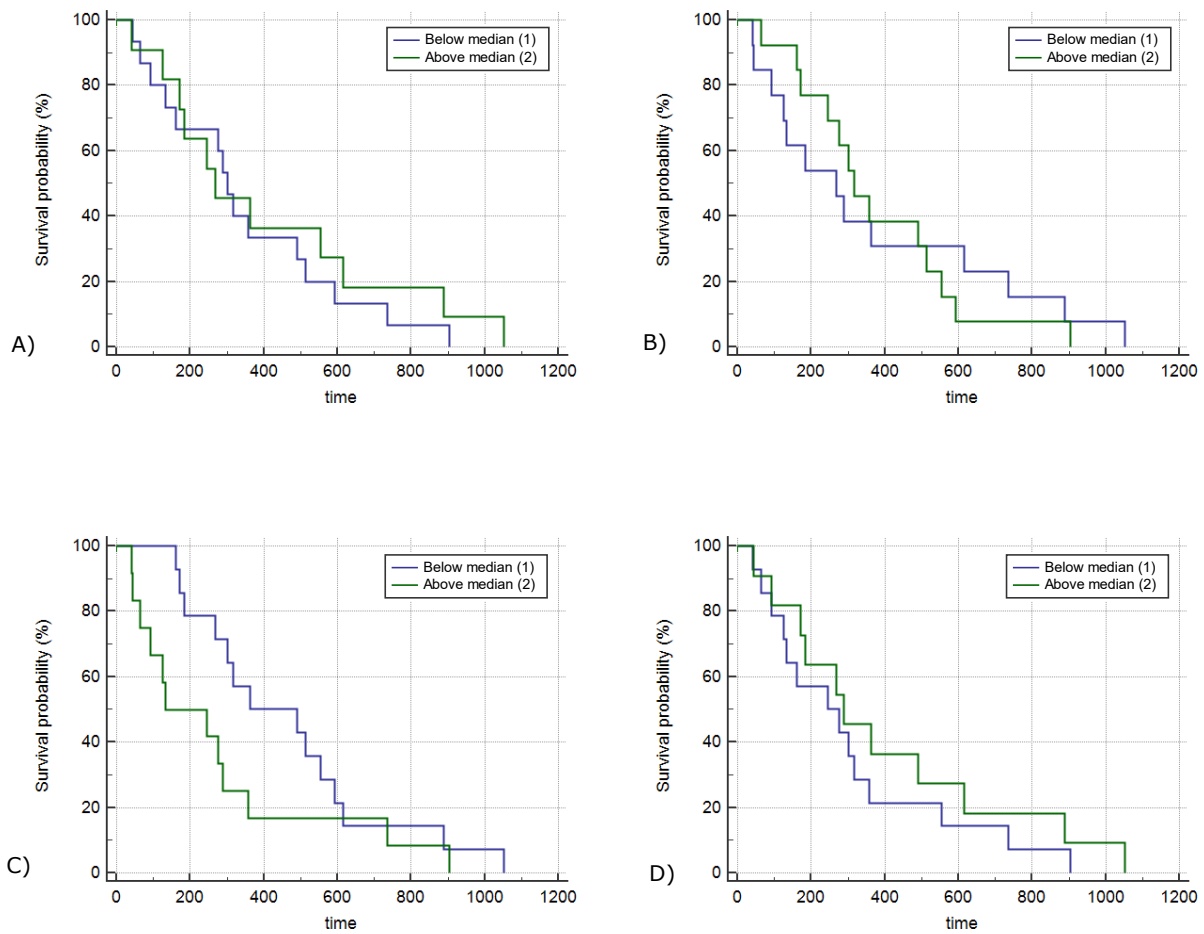
$b=50$ (shh) [ $\text{s/mm}^2$ ]	Cox regression	Likelihood ratio test	Wald test	Log-rank test
Cluster 1	<b>0,021</b>	<b>0.031</b>	<b>0.029</b>	<b>0.020</b>
Cluster 2	0,695	0.700	0.698	0.693
Cluster 3	0,134	0.144	0.130	0.140
Cluster 4	0,682	0.691	0.684	0.681

4.2.2.5  $b=100 \text{ s/mm}^2$ 

**Figure 4.30:** Kaplan-Meier plots for the survival difference between the two patient groups in cluster 1 (A), cluster 2 (B), cluster 3 (C) and cluster 4 (D) from the diffusion-weighted images ( $b=100 \text{ s/mm}^2$ ), divided by the median volume with Cox regression analysis (Plotted with MedCalc®). The investigated endpoints are local recurrence, metastasis or death. Survival is indicated in the portion of patients with progression-free survival (PFS). The estimated difference in the two groups results in p-values shown in **Table 4.29** (For all clusters there is no significant difference at the selected significance level  $p=0.05$ )

**Table 4.29:** P-values for the comparison of the two patient groups from the Cox-regression analysis (based on Wald test with MedCalc®) and the three tests of the Cox regression with R console for the diffusion-weighted images ( $b=100 \text{ s/mm}^2$ ).

$b=100$ [ $\text{s/mm}^2$ ]	Cox regression	Likelihood ratio test	Wald test	Log-rank test
Cluster 1	0,705	0.721	0.708	0.701
Cluster 2	0,123	0.134	0.128	0.122
Cluster 3	0,684	0.690	0.686	0.679
Cluster 4	0,843	0.854	0.849	0.844

4.2.2.6  $b=500 \text{ s/mm}^2$ 

**Figure 4.31:** Kaplan-Meier plots for the survival difference between the two patient groups in cluster 1 (A), cluster 2 (B), cluster 3 (C) and cluster 4 (D) from the diffusion-weighted images ( $b=500 \text{ s/mm}^2$ ), divided by the median volume with Cox regression analysis (Plotted with MedCalc®). The investigated endpoints are local recurrence, metastasis or death. Survival is indicated in the portion of patients with progression-free survival (PFS). The estimated difference in the two groups results in p-values shown in **Table 4.30** (For all clusters there is no significant difference at the selected significance level  $p=0.05$ )

**Table 4.30:** P-values for the comparison of the two patient groups from the Cox-regression analysis (based on Wald test with MedCalc®) and the three tests of the Cox regression with R console for the diffusion-weighted images ( $b=500 \text{ s/mm}^2$ ).

$b=500$ [ $\text{s/mm}^2$ ]	Cox regression	Likelihood ratio test	Wald test	Log-rank test
Cluster 1	0,558	0.589	0.563	0.560
Cluster 2	0,870	0.923	0.890	0.873
Cluster 3	0,123	0.134	0.128	0.122
Cluster 4	0,387	0.410	0.392	0.390

4.2.2.7  $b=1000 \text{ s/mm}^2$

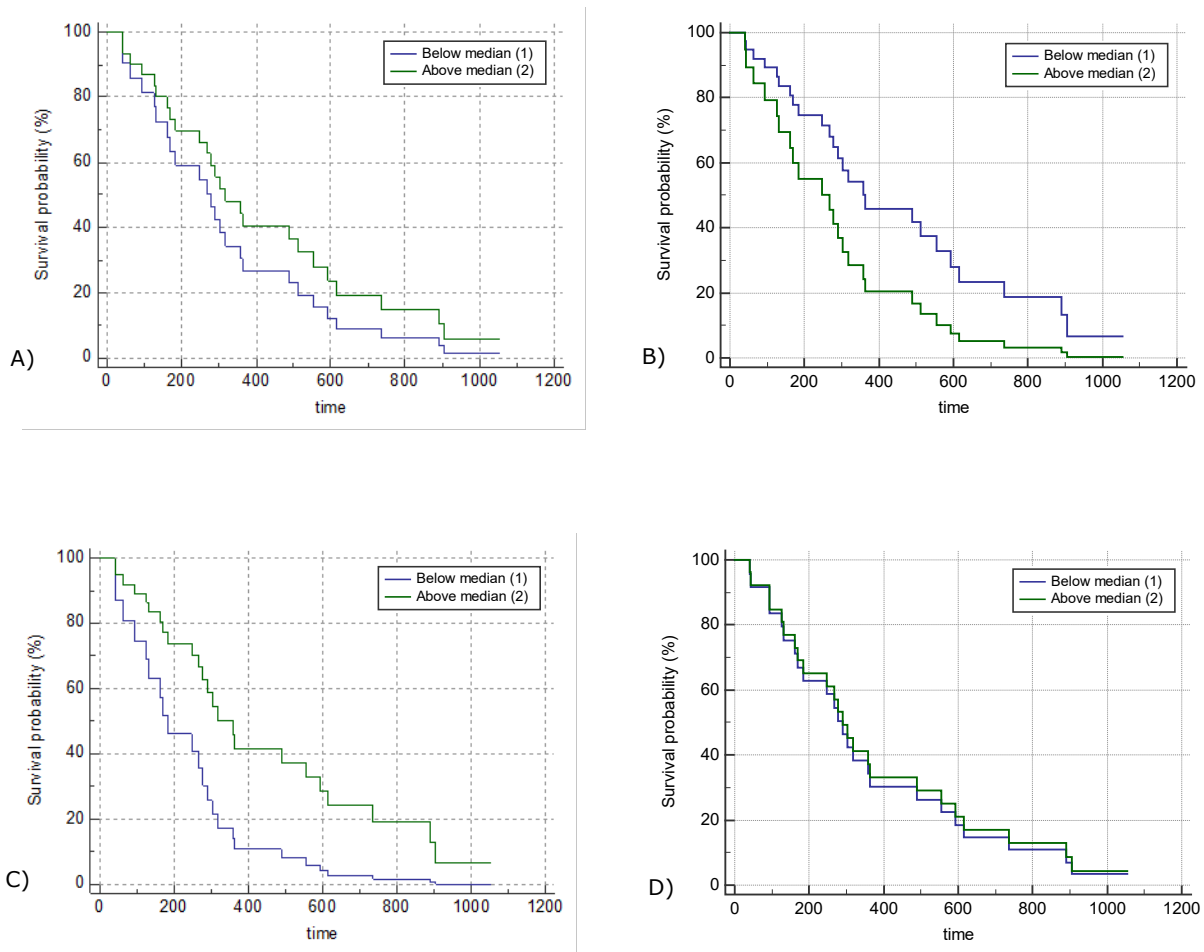


**Figure 4.32:** Kaplan-Meier plots for the survival difference between the two patient groups in cluster 1 (A), cluster 2 (B), cluster 3 (C) and cluster 4 (D) from the diffusion-weighted images ( $b=1000 \text{ s/mm}^2$ ), divided by the median volume with Cox regression analysis (Plotted with MedCalc®). The investigated endpoints are local recurrence, metastasis or death. Survival is indicated in the portion of patients with progression-free survival (PFS). The estimated difference in the two groups results in p-values shown in Table 4.31 (For Cluster 3 there is significant difference at the selected significance level  $p=0.05$ )

**Table 4.31:** P-values for the comparison of the two patient groups from the Cox-regression analysis (based on Wald test with MedCalc®) and the three tests of the Cox regression with R console for the diffusion-weighted images ( $b=1000 \text{ s/mm}^2$ ).

<b><math>b=1000</math> [<math>\text{s/mm}^2</math>]</b>	Cox regression	Likelihood ratio test	Wald test	Log-rank test
Cluster 1	0.348	0.356	0.349	0.344
Cluster 2	0.083	0.095	0.084	0.083
Cluster 3	<b>0.031</b>	<b>0.050</b>	<b>0.043</b>	<b>0.030</b>
Cluster 4	0.850	0.867	0.855	0.849



## 4.2.2.8 ADC maps

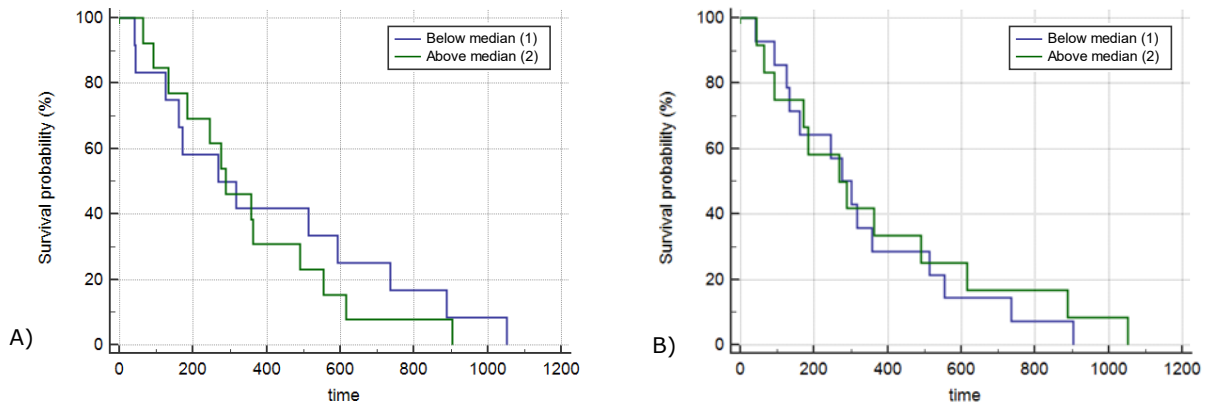
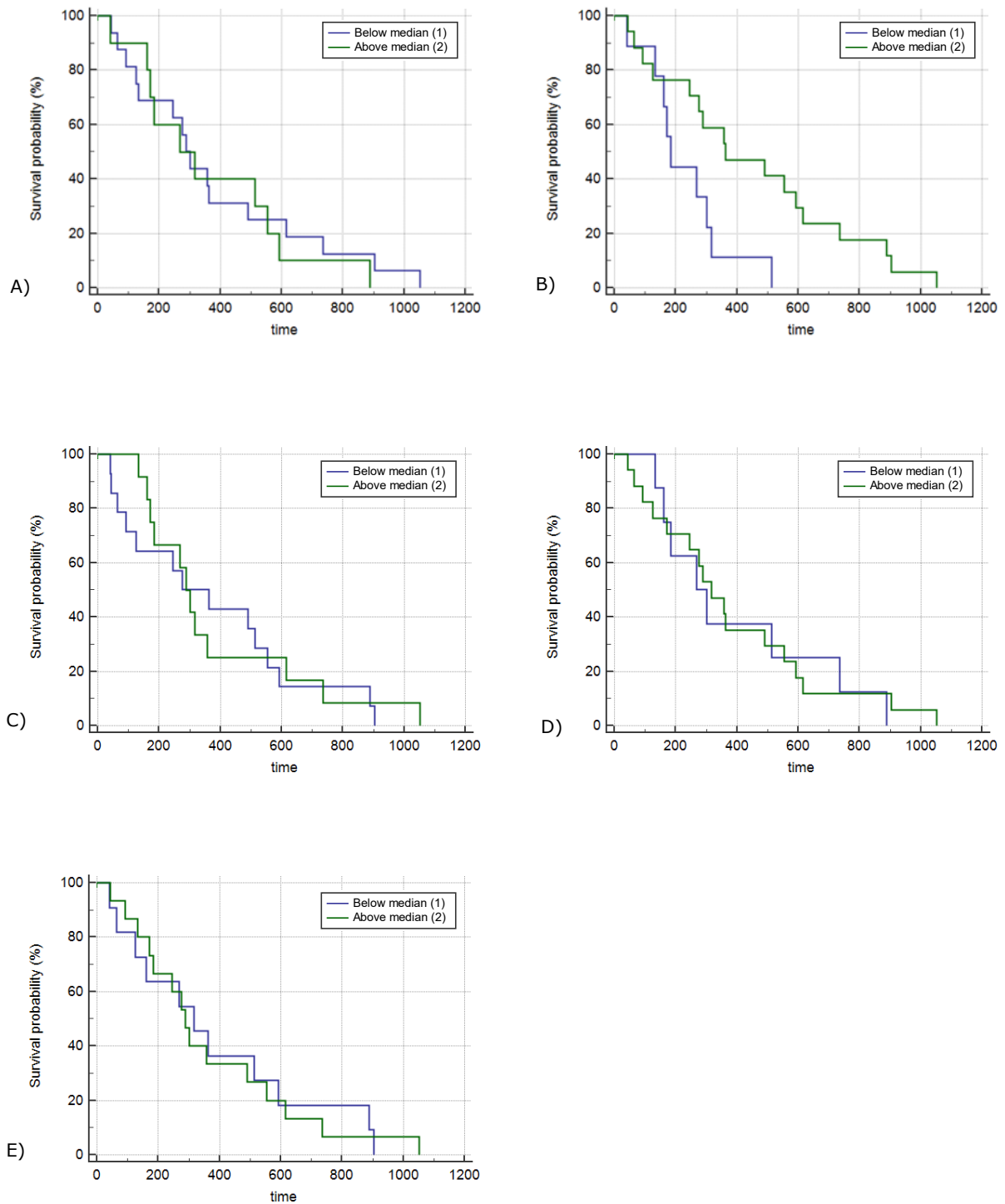


Figure 4.33: **Kaplan-Meier plots for the survival difference between the two patient groups in cluster 1 (A) and cluster 2 (B) from the ADC maps, divided by the median volume with Cox regression analysis (Plotted with MedCalc®). The investigated endpoints are local recurrence, metastasis or death. Survival is indicated in the portion of patients with progression-free survival (PFS). The estimated difference in the two groups results in p-values shown in**

**Table 4.32:** P-values for the comparison of the two patient groups from the Cox-regression analysis (based on Wald test with MedCalc®) and the three tests of the Cox regression with R console for the ADC maps.

ADC	Cox regression	Likelihood ratio test	Wald test	Log-rank test
Cluster 1	0.598	0.612	0.600	0.599
Cluster 2	0.687	0.703	0.693	0.788

4.2.3 T<sub>2</sub>-weighted and diffusion-weighted images

**Figure 4.34:** Kaplan-Meier plots for the survival difference between the two patient groups in cluster 1 (A), cluster 2 (B), cluster 3 (C), cluster 4 (D) and cluster 5 (E) for the combined data from diffusion-weighted images ( $b=25 \text{ s/mm}^2$ ) and T<sub>2</sub>-weighted images based on the delineation by radiologist - "shh" divided by the median volume with Cox regression analysis (Plotted with MedCalc®). The investigated endpoints are local recurrence, metastasis or death. Survival is indicated in the portion of patients with progression-free survival (PFS). The estimated difference in the two groups results in p-values shown in **Table 4.33** (For Cluster 2 there is significant difference at the selected significance level  $p=0.05$ )

**Table 4.33:** P-values for the comparison of the two patient groups from the Cox-regression analysis (based on Wald test with MedCalc®) and the three tests of the Cox regression with R console for the combined data from diffusion-weighted images ( $b=25 \text{ s/mm}^2$ ) and T<sub>2</sub>-weighted images (radiologist – “shh”).

<b>T<sub>2</sub>+DWI</b> ( $b=50 \text{ s/mm}^2$ ) (shh)	Cox regression	Likelihood ratio test	Wald test	Log-rank test
Cluster 1	0.696	0.710	0.703	0.699
Cluster 2	<b>0,021</b>	<b>0.031</b>	<b>0.027</b>	<b>0.022</b>
Cluster 3	0,774	0.798	0.780	0.777
Cluster 4	0,856	0.887	0.867	0.858
Cluster 5	0,963	1.000	0.974	0.972

## 5 Discussion

In this chapter we look at the limitations and strengths of the applied methods, followed by the discussion of the obtained results. The chapter ends with the implications of the conclusions and the potential for future work.

### 5.1 Materials and Methods

47 patients did not receive CRT and only underwent surgery, while the other 40% of the studied cohort received CRT (Table 3.1). However, some of the patients with LARC did not receive CRT because they were too sick or too old. Although it is impossible to assess, there might be a possibility that these patients would have responded differently if they were treated with the standard regime. This could indicate different results, but because only 4% of the LARC patients did not undergo CRT, the effect on the overall results is considered to be negligible.

The ideal prognostic system is expected to provide homogeneity in the same stage, good discrimination between different stages and monotonicity of the gradients that predict survival outcomes which are consistent with the severity of the cancer staging. However, there is some research indicating that the current TNM staging system by AJCC gives unsatisfactory gradient monotonicity. Although this might be problematic and influence the clinical implications of the results, there is a lack of understanding in the causes for defects in gradient monotonicity, so the matter will not be further discussed within the scope of this thesis.[66]

The acquisition of the MR images from the patients in the study group had included several sequences, which increase the probability of movement because of the required extended period inside the scanner. Additionally, bowel movements are difficult to annulate and they can cause motion artefacts. In

order to reduce these movements, peristaltic agents were used. They act directly on the muscles of the intestinal wall and result in slowed intestinal motility [69]

There is a high degree of uncertainty related to the tumor volume. In radiotherapy, one of the main challenges is the delineation of the tumors (ROIs). In clinical practice the current contouring of the target volumes is based on the guidelines by the International Commission on Radiation Units and Measurements (ICRU). However, there is a significant interobserver variability in tumor delineation which is influenced by different factors such as imaging modality and the technique. Considering the context of this thesis (the delineations were drawn on the same images by two radiologists) the biggest source of variability comes from the observer's specialty, training and personal bias.[67] A study by Weiss and Hess [68] based on interobserver variability suggests that "the contouring of a target volume is influenced to a large extent by the observer's subjective interpretation of what he or she sees on the images". They also emphasize the important contributions to variations by difference in training and the instructions for contouring, as well as experience. Generally (although speculative) it is reported that less experienced radiologists contour larger tumor volumes. [68] It is important to note that in some cases the normal tissue might have been included in the regions of interest while excluding the tumor in other cases. Such divergences will affect correlation with the parameters because the analyses are based on the pixels from each slice. A visual comparison of the variation is shown in Figure 4.1 where it is possible to observe the ROIs by the radiologist "shh" are significantly larger. This delineation difference needs to be considered in the interpretation of the results.

The ROIs are delineated on the T<sub>2</sub>-weighted images which have 512x512 pixels. Therefore, the image analyses need to include manual interpolation of the diffusion-weighted images (128x128), which is an essential rescaling process required for applying the ROIs on the DWI. However, this can give rise to inaccuracies caused by movement between the two imaging sequences as described before, differences in the slice selections and/or errors in the

rescaling. These discrepancies would mainly be indicated in extreme pixel values which require some correction. On the other hand, the K-means algorithm is based on medians, so we do not have to implement such corrections. Additionally, irregularities resulting from errors in the interpolation are investigated visually for each patient and in some cases the ROIs from the NIfTI files are manually adjusted to match the direction and orientation of the images.

The choice of the optimal clustering number is very important for avoiding over- or under-partitioning of the data. The method used for defining  $k$ , explained in Chapter 3.2.3.1, is robust and efficient, but there are also other more complex methods that could have been used if the time frame of the project had been longer.

The number of the studied patients is relatively limiting, so in some endpoints the groups have a low number of patients. This has been taken into consideration by choosing the Wilcoxon rank-sum test as an optimal option which does not require normally distributed data.

The survival analyses include only the patients that reached one of the endpoints within the latest follow-up. Nevertheless, some of the patients have been included in the study group at the earliest (2013) and some have joined at the latest (2017). This indicates different follow-up times depending on the date of inclusion, so a degree of uncertainty is expected to arise. The patients which have been followed the least have not completed the five-year following period and we do not know if they will reach one of the endpoints. Further on, if a patient has not reached any of the endpoints it is censored and not included in the analyses. The effect can be remedied by examining multiple survival endpoints at different times (ex. six months, one year, two years) or by using the time component as a grouping factor in the Cox proportional-hazards analysis.

## 5.2 Results

### 5.2.1 Statistical analyses

#### 5.2.1.1 T<sub>2</sub>-weighted images

The correlation of the pre-treatment and post-treatment parameters is different for the ROIs by the two radiologists “an” and “shh”. The comparison of the results shows that the cluster centers are relatively unchanged. This is expected since the delineations are based on the same MR images. However, there is a median difference of 2.4% between the median CVFs of the two different ROIs which makes Cluster 2 the most dominant (Figure 5.1). This is a consequence of the variation in the delineations which is caused by the subjective interpretation as discussed in Chapter 5.1.

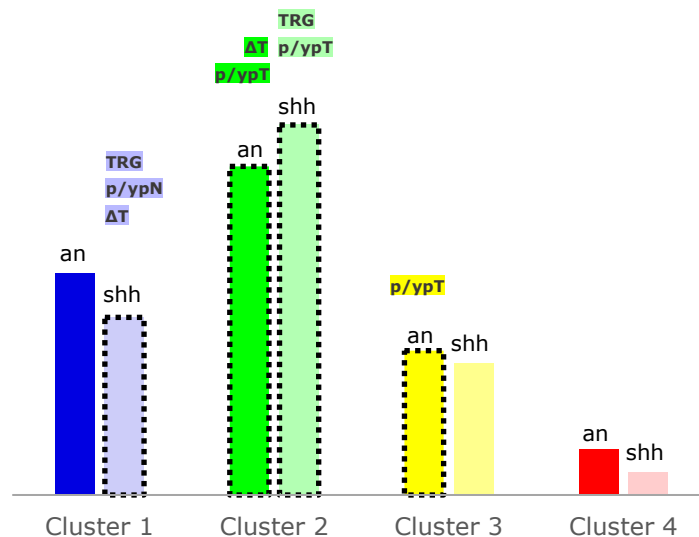


**Figure 5.1:** Median cluster volume fractions (%) for each cluster for the two delineations drawn by radiologist “an” and “shh” respectively. The median change in the fractions is 2.4%. For the ROIs from “shh” the median cluster fraction in Cluster 2 increases, while decreasing in the other clusters. (The dotted contours indicate statistical significance in the difference between the two groups for the cluster with the correlated parameter(s) at the top)

The results indicate higher correlation sensitivity to the parameters for the delineation by “shh”. Cluster 1 shows statistical significance in the difference between the two patient groups for the parameters p/ypT, ΔT, p/ypN and TRG, while Cluster 2 is correlated to p/ypT and TRG. Although it is difficult to assess the sensitivity of correlation with the parameters, it is possible to conclude that larger ROIs provide clustering that yields improved association to the parameters in the case of T<sub>2</sub>-weighted images. We could explain the increased sensitivity, if we consider that larger delineations can include portions of the

normal tissue. The K-means algorithm is provided with data from a larger area where it has a wider range of pixel intensities, which make it easier to provide improved separation of the clusters. This allows higher precision in the distinguishment of the regions and therefore it can improve the investigation of potential correlation with the parameters.

### 5.2.1.2 Diffusion-weighted images

An overview of the results from the six b-values of the DW images ( $b = \{0; 25; 50; 100; 500; 1000\}$ ) shows that the highest correlation with the parameters can be obtained for  $b = 50 \text{ s/mm}^2$ .

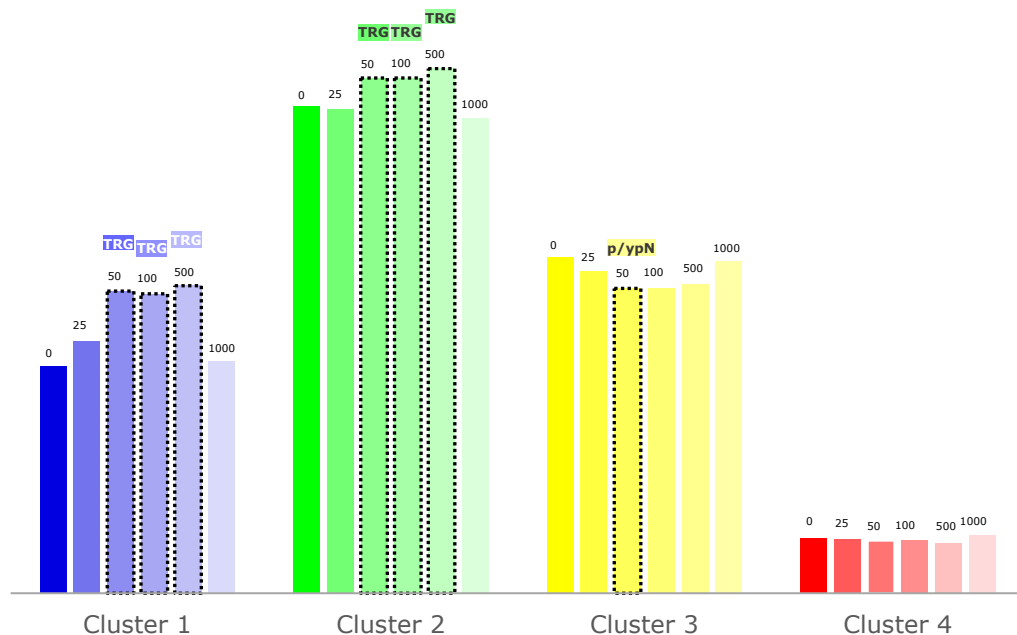


**Figure 5.2:** Median CVFs (%) for each cluster for the values of  $b = \{0, 25, 100, 500, 1000\}$  (radiologist "an"). (The dotted contours indicate statistical significance in the difference between the two groups for the cluster with the correlated parameter at the top)

There is a significant difference between the two groups in the clustered data for the DW images with  $b = 50 \text{ s/mm}^2$  (radiologist - "an") for the 'p/ypN' parameter in Cluster 3 and the 'TRG' parameter in cluster 1 and cluster 2. (Table 4.12). For  $b = 100 \text{ s/mm}^2$  (Table 4.14) there is correlation with the 'TRG' parameter in cluster 1 and cluster 2. For  $b = 500 \text{ s/mm}^2$  (Table 4.16) the difference in the groups is within the significance limit also for the parameter 'TRG' in cluster 1 and cluster 2. For  $b = 0 \text{ s/mm}^2$ ,  $b = 25 \text{ s/mm}^2$  and  $b = 1000 \text{ s/mm}^2$  there is no correlation between the clusters and the parameters.



The lack of correlation with the parameters for the low b-values is because these images do not contain enough diffusion signal which would help the K-means algorithm to produce effective differentiation of the clusters. In the higher b-values, on the other hand, there is too much diffusion which decreases the SNR as the noise is increased, so the algorithm becomes "confused" and cannot provide correct distinguishment. This results in poor clustering, which is not efficiently reflecting the different tumor regions, hence a correlation cannot be established.

The results demonstrate that for cluster 1 and cluster 2 from the DW images there is a strong correlation between the two patient groups (above/below the median volume) and the TRG. Therefore, the presence of a certain tumor properties illustrated through similar pixel intensities in the DW images can be used as an indicator for the expected grading of the tumor after the treatment (with neoadjuvant CRT and surgery). So, we can observe that the clustering approach used in this thesis shows strong evidence of a connection that will directly reflect the outcome of the treatment. Additionally, we can consider the evidence that TRG can be used as an independent predictor for survival (because patients graded with TRG0 have shown improved progression-free survival) (Chapter 3.1.2)[42]. This would amplify the drawn conclusion and we can go a step further by saying that the clustering based on pixel intensities for DW images can indicate the patient's survival. This has the potential to become a very powerful tool for assessing the patient's condition and for developing different treatment strategies in cases where the predicted outcome is expected to be negative.

In comparison, the DW images with  $b=50 \text{ s/mm}^2$  where the delineation has been performed by the radiologist - "shh" give results which show correlation to "p/ypT" for cluster 2 and " $\Delta T$ " and "p/ypT" for cluster 4. In this case, the connection with "TRG" is not visible in the results, which indicates that the larger ROIs are inefficient at providing precise data for better clustering. On the other side, the correlation with "p/ypT" is not present in the previous results, which could be a direct consequence of the smaller delineation, which does not include normal tissue to a significant extent. Therefore, further

analyses are needed, aimed at comparing all images with the two ROIs where a more precise conclusion might be drawn.

The data clustering from the ADC maps is attained at an optimal cluster number

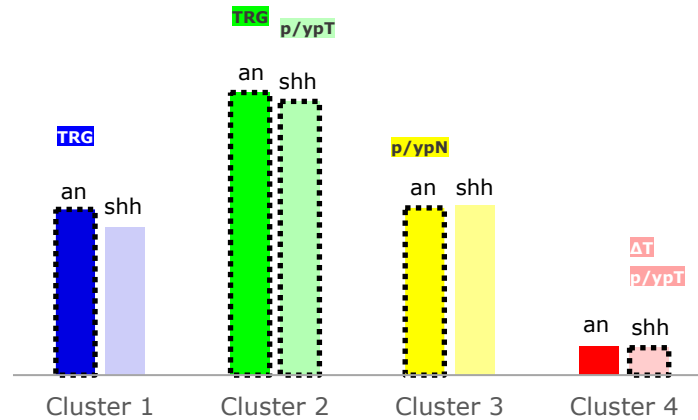


**Figure 5.3:** Median CVFs (%) for each cluster for the two delineations drawn by radiologist “an” and “shh” respectively for  $b=50$  s/mm<sup>2</sup>. The median change in the fractions is 0.97% which demonstrates a very small difference in the clustered results. (The dotted contours indicate statistical significance in the difference between the two groups for the cluster with the correlated parameter at the top)

$k=2$ . This is lower than the previous divisions where  $k=4$ , so an underlying reason could be the lack of detail compared to the anatomical  $T_2$ -weighted images and the DW images. The ADC maps represent only the diffusion, which is reflected in limited pixel intensity divergence. Such inability to truly reflect the distinction of the tumor regions results in poor correlation with the parameters. From this, we can conclude that the ADC maps are not suitable for clustering and cannot be used for further analyses.

### 5.2.1.3 $T_2$ -weighted and diffusion weighted

The project examines the possibility of combining data from the  $T_2$ -weighted and the DW images. The  $T_2$ -w images with the delineation which shows higher correlation to the parameters (radiologist – “shh”) are combined with the DW images with  $b$ -value that provides optimal results ( $b=50$  s/mm<sup>2</sup>; radiologist – “shh”)<sup>4</sup>. The script for defining the cluster number calculates  $k=5$ , which is higher than the cluster number when the images are analyzed separately ( $k=4$ ). The results cannot detect a connection between the clusters. One

<sup>4</sup> Note that  $T_2$ -w and DW images can be combined only for the same delineation (ROI), as the clustering tables contain voxel coordinates that correspond to that delineation only.

reason for the poor outcome can be the combination of different information from the two sequences which “confuse” the algorithm. It becomes difficult to make a distinction between the tumor regions. However, this seems counterintuitive, so further studies would have to confirm if a combination of this type would be beneficial for the correlation with the parameters.

### 5.2.2 Survival analyses

The investigation of the PFS in the survival analyses for the T<sub>2</sub>-weighted images does not show any correlation for the clustered data.

In the DW images with  $b=1000$  s/mm<sup>2</sup> the most dominant cluster (cluster 2 with median CVF=35,2%) demonstrates that PFS can be indicated directly from the clustering. Although, higher b-values are expected to provide lower SNR and result in poor correlation with the statistical parameters, this result shows the opposite in the case of investigating PFS. The advantage comes from the higher diffusion in the image, which causes a certain property of the tumor to become more visible. Then the K-means algorithm is able to distinguish this property (in this case a dominant region of the tumor) and directly connect its presence with a treatment outcome. Further studies would have to investigate how this relation can be defined more precisely and whether even higher b-values could provide correlation for smaller regions (clusters with lower median volume fractions).

For the data of the DW images with  $b=50$  s/mm<sup>2</sup>, where the ROIs have been drawn by the radiologist “shh” a statistical significance for  $p<0.05$  shows that cluster 1 can predict the treatment outcome. Once more, this can be explained with the larger delineation which in some cases can include normal tissue. Such conditions are beneficial for the algorithm as they provide higher contrast in the pixel intensities and the grouping can be performed more precisely.

A combination of the T<sub>2</sub>-weighted images and the DW images, as discussed in Chapter 5.2.1.3 (T<sub>2</sub>-w (“shh”) and DW ( $b=50$  s/mm<sup>2</sup> (“shh”))), is investigated for the survival analyses. The results indicate that the most dominant group (cluster 2 with median CVF of 39.6%) can be related with PFS. In this case, the largest area with similar pixel intensities (corresponding to a certain

approximately homogenous tumor region) is detected. This confirms the previous speculation that further investigation is in order, based on the expected increase in sensitivity due to the combined data. From the result we can observe that the joint information from the two sequences can help the algorithm in identifying tumor regions with similar properties, which directly influence the outcome of the treatment. Additionally, it is expected that this approach can be improved and extended for detecting correlation in smaller regions if more data is provided. Furthermore, this finding suggests a potential in combining data from different sequences and modalities to “feed” the algorithm with enough information for providing the required feedback.

### **5.3 Clinical implications**

The traditional morphological imaging mainly provides information about the size and the staging of the tumor but lacks quantitative information. The main aim of this thesis is to investigate predictive markers for the response to the treatment in rectal cancer patients. This would enhance the visual inspection with measurable quantities that reflect the heterogeneity of the tumor and can be compared for different patients. By introducing individualization in the treatment approach, it is possible to adjust the treatment and avoid surgery, use more aggressive CRT and/or intensify the follow-ups. The clustering technique is used for identifying tumor regions that are expected to yield a certain treatment outcome. For example, if the expected survival rate is high, based on the model’s prediction, it would be possible to avoid surgical interventions which have their adverse risks. Otherwise, if the analysis suggests high risk of developing distant metastases, then a more aggressive CRT can be utilized, and early detection can be obtained by increasing the number of follow-ups.

The results indicate that the survival of the patients can be directly predicted from DW images with higher b-values (investigated for  $b=1000$  s/mm<sup>2</sup>) and indirectly predicted ( $b=50$  s/mm<sup>2</sup>) through the TRG parameter as TRG0 is known to be correlated with PFS.[44] After more detailed analysis the outcome has the potential to be used in clinical practice for treatment prediction and

consequent treatment adjustment. That would require a program that will execute a combined and refined version of the scripts from the Appendices. Another option is to write a script for a toolbox for the MATLAB® directory, but this would require the user to have a certain knowledge in scripting for manually inserting the data. However, the approach currently has drawbacks, as it requires a powerful computer and long time for the image sorting and interpolation, coordinate extraction, clustering for different k-values and running the analyses.

## 5.4 Future work

The MRI scanners used in the Oxy-target study use a magnetic field ( $B_0$ ) with strength 1,5 Tesla. If we consider an increase in the field strength, we would get a higher excess in the  $\alpha$  population of the two eigenstates, which yields higher sensitivity. This would provide better SNR that could have been useful for more precise delineation and staging of the tumors. However, that would also increase the sensitivity to movement and susceptibility artefacts. As a result, a trade-off has to be made for the optimal choice of field strength, but other datasets can investigate if a stronger field would improve the correlation results.

As the analysis indicated that an increase in ROI area could provide improved separation of the pixels, it can be expected that an increased sensitivity would give better distinguishment as well. Additionally, there can be investigations of less precise delineations where larger portions of the normal tissue are included. It is expected that the algorithm would then easily identify the normal tissue and create a cluster corresponding to its properties. This indicates that the precision of the ROI is not as important in the cluster analyses, as it is for the radiotherapy in dose distribution calculations, and it could even be more beneficial for less precise delineations. However, within the scope of the "Oxy-target" dataset, this could be investigated in future studies by clustering for all images for the larger delineations drawn by radiologist "shh".

Based on the explained uncertainty in Chapter **Error! Reference source not found.** from the period of inclusion in the study and the time for follow-up for

the calculation of PFS, a future study could investigate multiple survival endpoints at different times. If the PFS is probed for one and/or two years additionally and the results indicate relation between the clusters and the survival, then it would be possible to confirm the findings with less uncertainty. Otherwise, it is possible to complement the Cox-proportional hazards regression with an additional covariate – “time” and get the same effect.

The combination of the two sequences improves the predictability of the treatment outcome, but within the time frame of this project only one combination was probed. Future work could investigate other (if not all) combinations.

## 6 Conclusion

In this project,  $T_2$ -weighted, DW MR images and patient data from 79 rectal cancer patients were analyzed. The results show that it is possible to identify different regions in the tumors based on the K-means clustering technique. The statistical analyses indicate that the relative size of several of the identified regions can be correlated to pre- and post-treatment parameters. The survival analyses showed strong link between the largest region (dominant cluster) and the outcome of the treatment for a larger b-value ( $b=1000 \text{ s/mm}^2$ ) when using DW MR images as input to the analysis. This can be beneficial in clinical practice as it introduces quantitative properties based on clustering based on images routinely acquired in clinical practice. Individualization of the assessment can provide valuable information about the expected outcome so that the treatment can be adjusted and better results can be obtained.

A strong correlation between the DW MR images ( $b=50 \text{ s/mm}^2$ ) and the TRG parameter show that this approach can be a powerful tool for assessing response to CRT in patients with LARC. A combination of  $T_2$ -weighted and DW images demonstrates more efficient clustering which reflects the tumor heterogeneity more precisely and gives better conditions for assessing the treatment results. This could also be considered as a potential pointer that combined data from different MR sequences could give even more information to the algorithm and result in improved clustering.

This approach is highly dependent on the delineation of the tumor. However, the results indicate that a larger ROI where some portions of the normal tissue might be included are beneficial for improved distinction of the tumor regions. A comparison between the ROIs drawn by two radiologists where the first case is more precise and the other is larger, showed that the latter yields better

results. This is based on the improved clustering which gives better reflection of the distinguishment in the relatively homogenous tumor regions.

Future studies could investigate other datasets for confirming if the results are reproducible and for determining which tumor property is an indicator for predicting a certain treatment outcome.

Another point that could be studied further is the spatial distribution of the clusters. Appendix C.2 shows a script for visualizing the cluster distribution and Appendix C.3 displays tumor median sections with different outcomes. The spatial distribution analyses could be performed visually for the clusters that have shown correlation with the outcomes in the statistical analysis. This approach can provide information about the spatial characteristics of the grouped voxels. For the purpose of better observation, the median slices where the tumor is most advanced should be selected for each patient.



## References

- [1] R. Glynne-Jones, L. Wyrwicz, G. Brown, C. Rodel, A. Cervantes, D. Arnold, on behalf of the ESMO Guidelines Committee, "Rectal cancer: ESMO Clinical Practice Guide for diagnosis, treatment and follow-up", *Annals of Oncology 28 (Supplement 4)*, 2017, pp.22-40.
- [2] International Agency for Research on Cancer, World Health Organization, *Data source: GLOBOCAN*, <https://www.gco.iarc.fr>, 2018, Accessed: 2019-01-26.
- [3] Cancer Registry of Norway, "Cancer in Norway 2016 - Cancer incidence, mortality, survival and prevalence in Norway," *Oslo: Cancer Registry of Norway*, 2012.
- [4] Marusyk A, Polyak K, "Tumor heterogeneity: causes and consequences", *Biochim Biophys Acta 1805(1)*, 2010, pp.105-117.
- [5] Gerlinger M, Rowan AJ, Horswell S, et al., "Intratumor heterogeneity and branched evolution revealed by multiregion sequencing", *N Engl J Med 366(10)*, 2012, pp.883-892.
- [6] Alic L, Niessen WJ, Veenland JF, "Quantification of heterogeneity as a biomarker in tumor imaging: a systematic review", *Plos One 9(10)*, 2014, pp.110-124.
- [7] World Health Organization, *Cancer*, <https://www.who.int/topics/cancer>, 2019, Accessed: 2019-02-12.
- [8] Strachan T, Goodship J, Chinnery P, "Genetics and genomics in medicine", *Garland Science, Taylor & Francis Group, LLC*, 2015, pp.373-384, ISBN: 978-0-8153-4480-3.
- [9] Hal EJ, Giaccia A, "Radiology for the radiologist - 7<sup>th</sup> edition", *Lippincott Williams & Wilkins*, 2012, pp.322-465, ISBN: 978-1-60831-193-4.
- [10] Chakraborty S, Rahman T, "The difficulties in cancer treatment", *Ecancermedicalscience 6*, 2012, pp.16-17.
- [11] Kufe D, Pollock RE, Wechselbaum RR, Bast RC, Gansler T, Holland JF, Frei E, "Cancer Medicine - 6<sup>th</sup> edition", *Hamilton (ON)*, 2003, pp.144-145, ISBN: 1-55009-213-8.
- [12] Grzywa TM, Paskal W, Włodarski PK, "Intratumor and intertumor heterogeneity in melanoma", *Transl Oncol. 10(6)*, 2017, pp.956-975.

- [13] "Surgery for rectal cancer", *Data source: Texas Oncology*, <https://www.texasoncology.com/types-of-cancer/rectal-cancer/surgery-for-rectal-cancer>, 2016, Accessed: 2019-02-13.
- [14] Stewart CB, Geoffrey C, "Magnetic Resonance Imaging: Physical and Biological Principles – 4<sup>th</sup> edition", *Elsevier Mosby*, 2015, pp.44-48, ISBN: 978-0-323-07354-7.
- [15] Månsson S, Bjornerud A, "The Chemistry of Contrast Agents in Medical Magnetic Resonance Imaging", *Chichester: Wiley*, 2001, pp. 1-35, ISBN: 978-1-119-99176-2.
- [16] Marinus TV, Jacques AB, "Magnetic Resonance Imaging: Theory and Practice – 3<sup>rd</sup> edition", *Springer*, 2003, pp.78-89, ISBN: 978-3-642-07823-1.
- [17] Westbrook C, Roth CK, Talbot J, "MRI in Practice – 4<sup>th</sup> edition", *Wiley-Blackwell*, 2011, pp.143-156, ISBN: 978-1-444-33743-3.
- [18] Tanner JE, Stejskal E, "Restricted Self-Diffusion of Protons in Colloidal Systems by the Pulsed-Gradient, Spin-Echo Method", *Journal of Chemical Physics* 49, 1968, pp.68-81
- [19] Heidi JB, Timothy EJB, "Diffusion MRI: From quantitative measurement to in-vivo neuroanatomy", *Elsevier*, 2009, pp.243-245, ISBN: 978-0-12-374709-9.
- [20] Jones DK, "Diffusion MRI: Theory, Methods and Applications", *Oxford University press*, 2011, pp.76-93, ISBN: 978-0-19-536977-9.
- [21] Philip K, Guilhem PS, Kaz N, Sendhil V, Vimalan V, Vijayasarathi N, Kai HG, "Stejskal – Tanner equation derived in full", *Singapore Bioimaging Consortium*, 2012, pp.4-7.
- [22] Bammer R, "Basic principles of diffusion-weighted images", *Eur J Radiol* 45(3), 2003, pp.169-184.
- [23] Afaq A, Andreou A, Koh DM, "Diffusion-weighted magnetic resonance imaging for tumour response assessment: why, when and how?", *Cancer imaging* 10(1A), 2010, pp.179-188.
- [24] Shai SS, Shai BD, "Understanding Machine Learning: from theory to algorithms", *Cambridge University Press*, 2014, pp.10-23, ISBN: 978-1-107-05713-5.
- [25] Alex S, Vishwanathan SVN, "Introduction to Machine Learning", *Cambridge University Press*, 2008, pp.46-49, ISBN: 0-521-82583-0.
- [26] Hurwitz J, Kirsch D, "Machine learning for dummies", *John Wiley & Sons Inc.*, 2018, pp. 24-38, ISBN: 978-1-119-45494-6.

- [27] Christopher MB, "Pattern Recognition and Machine Learning (Information Science and Statistics)", *Springer*, 2006, pp.87-89, ISBN:978-0387-31073-2.
- [28] "Learning", *Oxford University Press*, [www.oed.com/viewdictionaryentry/Entry/11125](http://www.oed.com/viewdictionaryentry/Entry/11125), 2019, Accessed: 2019-02-25.
- [29] Mehryar M, Afshin R, Ameet T, "Foundations of Machine Learning – 2<sup>nd</sup> edition", *MIT Press*, 2018, pp. 142-148, ISBN:978-0-262-01825-8.
- [30] Tuceryan M, Jain AK, "Texture Analysis: The Handbook of Pattern Recognition and Computer Vision", *World Scientific Publishing C.*, 1998, pp.3-14, ISBN:981-02-1136-8.
- [31] Pietikainen MK, "Texture analysis in machine vision", *World Scientific Publishing C.*, 2000, pp.186-192, ISBN: 978-9-81024373-9.
- [32] Nailon WH, Open access peer-reviewed chapter: "Texture analysis methods for medical image characterization", *IntechOpen*, 2010, pp.24-28, ISBN:978-953-307-071-1
- [33] "Texture analysis", *MathWorks*, <https://mathworks.com/help/images/texture-analysis.html>, 2019, Accessed on: 2019-03-05.
- [34] Castellano G, Bonilha L, Li LM, Cendes F, "Texture analysis of medical images", *Clinical radiology* 59(12), 2004, pp. 1061-1069.
- [35] Kurani AS, Xu D-H, Furst J, Raicu DS, "Co-occurrence matrices for volumetric data. Proceedings", *7<sup>th</sup> IASTED International Conference on Computer Graphics and Imaging*, 2004, pp.3-4.
- [36] Yankai M, Chongda Z, Shuangmei Z, Xinming Z, Kai X, Hongmei Z, Chunwu Z, "MRI texture analysis in predicting treatment response to neoadjuvant chemoradiotherapy in rectal cancer", *Oncotarget* 9(15), 2017, pp.11999-12008.
- [37] "The OxyTarget study", *Acredit*, <http://www.acredit.no/the-oxytarget-study/>, Accessed on: 2019-03-10.
- [38] "Functional MRI of Hypoxia-mediated rectal cancer aggressiveness (OxyTarget)", *U.S. National Library of Medicine*, <https://clinicaltrials.gov/ct2/show/NCT01816607>, Accessed on: 2019-03-10.
- [39] Blum J, "Xeloda in the Treatment of Metastatic Breast Cancer", *Oncology* 55(Suppl 1), 1999, pp.16-20.
- [40] Larsson P-A, Carlsson G, Gustavsson B, Glimelisu G, Graf W, "Different Intravenous Administration Techniques for 5-Fluorouracil Pharmacokinetics and Pharmacodynamic Effects", *Acta Oncologica* 35(2), 1996, pp.207-212.

- [41] Edge SB, Compton CC, "The American Joint Committee on Cancer: the 7th Edition of the AJCC Cancer Staging Manual and the Future of TNM", *Official journal of the society of surgical oncology*, 2010.
- [42] Thies S, Lange R, "Tumor Regression Grading of Gastrointestinal Carcinomas after Neoadjuvant therapy", *Virchows Arch.* 472(2), 2018, pp.175-186.
- [43] Gress DM, Edge ST, Greene FL, et al. "Principles of cancer staging", *AJCC*, 2017, pp.28-31.
- [44] Kim SH, Chang HJ, Kim DY, et al. "What Is the Ideal Tumor Regression Grading System in Rectal Cancer Patients after Preoperative Chemoradiotherapy?", *Official journal of Korean Cancer Association* 48, 2015, pp.189-196.
- [45] Redalen KR, et al, "MRI volumetry for prediction of tumour response to neoadjuvant chemotherapy followed by chemoradiotherapy in locally advanced rectal cancer", *The British Journal of radiology* 88(1051), 2015.
- [46] Srinivasan A, Galban CJ, Johnson TD, et al., "Utility of the K-means clustering algorithm in differentiating apparent diffusion coefficient values of benign and malignant neck pathologies", *AJNR* 31, 2010, pp. 156-173.
- [47] "Outlier", *Oxford Dictionaries*, <http://www.oxforddictionaries.com/definition/english/outlier>.
- [48] Raykov YP, Boukouvalas A, Baig F, "What to do when K-Means Clustering Fails: A simple yet principled alternative algorithm", *Plos One* 11(9), 2016, pp.162-173.
- [49] Ortega J, Boone J, García María, "Research issues on K-means Algorithm: An Experimental Trial Using Matlab", *CEUR Workshop Proceedings* 534, 2009.
- [50] Maimon O, Rokach L, "Data mining and knowledge discovery handbook – 2<sup>nd</sup> edition", *Springer*, 2010, pp. 256-277, ISBN 978-0-387-09822-7.
- [51] Seif G, "The 5 clustering algorithms data scientists need to know", *Medium*, <https://towardsdatascience.com/the-5-clustering-algorithms-data-scientists-need-to-know-a36d136ef68>, 2018, Accessed on: 2019-04-01.
- [52] "NCI Dictionary of cancer terms", *National Cancer Institute*, <https://www.cancer.gov/publications/dictionaries/cancer-terms>, 2019, Accessed on: 2019-03-28.
- [53] Clark TG, Bradburn MJ, Love SB, Altman DG, "Survival Analysis Part I: Basic concepts and first analyses", *British Journal of Cancer* 89, 2003, pp.185-193.

- [54] Stephen J W, "What is a Cox model?", *Hayward Medical Communications*, 2009, pp. 1-4.
- [55] Bewick Viv, Cheek L, Ball J, "Statistics review 12: Survival analysis", *Clinical care* 8(5), 2004, pp.389-394.
- [56] "Hazard function", *Wolfram® MathWorld*, <http://mathworld.wolfram.com/HazardFunction.html>, Accessed on: 2019-03-28.
- [57] Bradburn MJ, Clark TG, Love SB. Altman DG, "Survival Analysis Part II: Multivariate data analysis – an introduction to concepts and methods", *British Journal of Cancer* 89, 2003, pp.45-58.
- [58] Bhattacharya B, Habtzghi B, "Median of the p value under the alternative hypothesis", *The American Statistician* 56(3), 2002, pp.132-145.
- [59] Wasserstein RL, Nicole A, "The ASA's Statement on p-Values: Context, Process, and Purpose", *The American Statistician* 135, 2016, pp.38-44.
- [60] Harrington David, "Linear Rank Tests in Survival Analysis". *Encyclopedia of Biostatistics*, 2005, pp.387-410, ISBN: 978-0-470-011-812.
- [61] Goel MK, Khanna PKJ, "Understanding survival analysis: Kaplan-Meier estimate", *International journal of Ayurveda research* 44(2), 2010, pp.56-67.
- [62] Mendes M, Pala A, "Type I Error Rate and Power of Three Normality Tests", *Pakistan Journal of Information and Technology* 2(2), 2003, pp.135-139.
- [63] Razali M, Bee N&Y, (2011). "Power Comparisons of Shapiro-Wilk, Kolmogorov-Smirnov, Lilliefors and Anderson-Darling Tests", *Journal of Statistical modeling and Analytics* 2(1), 2011, pp.25-27.
- [64] Kim TK, "T test as a parametric statistic" *Korean journal of anesthesiology* 68(6), 2015, pp.540-546.
- [65] Bridge PD, Sawilowsky SS, "Increasing Physicians' awareness of the impact of Statistics on research outcomes: Comparative power of the t-test and Wilcoxon Rank-Sum test in small samples applied research", *Journal of Clinical Epidemiology* 52(3), 1999, pp. 230-231.
- [66] Li, Jun et al., "TNM Staging of Colorectal Cancer Should be Reconsidered According to Weighting of the T Stage (Verification Based on a 25-Year Follow-Up)", *Medicine Journal* 95(6), 2016, pp.271-281.
- [67] Njeh C.F, "Tumor delineation: The weakest link in the search for accuracy in radiotherapy" *Journal of medical physics*, 33(4),2008, pp. 136–140.

[68] Weiss E, Hess CF, "The impact of gross tumor volume (GTV) and clinical target volume (CTV) definition on the total accuracy in radiotherapy theoretical aspects and practical experiences", *Journal of medical physics*, 171(9),2003, pp. 21-30.

[69] Luigi S, "Intestinal motility disorders medication", MedScape, <http://emedscience.medscape.com/article/179937-medication>, 2017, Accessed on: 11-08-2019.

# Appendix A

## Matlab scripts

### A1: Image sorting

```
function data = loadAndSortDICOM(patientFolder, imgType)
    %%%%%%%%%%%%%%%%%%%%%%%%%%%%%%%%%%%%%%%%%%
    %    %%Test inputs
    %    clearvars
    %    patientFolder = 'C:/Users/HP/Desktop/Master_Thesis/Data/';
    %    imgType = 'DWI'; % or 'T2'
    %%%%%%%%%%%%%%%%%%%%%%%%%%%%%%%%%%%%%%%%%%

    %%This script works for both image types, T2 and DWI
    %%(as the T2 images have all DiffusionBValue = 0)

    % List all image files and count them
    imList = dir(fullfile(patientFolder, imgType, '*#.dcm'));
    nIm = size(imList,1);

    % read all headers, store the needed information
    for imgNr = nIm : -1 : 1 % loop backwards to do preallocation
        info(imgNr) = dicominfo(fullfile(patientFolder, imgType, imList(imgNr).name));
    end

    % Extract the information needed to sort the images
    % get list with b-values
    bValue = [info.DiffusionBValue]';

    % get a list with the patient position
    IPP = [info.ImagePositionPatient]';
    zValue = IPP(:,3); % extract the z-value

    % Determine how to sort the images
    sortInd = table( zValue, bValue ); % combine both sort-variables in a table
    sortInd.fileName = {info.FileName}'; % add the file name to the table;

    [~,~, sortInd.zValueIndex] = unique(sortInd.zValue);
    [~,~, sortInd.bValueIndex] = unique(sortInd.bValue);

    % Add the info needed to scale the image
    sortInd.RescaleIntercept = [info.RescaleIntercept]';
    sortInd.RescaleSlope = [info.RescaleSlope]';

    % Load the images in a sorted way
    nSlices = length(unique(zValue)); % number of slices
    nbv = length(unique(bValue)); % number of b-values
    data.img = nan(info(1).Height, info(1).Width, nSlices, nbv); % Preallocate
```

```

for zValueIndex = 1:nSlices
    for bValueIndex = 1:nbv
        % find image with the correct idxSlice and bValueIndex
        imgInfo = sortInd(sortInd.zValueIndex == zValueIndex & ...
            sortInd.bValueIndex == bValueIndex,:);
        % load the image and save it
        data.img(:,:,zValueIndex, bValueIndex) = ...
            double(dicomread( imgInfo.fileName{1})) * imgInfo.RescaleSlope +
imgInfo.RescaleIntercept;
        end
    end % All images are read

    % also store the b values
    data.bValue = unique(sortInd.bValue);

    % Save the spatial information (needed to determine the image grid)
    data.ImageOrientationPatient = info(1).ImageOrientationPatient;
    data.PixelSpacing           = info(1).PixelSpacing;

    % save the Image position patient
    % ( it is the same for all b values, so only store b=0)
    for zValueIndex = 1:nSlices
        data.ImagePositionPatient(zValueIndex,:) = IPP(...
            sortInd.zValueIndex == zValueIndex & ...
            sortInd.bValue == 0, :);
    end
end
end

```

## A2: Grid coordinates

```

function grid = getGridCoordinates(imgData)

% function to get the grid coordinates for an image, requires as input the
% data form loadAndSortDicom.m

%%%%%%%%%%%%%%%%%%%%%%%%%%%%%%%%%%%%%%%%%%
%   %%Test input
%   clearvars
%   imgData = load('C:/Users/HP/Desktop/Master_Thesis/Data/Oxytarget_103
PRE/DWI/ImgData.mat');
%%%%%%%%%%%%%%%%%%%%%%%%%%%%%%%%%%%%%%%%%%

% Set up the coordinates
xq = zeros( size(imgData.img(:,:,:,1)));% % preallocate empty matrix, use only the spatial
dimensions
yq = xq;
zq = xq;

Xq      = imgData.ImageOrientationPatient(1:3)';    % row values
Yq      = imgData.ImageOrientationPatient(4:6)';    % column values
dimPix  = imgData.PixelSpacing(1);                 % in mm

```



```

idx = double(0:size(imgData.img,1)-1);
[cMat,rMat] = meshgrid(idx,idx);

PatientsPosition = imgData.ImagePositionPatient;

% Get voxel coordinates
for k_idx = 1:size(imgData.img,3)
    S = PatientsPosition(k_idx,:);
    xq(:,:,k_idx) = (Xq(1)*rMat+Yq(1)*cMat)*dimPix + S(1);
    yq(:,:,k_idx) = (Xq(2)*rMat+Yq(2)*cMat)*dimPix + S(2);
    zq(:,:,k_idx) = (Xq(3)*rMat+Yq(3)*cMat)*dimPix + S(3);
end

%combine grid coordinates
grid.x = xq;
grid.y = yq;
grid.z = zq;

end

```

### A3: Interpolate DWI to T<sub>2</sub>-weighted image

```

function intImg = interpolateToGrid(dataT2, dataDWI)

posq = [dataDWI.grid.x(:), dataDWI.grid.y(:), dataDWI.grid.z(:)]; %DWI
pos = [dataT2.grid.x(:), dataT2.grid.y(:), dataT2.grid.z(:)]; % T2

% prepare empty image to save the result
intImg = zeros([size(dataT2.img), size(dataDWI.img,4)]);

% Loop over all images in 3d (-> different b values)
for idx = 1:size(dataDWI.img,4)
    % Get corresponding image;
    Vq = dataDWI.img(:,:,,idx);

    % interpolate the image
    % (Use linear interpolation between sample points, set outside values
    % to NaN);
    F = scatteredInterpolant(posq, Vq(:), 'linear', 'none');

    % get values of the image for the coordinates of the T2 image'
    V = F(pos);

    % rearrange from vector to matrix
    intImg(:,:,,idx) = reshape(V, size(dataT2.img));
end

% display the result to check
view3dgui(interpolatedDWI(:,:,,3))

% save the result
save([patientFolder '/InterpolatedDWI.mat']);

```

## A4: Extract pixel intensity for ROI

```

% This script demonstrates a simplified extraction for one b-value of the DWI
% but it can be used for all b-values and the T2-weighted images

% Load Region of Interest (Load NIFTI file)
filePath = 'C:/Users/HP/Desktop/Master_Thesis/Data/';

patientList = [24 48 49 50 51 52 55 56 57 58 59 61 64 65 67 68 69 72 74 ...
  77 78 79 80 83 85 87 88 89 90 91 94 95 96 99 103 110 113 115 116 118 ...
  120 121 122 123 125 127 128 131 133 134 138 143 144 145 146 148 149 ...
  150 153 154 155 156 157 160 163 164 165 166 170 171 172 173 174 175 ...
  177 176];

n = length(patientList);

%Create a loop that will read the ROIs for the analyzed patients
for patient = 1:n

    patientNr = patientList(patient);
    patientNr = int2str(patientNr);

    %Load the saved matrices from the previous step
    load([filePath 'Oxytarget_' patientNr ' PRE/InterpolatedDWI.mat']);

    %Load the ROI from the NIFTI file
    nifty = load_untouch_nii([filePath 'Oxytarget_' patientNr...
        ' PRE/binary/an/tumour.nii']);
    info = niftiinfo([filePath 'Oxytarget_' patientNr...
        ' PRE/binary/an/tumour.nii']);

    % Check if z-axis needs to be inverted
    [~,~,z1] = transformPointsForward(info.Transform,1,1,1);
    [~,~,z2] = transformPointsForward(info.Transform,1,1,100);
    neededInversion = (z2-z1)<0;

    % Modify to match with T2
    ROI = nifty.img;
    ROI = imrotate(flip(ROI), -90)>0;
    if neededInversion
        ROI = ROI(:,:,size(ROI,3):(-1):1);
    end

    % Visual inspection
    figure
    view3dgui(imT2)

    % Extract pixel intensity for the ROI only
    b0_all = interpolatedDWI(:,:,,1);
    b0 = b0_all(ROI);

    save([filePath 'Oxytarget_' patientNr ...
        ' PRE/ROI.mat'],'ROI');
    save([filePath 'Oxytarget_' patientNr ...
        ' PRE/DWI_b0.mat'],'b0');
end

```

## A5: Extract voxel coordinates for ROI

```

clear all

filePath = 'C:/Users/HP/Desktop/Master_Thesis/Data/';

patientList = [24 48 49 50 51 52 55 56 57 58 59 61 64 65 67 68 69 72 74 ...
  77 78 79 80 83 85 87 88 89 90 91 94 95 96 99 103 110 113 115 116 118 ...
  120 121 122 123 125 127 128 131 133 134 138 143 144 145 146 148 149 ...
  150 153 154 155 156 157 160 163 164 165 166 170 171 172 173 174 175 ...
  177 176];

n = length(patientList);

%Create a loop that will read the ROIs for the analyzed patients
for patient = 1:n

    patientNr = patientList(patient);

    %Load the saved matrices from the previous steps
    load([filePath 'Oxytarget_' int2str(patientNr)...
        ' PRE/imT2.mat']);
    load([filePath 'Oxytarget_' int2str(patientNr)...
        ' PRE/ROI.mat']);

    % List the image files
    imList = dir([filePath 'Oxytarget_' int2str(patientNr) ' PRE/T2/*#*']);
    nSlicesT2 = length(imList);

    for imageNr = 1:nSlicesT2

        info = dicominfo([filePath 'Oxytarget_' int2str(patientNr) ...
            ' PRE/T2/' imList(imageNr).name]);

        % Set up coordinates
        x = zeros(info.Width, info.Height, nSlicesT2);
        y = x;
        z = x;

        X = info.ImageOrientationPatient(1:3)';           % row values
        Y = info.ImageOrientationPatient(4:6)';           % column values
        dimPix = info.PixelSpacing(1);                     % in mm

        % idx = double(1:info.dimSlice);
        idx = double(0:info.Width-1);
        [cMat,rMat] = meshgrid(idx,idx);

        % Define 'PatientsPosition' as a 26x3 double containing x, y,
        % and z coordinates of the upper left corner of each image slice
        PatientsPosition = ones(nSlicesT2,3);

        for position = 1:3 % Extract information for x, y, and z
            PatientsPosition(imageNr,position) = ...
                info.ImagePositionPatient(position);
        end
    end
end

```

```

% Get voxel coordinates
for k_idx = 1:nSlicesT2
    %if imT2(512,512,k_idx) == 1
    S = PatientsPosition(k_idx,:);
    x(:,:,k_idx) = (X(1)*rMat+Y(1)*cMat)*dimPix + S(1);
    y(:,:,k_idx) = (X(2)*rMat+Y(2)*cMat)*dimPix + S(2);
    z(:,:,k_idx) = (X(3)*rMat+Y(3)*cMat)*dimPix + S(3);
end

% Logical indexing to get coordinates for ROI only
X = x(ROI);
Y = y(ROI);
Z = z(ROI);

% Save the coordinates for each patient in the corresponding folder
save([filePath 'Oxytarget_' int2str(patientNr) ...
    ' PRE/ROI_coordinates.mat'],'X','Y','Z')
end

```

## A6: Create matrix for K-means clustering

```

% Create cell arrays to store the values of all patients
Xn = cell(n,1);
Yn = Xn;
Zn = Xn;

for patient = 1:n

    patientNr = patientList(patient);

    load([filePath 'Oxytarget_' int2str(patientNr) ...
        ' PRE/ROI_coordinates.mat']);

    % Read in the coordinates for each patient into the array
    Xn{patient} = X;
    Yn{patient} = Y;
    Zn{patient} = Z;

    % Generate an array with the patients numbers
    patient_ = cell(length(X),1);
    patient_(:,1) = {patientNr};
    patient_ = cell2mat(patient_);
    patients{patient} = patient_;
end

% Convert to matrix
Xn = cell2mat(Xn);
Yn = cell2mat(Yn);
Zn = cell2mat(Zn);
Patient_number = cell2mat(patients);

% Generate a table to check the data
T_patient = table(Xn,Yn,Zn);
% Check with a small preview
T_preview = head(T_patient)

```

```
% Create a matrix to be used for the k-means analysis
b0_k = [xn Yn Zn b0];

save([filePath 'b0_k.mat'],'b0_k')
```

## A7: K-means clustering

```
clear all

filePath = 'C:/Users/HP/Desktop/Master_Thesis/Data/CODE/';

load([filePath 'ROI_voxel_coordinates_b2_shh.mat']);

% Run k-means and perform partition calculations
% K-means ++ is the default algorithm for initial cluster division
% The square of euclidean distance is the default distance target

% Save output to command window in a text file:
diary ('kmeansResults');

% Run k-means with k = 2 clusters:
rng (1); % Used so that the results can be reproducible
[idx2, C2, sumd2, D2] = kmeans (T2_k_4, 2, 'MaxIter', 500, 'Display', 'final', 'Replicates',
30);

% Count the number of data points belonging to cluster 1 and 2 respectively:
N21 = sum (idx2 (:) == 1);
N22 = sum (idx2 (:) == 2);

% Calculate MD21 and MD22 (average distance between observations and
% center):
MD21 = (sumd2 (1, 1)) / N21;
MD22 = (sumd2 (2, 1)) / N22;

% Calculate the subdivision target vu2 for k = 2 clusters:
vu2 = (MD21 + MD22) / 2;

% Find dmin2 (for k = 2 clusters, there's only one possibility):
dmin2 = pdist (C2);

% Calculate the target of overpartition vo2 for k = 2 clusters:
vo2 = 2 / dmin2;

% Run k-means with k = 3 clusters:
rng (1);
[idx3, C3, sumd3, D3] = kmeans(T2_k_4, 3, 'MaxIter', 500, 'Display','final', 'replicates',
30);

% Count the number of data points belonging to clusters 1, 2 and 3:
N31 = sum (idx3 (:) == 1);
N32 = sum (idx3 (:) == 2);
N33 = sum (idx3 (:) == 3);
```

```

% Calculate MD31, MD32 and MD33:
MD31 = (sumd3 (1, 1)) / N31;
MD32 = (sumd3 (2, 1)) / N32;
MD33 = (sumd3 (3, 1)) / N33;

% Calculate the subdivision target Vu3 for k = 3 clusters:
Vu3 = (MD31 + MD32 + MD33) / 3;

% Find dmin3 for k = 3 clusters:
dmin3 = min (pdist (C3));

% Calculate the target of overpartition Vo3 for k = 3 clusters:
Vo3 = 3 / dmin3;

% Run k-means with k = 4 clusters:
rng (1);
[idx4, C4, sumd4, D4] = kmeans(T2_k_4, 4, 'MaxIter', 500, 'Display', 'final','Replicates',
30);

% Count the number of data points belonging to clusters 1, 2, 3 and 4:
N41 = sum (idx4 (:) == 1);
N42 = sum (idx4 (:) == 2);
N43 = sum (idx4 (:) == 3);
N44 = sum (idx4 (:) == 4);

% Calculate MD41, MD42, MD43 and MD44:
MD41 = (sumd4 (1, 1)) / N41;
MD42 = (sumd4 (2, 1)) / N42;
MD43 = (sumd4 (3, 1)) / N43;
MD44 = (sumd4 (4, 1)) / N44;

% Calculate the subdivision target Vu4 for k = 4 clusters:
Vu4 = (MD41 + MD42 + MD43 + MD44) / 4;

% Find dmin4 for k = 4 clusters:
dmin4 = min (pdist (C4));

% Calculate target of overpartition Vo4 for k = 4 clusters:
Vo4 = 4 / dmin4;

% Run k-means with k = 5 clusters:
rng (1);
[idx5, C5, sumd5, D5] = kmeans (T2_k_4, 5, 'MaxIter', 500, 'Display', 'final', 'replicates',
30);

% Count the number of data points belonging to clusters 1, 2, 3, 4 and 5:
N51 = sum (idx5 (:) == 1);
N52 = sum (idx5 (:) == 2);
N53 = sum (idx5 (:) == 3);
N54 = sum (idx5 (:) == 4);
N55 = sum (idx5 (:) == 5);

% Calculate MD51, MD52, MD53, MD54 and MD55:
MD51 = (sumd5 (1, 1)) / N51;
MD52 = (sumd5 (2, 1)) / N52;
MD53 = (sumd5 (3, 1)) / N53;
MD54 = (sumd5 (4, 1)) / N54;
MD55 = (sumd5 (5,1)) / N55;

```

```

% Calculate the subdivision target Vu5 for k = 5 clusters:
Vu5 = (MD51 + MD52 + MD53 + MD54 + MD55) / 5;

% Find dmin5 for k = 5 clusters:
dmin5 = min (pdist (C5));

% Calculate the target of overpartition Vo5 for k = 5 clusters:
Vo5 = 5 / dmin5;

% Runs k-means with k = 6 clusters:
rng (1);
[idx6, C6, sumd6, D6] = kmeans (T2_k_4, 6, 'MaxIter', 500, 'Display', 'final','Replicates',30)

% Count the number of data points belonging to groups 1, 2, 3, 4, 5 and 6:
N61 = sum (idx6 (:) == 1);
N62 = sum (idx6 (:) == 2);
N63 = sum (idx6 (:) == 3);
N64 = sum (idx6 (:) == 4);
N65 = sum (idx6 (:) == 5);
N66 = sum (idx6 (:) == 6);

% Calculate MD61, MD62, MD63, MD64, MD65 and MD66:
MD61 = (sumd6 (1, 1)) / N61;
MD62 = (sumd6 (2, 1)) / N62;
MD63 = (sumd6 (3, 1)) / N63;
MD64 = (sumd6 (4, 1)) / N64;
MD65 = (sumd6 (5, 1)) / N65;
MD66 = (sumd6 (6, 1)) / N66;

% Calculate the subdivision target Vu6 for k = 6 clusters:
Vu6 = (MD61 + MD62 + MD63 + MD64 + MD65 + MD66) / 6;

% Find dmin6 for k = 6 clusters:
dmin6 = min (pdist (C6));

% Calculate the target of overpartition Vo6 for k = 6 clusters:
Vo6 = 6 / dmin6;

% Create vectors with sub and overlay functions respectively
% k = 2,3,4,5,6:

Vuvector = [Vu2; Vu3; Vu4; Vu5; Vu6];
Vovektor = [Vo2; Vo3; Vo4; Vo5; Vo6];

% Find max and min for Vu:
maxVu = max (Vuvector);
minVu = min (Vuvector);

% Normalize Vuvector to enter values in range [0, 1]:
Vunorm = (Vuvector - minVu) / (maxVu - minVu);

% Find max and min for Vo:
maxVo = max (Vovektor);
minVo = min (Vovektor);

% Normalize Vovektor to enter values in range [0, 1]:
Vonorm = (Vovektor - minVo) / (maxVo - minVo);

```

```

% Add Vunorm and Vonorm:
Vsv = Vunorm + Vonorm;

% Find minimal Vsv:
minVsv = min (Vsv);

% Save all variables:
save 'Results K-means from T2.mat';

% Plot normalized vectors to inspect the value of the optimal cluster number
figure
plot(Vsv, '-o', 'MarkerSize',4, 'Linewidth',1.3)
ylabel('Normalized partitioning')
set(gca, 'YTick', (0:0.2:1))
xlabel('Number of clusters')
xlim([1 5])
set(gca, 'XTick', (1:1:6))
xticklabels({'2', '3', '4', '5', '6'})
hold on
plot(Vunorm, '--o', 'MarkerSize',3, 'Linewidth',1)
plot(Vonorm, '--o', 'MarkerSize',3, 'Linewidth',1)
hold off
legend('Vsv=Vo*+Vu*', 'Vu*=normalized subdivision vector', 'Vo*=normalized overpartition
vector')

```

## A8: Calculation of Cluster Volume Fraction (CVF)

```

clear all

filePath = 'C:/Users/HP/Desktop/Master_Thesis/Data/';

% Generate groups of patients median volume fraction for
% each cluster for the defined optimal cluster number - k

% Load the matrix from the previous step
load ([filePath 'Results K-means from T2.mat']);

patientList = [24 48 49 50 51 52 55 56 57 58 59 61 64 65 67 68 69 72 74 ...
    77 78 79 80 83 85 87 88 89 90 91 94 95 96 99 103 110 113 115 116 118 ...
    120 121 122 123 125 127 128 131 133 134 138 143 144 145 146 148 149 ...
    150 153 154 155 156 157 160 163 164 165 166 170 171 172 173 174 175 ...
    177 176];

n = length(patientList);

% Get idx4 in an array for each patient separately (in this case k=4)
result = cell(n,1);
k = 1;
for patient = 1:n
    patientNr = patientList(patient);

    % Load the saved coordinates from the previous step
    load([filePath 'Oxytarget_' int2str(patientNr) ...
        ' PRE/T2/ROI_coordinates.mat']);

```



```

    result{patient} = idx4(k:(k+length(X)-1));
    k = k + length(X);
end

% Counts the number of voxels with values 1, 2 and 3 for each patient:
cluster1 = cellfun( @(x) sum( x == 1, 1 ), result, 'UniformOutput', 0);
cluster2 = cellfun( @(x) sum( x == 2, 1 ), result, 'UniformOutput', 0);
cluster3 = cellfun( @(x) sum( x == 3, 1 ), result, 'UniformOutput', 0);
cluster4 = cellfun( @(x) sum( x == 4, 1 ), result, 'UniformOutput', 0);

% Clusters 1,2 and 3 are concatenated into a matrix
clusters = cell2mat( horzcat( cluster1, cluster2, cluster3, cluster4));

% Total number of voxels with values 1, 2, 3 and 4 for each tumor(patient)
% (the sum is along the rows (second dimension))
clusters(:, 5) = sum( clusters, 2);

% Generate matrices for the results
% (CVF = Cluster Volume Fraction)
CVF1 = zeros(n,1);
CVF2 = zeros(n,1);
CVF3 = zeros(n,1);
CVF4 = zeros(n,1);

% Calculate the volume fraction of clusters 1,2 and 3 for each patient
for patient = 1:n
    CVF1(patient, 1) = clusters(patient, 1)/clusters(patient, 5);
    CVF2(patient, 1) = clusters(patient, 2)/clusters(patient, 5);
    CVF3(patient, 1) = clusters(patient, 3)/clusters(patient, 5);
    CVF4(patient, 1) = clusters(patient, 4)/clusters(patient, 5);
end

% Find the median value for each cluster
medianCVF = [median(CVF1); median(CVF2); median(CVF3); median(CVF4)];

% Group patients in two groups above and below the median volume
% for each cluster (if CVF > median the value is stored % in column 2
% if CVF < median the value is stored in column 3)

% Cluster 1:
for patient = 1:n
    if CVF1(patient,1) > median(CVF1(:,1));
        CVF1(patient,2) = CVF1(patient,1);
    elseif CVF1(patient,1) < median(CVF1(:,1));
        CVF1(patient,3) = CVF1(patient,1);
    end
end

% Cluster 2:
for patient = 1:n
    if CVF2(patient,1) > median(CVF2(:,1));
        CVF2(patient,2) = CVF2(patient,1);
    elseif CVF2(patient, 1) < median(CVF2(:,1));
        CVF2(patient,3) = CVF2(patient,1);
    end
end
end

```

```

% Cluster 3:
for patient = 1:n
    if CVF3(patient,1) > median(CVF3(:,1));
        CVF3(patient,2) = CVF3(patient,1);
    elseif CVF3(patient, 1) < median(CVF3(:,1));
        CVF3(patient,3) = CVF3(patient,1);
    end
end

% Cluster 4:
for patient = 1:n
    if CVF4(patient,1) > median(CVF4(:,1));
        CVF4(patient,2) = CVF4(patient,1);
    elseif CVF4(patient, 1) < median(CVF4(:,1));
        CVF4(patient,3) = CVF4(patient,1);
    end
end

% Cluster 1
% Find row number and value for CVF1>median
[row11, ~, v11] = find (CVF1 (:, 2));
% Find row number and value for CVF1<median
[row12, ~, v12] = find (CVF1 (:, 3));
% Store new array for CVF1>median (h = high) and CVF<median (l=low)
GhCVF1 = [row11, v11];
GlCVF1 = [row12, v12];

% Cluster 2
% Find row number and value for CVF1>median
[row11, ~, v11] = find (CVF2 (:, 2));
% Find row number and value for CVF1<median
[row12, ~, v12] = find (CVF2 (:, 3));
% Store new array for CVF1>median (h = high) and CVF<median (l=low)
GhCVF2 = [row11, v11];
GlCVF2 = [row12, v12];

% Cluster 3
% Find row number and value for CVF1>median
[row11, ~, v11] = find (CVF3 (:, 2));
% Find row number and value for CVF1<median
[row12, ~, v12] = find (CVF3 (:, 3));
% Store new array for CVF1>median (h = high) and CVF<median (l=low)
GhCVF3 = [row11, v11];
GlCVF3 = [row12, v12];

% Cluster 4
% Find row number and value for CVF1>median
[row11, ~, v11] = find (CVF4 (:, 2));
% Find row number and value for CVF1<median
[row12, ~, v12] = find (CVF4 (:, 3));
% Store new array for CVF1>median (h = high) and CVF<median (l=low)
GhCVF4 = [row11, v11];
GlCVF4 = [row12, v12];

save ('CVF data for K-means with T2 for k = 4.mat');

```

## A9: Extract parameter data from Excel for statistical analyses

The recorded data for the tumor staging from the study is provided in an Excel file. The following script extracts the a column that is relevant for the analysis. The same code applies for all other parameters in the statistical analysis of this project.

```
% Load data from excel

clear all

filePath = 'C:/Users/HP/Desktop/Master_Thesis/Data/';

patientList =[24 48 49 50 51 52 55 56 57 58 59 61 64 65 67 68 69 72 74 ...
    77 78 79 80 83 85 87 88 89 90 91 94 95 96 99 103 110 113 115 116 118 ...
    120 121 122 123 125 127 128 131 133 134 138 143 144 145 146 148 149 ...
    150 153 154 155 156 157 160 163 164 165 166 170 171 172 173 174 175 ...
    177 176];

n = length(patientList);

% Read in patients numbers from first column in the sheet
[num,patient] = xlsread([filePath 'Outcome_data.xlsx'],'A1:A193');
patient=regexp(patient,'\d+(\.)(\d+)?','match');
patient=str2double([patient{:}]);
patient(~ismember(patient,patientList))= 0;
patient = patient(:);

% Read in column containing p/yPT
out = xlsread('Outcome_data.xlsx','AK1:AK193');

% Eliminate patients which have not been analyzed in the previous steps
ypN = [patient,out];
indices = find(ypN(:,1)==0);
ypN(indices,:) = [];

% Remove NaN values
ypT(any(isnan(ypT),2),:) = [];

% Save as a matrix
save ([filePath 'patients_ypN'], 'ypN');
```

## A10: Extract parameter data from Excel for survival analyses

The Progression Free Survival (PFS) needs to be calculated from the provided Excel data based on the three endpoints with the following script.

```
clear all

filePath = 'C:/Users/HP/Desktop/Master_Thesis/Data/';

patientList =[24 48 49 50 51 52 55 56 57 58 59 61 64 65 67 68 69 72 74 ...
    77 78 79 80 83 85 87 88 89 90 91 94 95 96 99 103 110 113 115 116 118 ...
```

```

120 121 122 123 125 127 128 131 133 134 138 143 144 145 146 148 149 ...
150 153 154 155 156 157 160 163 164 165 166 170 171 172 173 174 175 ...
177 176];

n = length(patientList);

% Read in patients numbers from first column in the sheet
[num,patient] = xlsread([filePath 'Outcome_data.xlsx'],'A1:A201');
patient=regexp(patient,'\d+(\.)?(\d+)?','match');
patient=str2double([patient{:}]);
patient(~ismember(patient,patientList))= 0;
patient = patient(:);

% Read in columns containing time difference from
% events and time of inclusion in the study
out = xlsread('Outcome_data.xlsx','DF:DH');
out(out<0)=0;

% Eliminate patients which have not been analyzed in the previous steps
patient1 = [patient,out];
indices = find(patient1(:,1)==0);
patient1(indices,:) = [];

% Estimate the min time between inclusion and first event
patient1(patient1 == 0) = inf;
min_time = min(patient1(:,2:4),[],2);

% Add column to the existing matrix
patient1 = [patient1, min_time];
patient1(patient1 == inf) = 0;

% Generate Progression Free Survival (PFS) column
m = size(patient1,1);
for i = 1:m
    if patient1(i,5) > 0
        patient1(i,6) = 1;
    else patient1(i,6) = 0;
    end
end

% Generate columns for better overview of the contained data
Columns = {'Patient number', 'Local recurrence [days]', 'Metastasis [days]' ...
'Death [days]', 'Min time to first event', 'PFS'};

save('patient_PFS.mat');

```

## A11: Create datasets for the statistical/survival analyses

The following script can be used for generating datasets for the survival analyses, by importing the obtained PFS parameter from A10: Extract parameter data from Excel for survival analyses. The same script is used for the datasets in the statistical analyses with the parameters from A9: Extract parameter data from Excel for statistical analyses.

```

filePath = 'C:/Users/HP/Desktop/Master_Thesis/Data/';

% Load matrix with data extracted from excel
load('patients_ypT');
% Load CVF matrix from previous step
load('CVF data for K means with T2 for k = 4.mat');

% Add ypT value to the 6 patient groups
GlCVF1(:, 3) = param ((GlCVF1(:, 1))', [2]);
GhCVF1(:, 3) = param ((GhCVF1(:, 1))', [2]);
GlCVF2(:, 3) = param ((GlCVF2(:, 1))', [2]);
GhCVF2(:, 3) = param ((GhCVF2(:, 1))', [2]);
GlCVF3(:, 3) = param ((GlCVF3(:, 1))', [2]);
GhCVF3(:, 3) = param ((GhCVF3(:, 1))', [2]);
GlCVF4(:, 3) = param ((GlCVF4(:, 1))', [2]);
GhCVF4(:, 3) = param ((GhCVF4(:, 1))', [2]);
% The first column is transposed because it contains the patient number
% so the correct rows can be extracted from the data.

% Remove NaN values
GlCVF1(any(isnan(GlCVF1),2), :) = [];
GhCVF1(any(isnan(GhCVF1),2), :) = [];
GlCVF2(any(isnan(GlCVF2),2), :) = [];
GhCVF2(any(isnan(GhCVF2),2), :) = [];
GlCVF3(any(isnan(GlCVF3),2), :) = [];
GhCVF3(any(isnan(GhCVF3),2), :) = [];

% Give group numbers for low CVF (1) and high CVF (2) so that
% the data fits the survival analysis
GlCVF1(:, 4) = 1; GlCVF2(:, 4) = 1; GlCVF3(:, 4) = 1; GlCVF4(:, 4) = 1;
GhCVF1(:, 4) = 2; GhCVF2(:, 4) = 2; GhCVF3(:, 4) = 2; GhCVF4(:, 4) = 2;

% Columns for overview:
Columns = {'Patient row', 'CVF', 'ypN', 'Group in R'};
% Store data sets for ypT for each cluster.
% Cluster 1:
ypN_cluster1 = vertcat (GlCVF1(:, [3,4]), GhCVF1(:, [3,4]));
% Cluster 2:
ypN_cluster2 = vertcat (GlCVF2(:, [3,4]), GhCVF2(:, [3,4]));
% Cluster 3:
ypN_cluster3 = vertcat (GlCVF3(:, [3,4]), GhCVF3(:, [3,4]));
% Cluster 4:
ypN_cluster4 = vertcat (GlCVF4(:, [3,4]), GhCVF4(:, [3,4]));

% Remove rows of NaNs from the datasets (for patients with unknown survival time)
% Cluster 1:
ypN1 = ypN_cluster1 (~ any (isnan (ypN_cluster1), 2), :);
% Cluster 2:
ypN2 = ypN_cluster2 (~ any (isnan (ypN_cluster2), 2), :);
% Cluster 3:
ypN3 = ypN_cluster3 (~ any (isnan (ypN_cluster3), 2), :);
% Cluster 4:
ypN4 = ypN_cluster4 (~ any (isnan (ypN_cluster4), 2), :);

save ([filePath 'Survival data T2_parameter ypT.mat'] 'ypN1', 'ypN2', 'ypN3', 'ypN4');

```

## A12: Create delimiter tables in .txt to be used for R-console

```

clear all

% Load the datasets from the previous step
load ('Survival data T2_parameter ypT.mat');

% For Cluster 1:
CVFh1=ypN1(:,2); % Cluster Volume Fraction: high - low
ypN = ypN1(:,1); % ypT value
for i = 1:length(ypN1(:,1))
group{i,1}=sprintf('%.1f',CVFh1(i));
group{i,2}=ypN(i);
end
table1 = cell2table(group);
%%Modify variable names in table
table1.Properties.VariableNames = {'median' 'ypN'};
writetable(table1,'ypN1.txt','Delimiter','\t','writeRowNames',true);

% For Cluster 2:
CVFh1=ypN2(:,2); % Cluster Volume Fraction: high - low
ypN = ypN2(:,1); % ypT value
for i = 1:length(ypN2(:,1))
group{i,1}=sprintf('%.1f',CVFh1(i));
group{i,2}=ypN(i);
end
table2 = cell2table(group);
%%Modify variable names in table
table2.Properties.VariableNames = {'median' 'ypN'};
writetable(table2,'ypN2.txt','Delimiter','\t','writeRowNames',true);

% For Cluster 3
CVFh1=ypN3(:,2); % Cluster Volume Fraction: high - low
ypN = ypN3(:,1); % ypT value
for i = 1:length(ypN3(:,1))
group{i,1}=sprintf('%.1f',CVFh1(i));
group{i,2}=ypN(i);
end
table3 = cell2table(group);
%%Modify variable names in table
table3.Properties.VariableNames = {'median' 'ypN'};
writetable(table3,'ypN3.txt','Delimiter','\t','writeRowNames',true);

% For Cluster 4
CVFh1=ypN4(:,2); % Cluster Volume Fraction: high - low
ypN = ypN4(:,1); % ypT value
for i = 1:length(ypN4(:,1))
group{i,1}=sprintf('%.1f',CVFh1(i));
group{i,2}=ypN(i);
end
table4 = cell2table(group);
%%Modify variable names in table
table4.Properties.VariableNames = {'median' 'ypN'};
writetable(table4,'ypN4.txt','Delimiter','\t','writeRowNames',true);

```

# Appendix B

## R scripts

### B1: Cox proportional-hazards regression

```
library("survival")
library("survminer")

PFS1 <- read.table (file = file.choose (), header = T)

Rescox <- coxph(Surv(time, event) ~ group, data=PFS1)
summary(Rescox)

# Create the new data
group_df <- with(PFS1,data.frame(group = c(1, 2)))
group_df

# Survival curves
fit <- survfit(Rescox, newdata = group_df, data=PFS1)
ggsurvplot(fit, conf.int = TRUE, palette = c("blue", "red"),
           legend.labs=c("Volume share <median", "Volume share >median"),
           ggtheme = theme_minimal())
```

### B2: Wilcoxon rank-sum test

```
data <- read.table (file = file.choose (), header = T)

# Testing normal distribution of the data
# Shapiro-Wilk normality test for below ypN
with(data, shapiro.test(param[median == "1"]))
```

```
# Shapiro-Wilk normality test for above ypN
with(data, shapiro.test(param[median == "2"]))

res <- wilcox.test(param ~ median, data = data,
                  exact = FALSE)

res
```



# Appendix C

## Cluster distribution

### C1: Matlab script for voxel coordinates of tumor median sections

```

clear all

filePath = 'C:/Users/HP/Desktop/Master_Thesis/Data/';

patientList = [24 48 49 50 51 52 55 56 57 58 59 61 64 65 67 68 69 72 74 ...
              77 78 79 80 83 85 87 88 89 90 91 94 95 96 99 103 110 113 115 116 118 ...
              120 121 122 123 125 127 128 131 133 134 138 143 144 145 146 148 149 ...
              150 153 154 155 156 157 160 163 164 165 166 170 171 172 173 174 175 ...
              176 177 179];

n = length(patientList);

% Load x, y and z coordiantes in one cell
xyzdata = cell(n,1);
for patient = 1:n

    patientNr = patientList(patient);

    % Load the saved coordinates from the previous step
    load([filePath 'Oxytarget_' int2str(patientNr) ...
          ' PRE/Coordinates.mat']);

    % Read in the coordinates for each patient into the array
    xyzdata{patient}(:,1) = X;
    xyzdata{patient}(:,2) = Y;
    xyzdata{patient}(:,3) = Z;
end

% Load previous results
load([filePath 'Results K-means from T2.mat']);

% Add the cluster number to each voxel:
k = 1;
for I = 1 : n
    xyzdata {I} (:,4) = idx4(k: (k + length (xyzdata{I}) - 1));
    k = k + length (xyzdata{I});
end
% idx4 contains the voxel cluster number for k = 4 clusters.
% Number of clusters.
k = 4;

% Duplicate cell array before pre-loop
data = xyzdata;

```

```

% Add data for the median section of each tumor in the cell array data:
for I = 1: n
    for i = 1: length (xyzdata {I})
        if xyzdata {I} (i, 3) == median (xyzdata {I, 1} (:, 3))
            data {I} (i, :) =xyzdata {I} (i, :);
        else data {I} (i, :) = nan;
        end
    end
end
% Everything other than median section is now set equal to nan in data.

% Find the xy coordinates of the center of the median section for each tumor:
center = cellfun(@nanmean, data, 'UniformOutput', 0);

% Calculate the distance to the mass center provided that the voxel belongs to the median cut:
for I = 1: n
    for i = 1: length (data {I})
        if ~isnan (data {I} (i, 1))
            data {I} (i, 5) = sqrt (((data {I} (i, 1) - center {I} (1,1)) ^ 2 ) + ((data {I,
1} (i, 2) - center {I} (1,2)) ^ 2));
        end
    end
end

% Sort the distance calculations by cluster affiliation:
distance = cell (n, 1);
% Make empty cell array before the pre-loop.
for I = 1: n
    for i = 1: length (data {I})
        if data {I} (i, 4) == 1
            distance {I} (i, 1) = data {I} (i, 5);
        else distance {I} (i, 1) = 0;
        end
    end

    for l = 1:3
        if data {I} (i, 4) == 2
            distance {I} (i, 2) = data {I} (i, 5);
        else distance {I} (i, 2) = 0;
        end
    end

    for l = 1:3
        if data {I} (i, 4) == 3
            distance {I} (i, 3) = data {I} (i, 5);
        else distance {I} (i, 3) = 0;
        end
    end
end

% Column 1 now contains the distance to the center of the cluster 1.
% Column 2 now contains the distance to the center of the cluster 2.
% Column 3 now contains the distance to the center of the cluster 3.
% Set all rows except median sections equal to nan in cell the array distance:
for I = 1: n
    for i = 1: length (distance {I})
        for j = 1: k

```

```

        if distance{I}(i, j) == 0
            distance {I} (i, j) = nan;
        end
    end
end
end
end

% Calculate the average distance to the center of the median section for each
% patient for cluster 1,2,3:
incisionpass = cell2mat (cellfun(@nanmean, distance, 'UniformOutput', 0));

save([filePath 'xyzdata from T2.mat'],'xyzdata');

```

## C2: Matlab script for displaying cluster distribution

This script uses the results from the previous step and displays the distribution of the clusters in the median sections of the tumors.

```

clear all

filePath = 'C:/Users/HP/Desktop/Master_Thesis/Data/';

% Load results from the K-means
load([filePath 'Results K-means from T2.mat']);

patientList = [24 48 49 50 51 52 55 56 57 58 59 61 64 65 67 68 69 72 74 ...
    77 78 79 80 83 85 87 88 89 90 91 94 95 96 99 103 110 113 115 116 118 ...
    120 121 122 123 125 127 128 131 133 134 138 143 144 145 146 148 149 ...
    150 153 154 155 156 157 160 163 164 165 166 170 171 172 173 174 175 ...
    177 176];

n = length(patientList);

% Load x, y and z coordiantes in one cell
xyzdata = cell(n,1);
mask_median = cell(n,1);
mask_tomedian = cell(n,1);
points_median = cell(n,1);
points_tomedian = cell(n,1);

for patient = 1:n
    patientNr = patientList(patient);

    % Load the saved matrices from the previous step
    load([filePath 'Oxytarget_' int2str(patientNr) ...
        ' PRE/imgT2.mat']);

    % calculate number of pixels in the median section
    nSliceT2_2 =round(nSlicesT2 / 2);
    mask_median{patient} = ROI(:, :, nSliceT2_2);
    points_median{patient} = sum(sum(mask_median{patient}>0,2));

    % calculate number of pixels to the median section
    mask_tomedian{patient} = ROI(:, :, [1:nSliceT2_2]);

```

```

points_tomedian{patient} =
sum(sum(sum(mask_tomedian{patient,1}(:, :, [1:nSliceT2_2])>0,2)));

% Load the saved coordinates from the previous step
load([filePath 'Oxytarget_' int2str(patientNr) ...
      ' PRE/Coordinates.mat']);

% Read in the coordinates for the pixel interval corresponding to the median section
xyzdata{patient}(:,1) = X([points_tomedian{patient}:(points_tomedian{patient} +
points_median{patient})],1);
xyzdata{patient}(:,2) = Y([points_tomedian{patient}:(points_tomedian{patient} +
points_median{patient})],1);
xyzdata{patient}(:,3) = Z([points_tomedian{patient}:(points_tomedian{patient} +
points_median{patient})],1);
xyzdata{patient}(:,4) = idx4([points_tomedian{patient}:(points_tomedian{patient} +
points_median{patient})],1);

end

% Plot cluster distribution in median section
figure1 = figure(1);
l=gscatter(xyzdata{patient,1}(:,1),xyzdata{patient,1}(:,2),xyzdata{patient,1}(:,4),'gryb',8);
legend({'Cluster1', 'Cluster2', 'Cluster3', 'Cluster4'}, 'Location', 'southeast')
set(gca, 'visible', 'off')
rotate(1,[0 0 1], -90);
saveas(figure1, 'Median.png')

```

### C3: Cluster distribution in median tumor sections

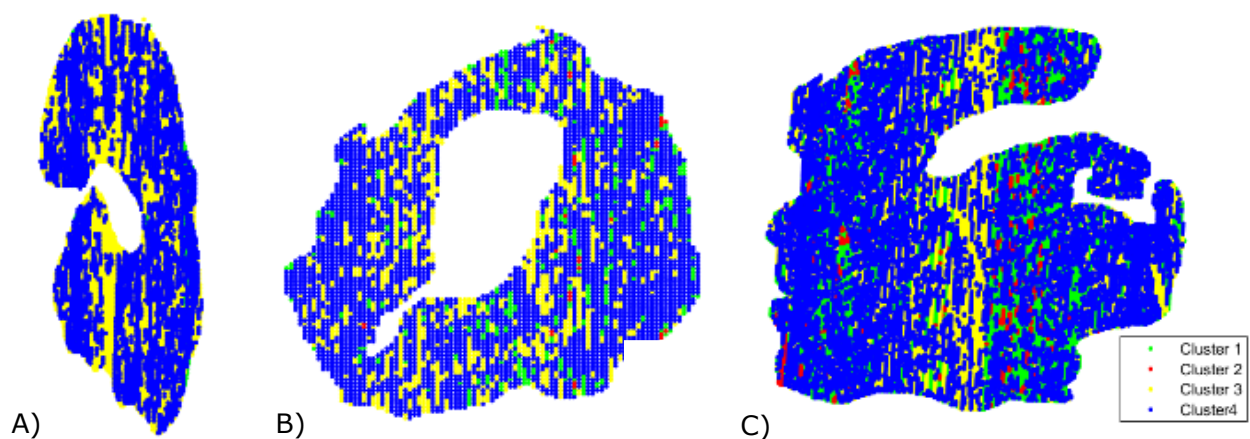


**Figure C3.1:** Intensity-based voxel clusters in the central slice of tumors from three different patients. The treatment for these patients resulted in local recurrence (A), metastasis (B) or progression-free survival (C).

## Appendix D

### Kaplan-Meier plots

The calculations in the survival analyses with the Cox proportional-hazards regression were controlled with Kaplan-Meier plots in the R console and MedCalc®.

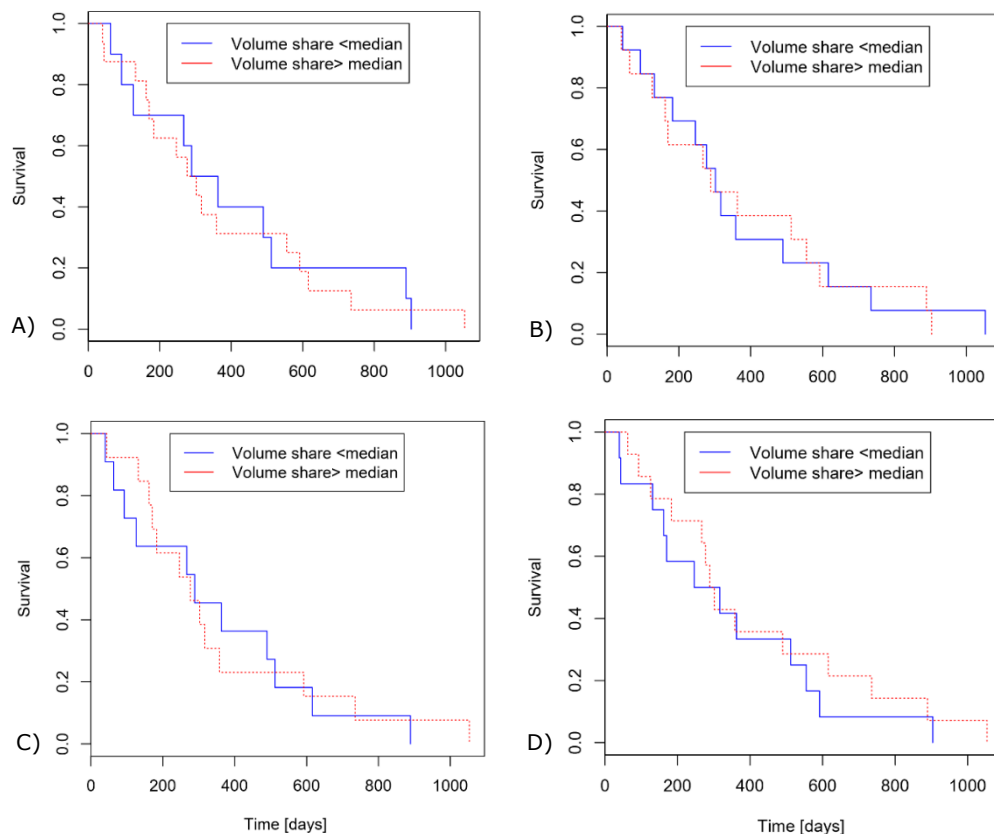


**Figure D.1:** Kaplan-Meier survival plot for the survival difference between the two patient groups in cluster 1 (A), cluster 2 (B), cluster 3 (C) and cluster 4 (D), divided by the median volume with log-rank test. The investigated endpoints are local recurrence, metastasis or death. Survival is indicated in the portion of patients with progression-free survival (PFS).

# Appendix E

## Normality tests

The following tables show the results from Saphiro-Wilk normality tests performed on the data. Only in several outliers the results indicated p-values higher than 0.05, which showed that the data is not normally distributed. Consequently the Wilcoxon rank-sum test was chosen for the statistical analyses.

$T_2(\text{shh})$	mrT		p/ypT		$\Delta T$		mrN		p/ypN		$\Delta N$		TRG	
Cluster 1	1.175e-05	6.088e-06	1.539e-05	3.197e-06	9.418e-06	1.225e-07	9.464e-06	1.764e-05	4.248e-07	1.616e-05	2.593 e-04	2.707 e-04	0.03487	4.506e-06
Cluster 2	1.061e-05	1.682e-05	5.401e-05	5.456e-07	8.635e-07	7.417e-06	1.061e-05	1.682e-05	7.623e-07	4.053e-06	9.416 e-04	1.051 e-04	0.01128	3.423e-06
Cluster 3	1.609e-05	1.118e-05	1.082e-05	2.791e-06	4.468e-08	5.636e-05	7.029e-06	4.939e-06	1.117e-06	5.329e-06	3.286 e-04	1.886 e-04	0.0003286	1.886e-04
Cluster 4	1.636e-05	4.255e-06	1.786e-04	7.131e-07	2.319e-06	1.471e-06	1.578e-06	1.251e-05	3.356e-07	3.557e-06	5.408e-04	1.334e-05	5.408e-04	1.334e-05

$b=0$ [s/mm <sup>2</sup> ]	mrT		p/ypT		$\Delta T$		mrN		p/ypN		$\Delta N$		TRG	
Cluster 1	1.437e-05	8.787e-06	0.000243	3.397e-07	4.876e-07	3.126e-05	4.020e-06	2.461e-05	1.172e-07	2.267e-06	0.0004142	0.0004954	0.04808	0.01786
Cluster 2	1.907e-05	1.162e-05	3.626e-05	2.111e-05	2.352e-06	4.575e-06	7.256e-07	8.779e-05	3.407e-08	7.813e-06	1.185e-05	0.0010050	0.004826	0.04285
Cluster 3	2.766e-05	1.130e-05	0.0003881	1.657e-06	2.159e-07	7.284e-06	4.275e-05	2.985e-06	2.481e-06	2.609e-07	0.001490	6.679e-05	0.00728	0.01210
Cluster 4	2.111e-05	1.525e-05	1.765e-06	0.000103	8.326e-05	4.222e-08	6.633e-06	1.297e-05	1.150e-06	5.397e-07	0.003613	1.032e-05	0.01210	0.00324

$b=25$ [s/mm <sup>2</sup> ]	mrT		p/ypT		$\Delta T$		mrN		p/ypN		$\Delta N$		TRG	
Cluster 1	8.787e-06	2.114e-05	3.207e-05	5.327e-05	6.314e-06	3.299e-06	1.583e-05	4.080e-06	7.623e-07	1.334e-06	3.74e-04	3.881e-04	0.0007407	6.878e-05
Cluster 2	1.127e-05	1.829e-05	1.461e-06	7.374e-05	3.03e-06	6.612e-06	3.605e-05	2.687e-06	9.076e-07	6.619e-07	0.0003294	0.0001708	0.0083650	3.894e-05
Cluster 3	2.620e-05	1.007e-05	1.984e-05	2.226e-05	1.447e-04	2.548e-07	1.087e-05	4.782e-06	1.901e-07	3.413e-06	0.0004564	0.0003487	0.0016630	5.072e-05
Cluster 4	1.907e-05	7.475e-06	1.859e-06	4.005e-05	1.652e-06	4.28e-06	4.182e-06	1.177e-05	1.233e-07	6.510e-06	0.0006348	0.0002052	<b>0.069660</b>	6.578e-06

$b=50$ [s/mm <sup>2</sup> ]	mrT		p/ypT		$\Delta T$		mrN		p/ypN		$\Delta N$		TRG	
Cluster 1	1.907e-05	1.162e-05	3.626e-05	2.111e-05	2.352e-06	4.575e-06	7.256e-07	8.779e-05	3.407e-08	1.614e-06	1.185e-05	0.000445	0.0048260	0.042850
Cluster 2	2.766e-05	1.130e-05	0.0003881	1.657e-06	2.159e-07	7.284e-06	4.275e-05	2.985e-06	2.481e-06	8.674e-08	0.001490	4.788e-05	0.0072890	0.012100
Cluster 3	2.111e-05	1.525e-05	1.765e-06	0.000103	8.326e-05	4.222e-08	6.633e-06	1.297e-05	1.150e-06	1.819e-07	0.003613	1.187e-05	<b>0.090410</b>	0.003243
Cluster 4	1.437e-05	8.787e-06	0.0002434	3.397e-07	4.876e-07	1.767e-05	4.020e-06	2.461e-05	1.172e-07	3.613e-07	0.0004142	0.000402	0.0480800	0.011850

<b>b=50</b> [s/mm <sup>2</sup> ] (shh)	mrT	p/ypT	$\Delta T$	mrN	p/ypN	$\Delta N$	TRG
Cluster 1	5.310e-06 1.867e-05	1.578e-05 7.374e-05	4.011e-06 4.178e-06	4.433e-06 2.213e-05	4.482e-07 1.354e-06	0.000266 0.000266	0.063520 0.015570
Cluster 2	3.622e-05 1.376e-05	0.000234 1.939e-05	1.409e-05 1.368e-07	1.897e-05 3.770e-06	5.408e-07 2.221e-06	0.000245 0.002649	0.008319 0.006740
Cluster 3	2.246e-05 4.853e-06	1.634e-05 7.566e-05	7.566e-07 2.159e-05	7.144e-06 1.290e-05	5.397e-07 3.045e-06	0.000634 0.000456	0.009565 0.003747
Cluster 4	1.489e-05 2.451e-05	6.180e-05 9.365e-05	2.159e-05 7.566e-0	1.778e-05 3.572e-06	5.842e-07 2.320e-06	0.000611 0.000789	0.002293 0.005944

<b>b=100</b> [s/mm <sup>2</sup> ]	mrT	p/ypT	$\Delta T$	mrN	p/ypN	$\Delta N$	TRG
Cluster 1	1.437e-05 8.787e-06	0.000243 3.397e-07	4.876e-07 3.126e-05	4.020e-06 2.461e-05	1.172e-07 2.267e-06	0.0004142 0.0004954	0.04808 0.01786
Cluster 2	1.907e-05 1.162e-05	3.626e-05 2.111e-05	2.352e-06 4.575e-06	7.256e-07 8.779e-05	3.407e-08 7.813e-06	1.185e-05 0.0010050	0.004826 0.04285
Cluster 3	2.766e-05 1.130e-05	0.0003881 1.657e-06	2.159e-07 7.284e-06	4.275e-05 2.985e-06	2.481e-06 2.609e-07	0.001490 6.679e-05	0.00728 0.01210
Cluster 4	2.111e-05 1.525e-05	1.765e-06 0.000103	8.326e-05 4.222e-08	6.633e-06 1.297e-05	1.150e-06 5.397e-07	0.003613 1.032e-05	<b>0.09041</b> 0.00324

<b>b=500</b> [s/mm <sup>2</sup> ]	mrT	p/ypT	$\Delta T$	mrN	p/ypN	$\Delta N$	TRG
Cluster 1	1.144e-05 1.344e-05	0.000113 8.352e-06	4.876e-07 3.126e-05	5.534e-06 2.461e-05	2.679e-07 2.267e-06	0.000414 0.000495	0.041490 0.012560
Cluster 2	2.111e-05 1.344e-05	1.765e-06 6.681e-05	8.326e-05 7.363e-08	6.633e-06 1.965e-05	6.277e-07 1.648e-06	0.006019 8.258e-06	<b>0.096410</b> 0.003243
Cluster 3	1.525e-05 1.162e-05	1.084e-05 4.851e-05	4.116e-06 3.381e-06	3.720e-07 0.000116	3.407e-08 7.941e-06	4.279e-06 0.001130	0.0053030 0.033530
Cluster 4	4.94e-05 7.469e-06	0.000563 1.800e-06	2.510e-07 4.032e-06	7.513e-05 1.252e-06	3.560e-06 1.670e-07	0.002975 0.000259	0.005815 0.012100

<b>b=1000</b> [s/mm <sup>2</sup> ]	mrT	p/ypT	$\Delta T$	mrN	p/ypN	$\Delta N$	TRG
Cluster 1	1.175e-05 6.088e-06	1.539e-05 3.197e-06	9.418e-06 1.225e-07	9.464e-06 1.764e-05	4.248e-07 1.616e-05	2.593 e-04 2.707 e-04	0.03487 4.506e-06
Cluster 2	1.061e-05 1.682e-05	5.401e-05 5.456e-07	8.635e-07 7.417e-06	1.061e-05 1.682e-05	7.623e-07 4.053e-06	9.416 e-04 1.051 e-04	0.01128 3.423e-06
Cluster 3	1.609e-05 1.118e-05	1.082e-05 2.791e-06	4.468e-08 5.636e-05	7.029e-06 4.939e-06	1.117e-06 5.329e-06	3.286 e-04 1.886 e-04	0.0003286 1.886e-04
Cluster 4	1.636e-05 4.255e-06	1.786e-04 7.131e-07	2.319e-06 1.471e-06	1.578e-06 1.251e-05	3.356e-07 3.557e-06	5.408e-04 1.334e-05	5.408e-04 1.334e-05

<b>DWI + T<sub>2</sub></b> (b=50 s/mm <sup>2</sup> ) (shh)	mrT	p/ypT	$\Delta T$	mrN	p/ypN	$\Delta N$	TRG
Cluster 1	9.794e-06 2.601e-05	6.155e-05 3.549e-05	1.395e-06 4.832e-06	1.536e-05 3.924e-06	5.365e-06 6.435e-08	0.002198 5.471e-05	0.008864 0.078620
Cluster 2	6.646e-06 2.252e-05	2.469e-07 0.000710	9.104e-07 2.967e-05	4.239e-06 9.557e-06	1.344e-06 1.117e-06	0.000251 9.493e-05	0.020080 0.010620
Cluster 3	2.223e-05 2.100e-05	3.511e-05 0.000177	5.568e-05 2.207e-07	2.133e-05 2.808e-06	5.408e-07 1.127e-06	0.000981 0.000885	0.007322 0.003978
Cluster 4	2.035e-05 5.31e-06	0.0004252 2.729e-06	1.652e-06 1.613e-05	1.922e-06 1.778e-05	2.855e-07 3.045e-06	0.001465 0.000252	0.002371 0.000871